EXPERIMENTAL INVESTIGATIONS INTO ENHANCING THE MACHINABILITY OF EN-36C

A THESIS SUBMITTED IN FULFILMENT OF

THE REQUIREMENT FOR THE AWARD OF THE DEGREE

OF

DOCTOR OF PHILOSOPHY

IN

MECHANICAL ENGINEERING

BY

RAJESH KUMAR MAURYA

ROLL NO- (2K16/Ph.D./ME/52)

GUIDED BY

Prof. M. S. NIRANJAN

Mechanical Engineering Department
Delhi Technological University
Main Bawana Road, Shahabad Daulatpur, Delhi- 110042, India

CERTIFICATE

This is to certify that the work embodied in the thesis entitled **"Experimental Investigations into Enhancing the Machinability of EN-36C"** being submitted by **Rajesh Kumar Maurya (Roll No- 2K16/Ph.D./ME/52)** for the award of Doctor of Philosophy (Ph.D.) Degree in Mechanical Engineering at Delhi Technological University, Delhi is an authentic work carried out by him under my guidance and supervision. It is further certified that the work is based on original research and the matter embodied in this thesis has not been submitted to any other university/institute for award of any degree to the best of my knowledge and belief.

Date :

Place:

Prof. M. S. Niranjan
Department of Mechanical Engineering
Delhi Technological University
Delhi- 110042

ACKNOWLEDGEMENT

I would like to express my special appreciation and thanks to my supervisor Dr. M. S. Niranjan, for his invaluable guidance and unwavering support throughout my journey to complete my Ph.D. thesis. Your mentorship has been instrumental in shaping my academic and research endeavors, and I am immensely thankful for the opportunities you provided for growth and learning. Your expertise, dedication, and passion for the subject matter served as a constant source of inspiration. Your insightful feedback, constructive criticism, and patience during our countless discussions and meetings significantly enhanced the quality of my research. I have learned not only the intricacies of my field but also the importance of diligence, perseverance, and the pursuit of excellence through your mentorship.

I would like to express my gratitude to Prof. Prateek Sharma, Vice chancellor, Delhi Technological University, Delhi for providing this opportunity to carry out the research work in this prestigious institute. I would also like to express my deep sense of gratitude and indebtedness to my head, Department of Mechanical Engineering Prof. B. B. Arora for his motivation and support during my research work. I would also like to thank all technical staff for all possible help during the experiments.

I also convey my sincere thanks to my faculty colleague Dr.Virendra Pratap Singh, Dr. Vineet Kumar, Dr. Deepak Chauhan, Dr. Ambuj Saxena and Dr. Himmat Singh for their active support. I am greatly indebted to my parents for their love and blessings to see me scaling greater heights of life. I truly appreciate the moral support which I got from my father Mr. Basant Lal Maurya throughout my career. Without his motivation and encouragement, pursuit of this Ph.D. work would have never been possible.

With immense pleasure and delight, I would like to thank my wife Mrs. Kiran Maurya for giving me the mental and moral support in my highs and lows during this Ph. D. journey. I appreciate my daughter Palak Maurya, little son Pranjal Kumar Maurya for abiding my ignorance and patience as both showed during my Ph.D. Words can never say how grateful I am to my wife and to both of my loving children.

Date: **Rajesh Kumar Maurya**

Place: **Roll Number: 2K16/Ph.D./ME/52**

PREFACE

In this thesis the effect of different stages of tempering on EN-36C alloy steel has been carried out to check the mechanical behavioural, microstructural properties and residual stresses. The main objective behind this to enhancing the machinablity during CNC turning with preserving their properties. It would help the researchers to understand the technique how to increase the machinablity of any hard metal by this method. The contents of the thesis are as follows:

Chapter 1 In this chapter, conventional machining processes have been described along with its different types of classification. Merits and demerits of CNC machining over other conventional machining have been discussed. Various parts and their uses are included in this section. Later in this chapter, about material EN-36C, tempering process and their different stages has been discussed.

Chapter 2 A comprehensive review of the literature has been discussed on machinability of EN-36C alloy steel with and without tempered on CNC turning. In this section, the effect of various process parameters such as feed rate, depth of cut, cutting speed on output responses like material removal rate, surface finish, residual stress, tool tip temperature are reviewed. Effect of tempering on mechanical properties and microstructural behaviour of hard metals is also reviewed**.**

Chapter 3 In this chapter, the sample preparation of EN-36C alloy steel, chemical composition, tempering of prepared samples, testing of samples for mechanical and microstructural properties were carried out. A brief discussion was made on sequence of experimental processes.

Chapter 4 In this chapter, the discussion is made on Machinability and related factors which affect on it. Apart from this, a comparative study on mechanical properties of EN-36C alloy steel tempered and untempered has been carried out. The comparative study on surface roughness has also been carried out after conducting

the experiments on CNC lathe at same process parameters using cylindrical bar of tempered and untempered EN-36C alloy steel.

Chapter 5 This chapter discusses the design of experiments using Response Surface Methodology (RSM), utilizing statistical analysis and ANOVA to understand the process. The optimum process parameters were selected for minimum surface roughness, residual stress and tool wear and maximum material removal rate for demonstrating the effectiveness of the method in achieving desired results.

Chapter 6 This chapter elaborates scanning electron micrographs (SEM) and optical microscope obtained with CNC turned surfaces of tempered and non-tempered work piece of EN-36C alloy steel at optimum process parameters have been studied

Chapter 7 This chapter explains the residual stress of CNC turned surfaces of tempered and untempered EN-36C alloy steel using an X-ray residual stress analyzer. The process is analyzed using response surface methodology and ANOVA. The optimal process parameters are obtained for the response percentage reduction in residual stress.The regression analysis investigates the significance of process parameters like cutting speed (V), feed rate (f) and depth of cut (d) and tempering temperature on the output response percentage reduction in residual stress (%ΔRS).

Chapter 8 This chapter describes the results and discussion part of the investigations in this thesis. The effect of tempering on mechanical properties and behavioral of microstructure as well as the various process parameters such as cutting speed (V), feed rate (f) and depth of cut (d) on their responses like residual stress, surface roughnes, tool wear, material removal rate (MRR) are studied.

Chapter 9 This chapter contains the conclusions obtained from experimental investigations on EN-36C alloy steel with and without tempered during CNC turning. The process is thoroughly analyzed mechanical properties such as tensile strength,

hardness, toughness and percentage elongation, microstructural properties, surface roughness and residual stress by statistical analysis using response surface methodology. The results have been explained in brief and scope of future work is discussed.

TABLE OF CONTENTS

List of Figures

List of Tables

ABBREVIATIONS

CNC	Computer Numeric Control
CAD	Computer Aided Design
CAM	Computer Aided Manufacturing
TMM	Tool Makers Microscope
RSM	Response Surface Methodology
CFD	Computer Fluid Dynamics
CCD	Central Composite Design
ANOVA	Analysis of variance
GA	Genetic algorithm
MRR	Material removal rate
SR	Surface roughness
PCBN	Polycrystalline cubic boron nitride
CBN	Cubic boron nitride
MQL	Minimum quantity lubrication
UHS	Ultra high strength
XRD	X-ray diffraction
PSSD	Line sensitive Scintillation detectors
XEC	X-ray elastic constants

MET	Multiple exposure technique
MOGA	Multi-objective genetic algorithm
DSS	Duplex stainless steel
FSS	Ferritic stainless steel
OES	Optical emission spectroscope
UTM	Universal testing machine
ASTM	American society for testing and materials
EDAX	Energy dispersive X-ray analysis
SEM	Scanning electron microscope
NDT	Non-destructive testing
FWHM	Full-width at half-maximum
D-S	Debye-scherrer
HRB	Rockwell hardness of scale B
MRR_{TT}	Material removal rate at tempering temperature
MRR_{RT}	Material removal rate at room temperature
IPs	Imaging plates

NOMENCLATURES

V	Cutting speed
f	Feed Rate
d	Depth of Cut
R_a	Average surface roughness
R_q	Root mean square value
R_z	Peak to valley height
T_w	Tool wear
µm	Micro-meter
h_1	Indentation depth produced by the preliminary test force
h_2	Indentation depth produced by the test force
IPs	Imaging plates
mm	millimeter
kN	Kilo-Newton
J	Joule
Kg	Kilogram
MPa	Mega pascal

ABSTRACT

EN-36C alloy steel has a wide application in the field of automobile and aerospace sector due to its splendid mechanical and metallurgical properties. There are several studies available to investigate the mechanical and surface properties of EN-36C alloy steel. The intense demands of nickel chromium case hardened (EN-36C) alloy steel in different engineering applications are increasing day by day due to its cheap and easy availability. The samples of EN-36C alloy steel of diameter 32 mm and length of 150 mm are prepared. The tempering in box type muffle furnace has been carried out at 200°C, 300°C, 500°C and 700°C respectively. The effect of different stages of tempering on EN-36C alloy steel has been observed to study the mechanical behavioural and microstructural properties in the present work. The influence of tempering on mechanical properties such as tensile strength, hardness, toughness and percentage elongation has been observed. The experiments have been conducted on tempered and untempered EN-36C at cutting speed 550 rpm, feed rate 0.16 mm/rev and depth of cut 1.5 mm using CNC lathe. The effects of tempering on response variables such as material removal rate, surface roughness, tool tip temperature and residual stresses are evaluated. The cos α method is used to measure the residual stresses in the turned specimen using two-dimensional detectors such as imaging plates. Experimental results depicted that the ductility and toughness are improved without significant change in hardness in the specimen tempered at 500°C.The maximum value of material removal rate (12596.80 mm^3/min), minimum tool tip temperature (61.33°C), minimum surface roughness (R_a =1.93µm, R_q = 2.36µm, R_z =10.30µm) and minimum residual stress 217 MPa are observed in the specimens tempered at 500°C among all tempered and untempered specimens. After comparative study, the experimental plan has been developed for specimens tempered at 500°C using design of experiment. Statistical analysis using response surface methodology has been carried out for the selection of optimum process parameters such as cutting speed (V), feed rate (f), and depth of cut (d) in the turning

of EN-36C with tungsten carbide cutting insert (CNMG-120408-TMH-F) in dry machining environment for minimization of residual stress and tool wear as well as maximizing the material removal rate (MRR). Analysis of variance (ANOVA) has been done to develop regression models for tool wear, residual stress, and MRR. Optimum process parameters have been found for maximum MRR, minimum tool wear and residual stress individually. ANOVA revealed that more contribution towards cutting speed and feed rate has been observed than depth of cut for minimum residual stress and tool wear, while more contribution towards cutting speed and depth of cut observed than feed rate for maximization of MRR. The confirmatory experiments have been conducted at optimum process parameters obtained by regression model and tool wear, residual stress and MRR have been calculated which are found very close to predicted minimum tool wear, residual stress and maximum predicted MRR.

Keywords: *EN-36C alloy steel, Tempering, Mechanical properties, CNC turning, Microstructure, MRR, Residual stresses, Tool wear*

CHAPTER-1

Introduction

In this chapter, conventional machining processes have been described along with its different types of classification. Merits and demerits of CNC machining over other conventional machining have been discussed. Various parts and their uses are included in this section. Later in this chapter, about material EN-36C, tempering process and their different stages has been discussed.

1.1 Background

Turning is a very important operation use to remove unwanted materials from the surface of the rotating cylindrical bar with the use of single point cutting tool for getting usable finished product. This operation is used to decrease the diameter of the work-piece as per required application, and also achieve a good surface finish on the cylindrical bar. The cutting tool used for turning is fed linearly, parallel to the axis of rotation of cylindrical bar [1].

Now a day, industry requirements are to produce low cost, high quality products with maximum productivity. This common method is generally used for finishing the machined parts. For producing desired quality and maximum productivity, suitable cutting parameters should be selected [2].

Surface quality significantly impacts turning performance, improving fatigue strength, corrosion resistance, and creep life. Surface roughness affects functional attributes like contact friction, wearing, light reflection, heat transmission, lubricant distribution, load bearing capacity, and fatigue resistance. A good surface also enhances lubricant distribution and holding capacity. Therefore, the desired surface finish is usually specified and the appropriate processes are selected to reach the required quality [3]

There is a remarkable degree of demand for nickel chromium case hardened steel (EN-36C) alloy steel in various fields of engineering due to its good mechanical properties like yield strength, ultimate tensile strength, percentage elongation and hardness. It comes in a range of

sizes and forms, including billet, hexagonal, flat, square, and round bars. It is utilized in the automotive and aerospace industries to create a variety of high strength parts, including connecting rods, crankshafts, gear shafts, and specific kinds of collets. Because of its extreme hardness characteristic, optimization of the machining of samples for a final product presents a significant problem. It is important to greatly enhance the mechanical property in order to facilitate machining. Design, production, and metallurgical techniques can all be used to enhance a material's mechanical properties. One of the most significant heat treatment procedures is tempering, which involves heating martensitic steel below the eutectoid temperature to increase its ductility and softness. Without appreciably decreasing the alloy steel's hardness or strength, the tempering procedure lessens the steel's brittleness and stresses.

1.2 Lathe Machine Tool

Lathe is a crucial machine tool used for removing unwanted material from a work piece by rotating it against a single point cutting tool. Originating in France as early as 1569, wood lathes were later adapted for metal cutting during the Industrial Revolution in England. Hand controls are used to rotate the machine's horizontal spindle, which is often powered at different speeds and is supported by a tool rest. The tool is mounted onto a cross slide and driven on straight pathways either parallel or perpendicular to the work axis on an engine lathe. The tool's motion in a screw cutting lathe is precisely correlated with the spindle's rotation.

1.2.1 Classification of Lathe

Lathes are machines used for various purposes, including cutting, loading, tool changing, and part unloading.

Engine lathe

Engine lathe is a common type of lathe machine for general-purpose metal cutting, originally developed for machine engine blocks and driven by steam engines. It was the traditional lathe applied in the late 19th or 20th century, with automatic feed to the cutting tool.

Early engine lathes had cone heads with a spindle attached and a cone pulley designed to accept a flat belt. Modern engine lathes powered by small motors are smaller and more powerful than original machines. They can be mounted on a workbench and are often equipped with Computer Numerical Control, allowing them to perform complex CNC turning or machining works with fewer manual operations.

Bench lathes

Bench lathe machines are small, precision lathes used for small precision work. Mounted on a bench, they share similarities with engine and speed lathes but perform most operations, with only difference being their size. Bench lathe machines perform similar operations.

Tracer Lathe and Mills

Tracer lathes and mills were historically used in machining and manufacturing before the widespread adoption of CNC technology. These manually operated machines follow a template or master model, replicating complex contours and profiles onto the work-piece. Although not as precise or versatile as CNC machines, they were valuable tools for producing intricate parts. However, their use has decreased with the advent of CNC technology, offering greater automation, precision, and flexibility in machining operations.

Automatic lathes

Automatic lathes are a powerful tool in the machining industry, capable of producing precision parts with minimal human intervention, using various features like drilling, turning, boring, and threading.

Turret lathes

The turret lathe is a metalworking machine that evolved from earlier lathes by adding an indexable tool holder. This allows for multiple cutting operations with different tools on one machine, eliminating the need for operator setup or tool control. The early turret was a flattened cylindrical block mounted to the cross slide, rotating around the vertical axis and projecting tool

holders out to all sides. The turret lathe can automatically switch to the proper cutter, resulting in faster and more efficient production compared to traditional lathes.

Capstan Lathe

The Capstan Lathe, developed by Pratt and Whitney in 1860, is a modified version of the Engine Lathe and Center Lathe, replacing the tailstock with a hexagonal turret tool head. This was necessary due to the time consuming nature of changing tools and operations in the center lathe, which was not suitable for mass production. The Capstan Lathe is a modified form of the center lathe, allowing for more efficient and accurate work-piece operations.

Computer controlled lathes are highly automated machines that control cutting, loading, tool changing, and part unloading

1.2.2 An introduction to CNC machine

CNC machining is a manufacturing process where pre-programmed computer software controls the movement of factory tools and machinery, including grinders, lathes, mills, and routers. It allows for three-dimensional cutting tasks to be accomplished in a single set of prompts, similar to a robot. CNC programming is stored in a computer's memory and the code is written and edited by programmers. This allows for more expansive computational capacity and is not static, as new prompts can be added to pre-existing programs through revised code. CNC systems run more efficiently than manual control, which requires live operators to operate machine tools via levers, buttons, and wheels. Although CNC systems may not appear visually different from generic computer systems, the software programs and advanced components used in this process make them stand out from other forms of computation. The block diagram of CNC machine is given in Figure1.

1.2.3 Steps in CNC Machines to Make Parts

The process for creating a surface finished part is straightforward and involves the following steps.

- CAD software is used for designing idealized parts, creating 2D or 3D models with precise dimensions, akin to computer-aided drawing.
- CNC programming utilizes CAM software to convert CAD models into G-code, the language used to program CNC machines.
- The machine is set up with work holding, proper tooling, and loaded with G-code program and tool data, with the operator indicating part zero.
- The process of machine the parts are now complete after all the setup has been completed.

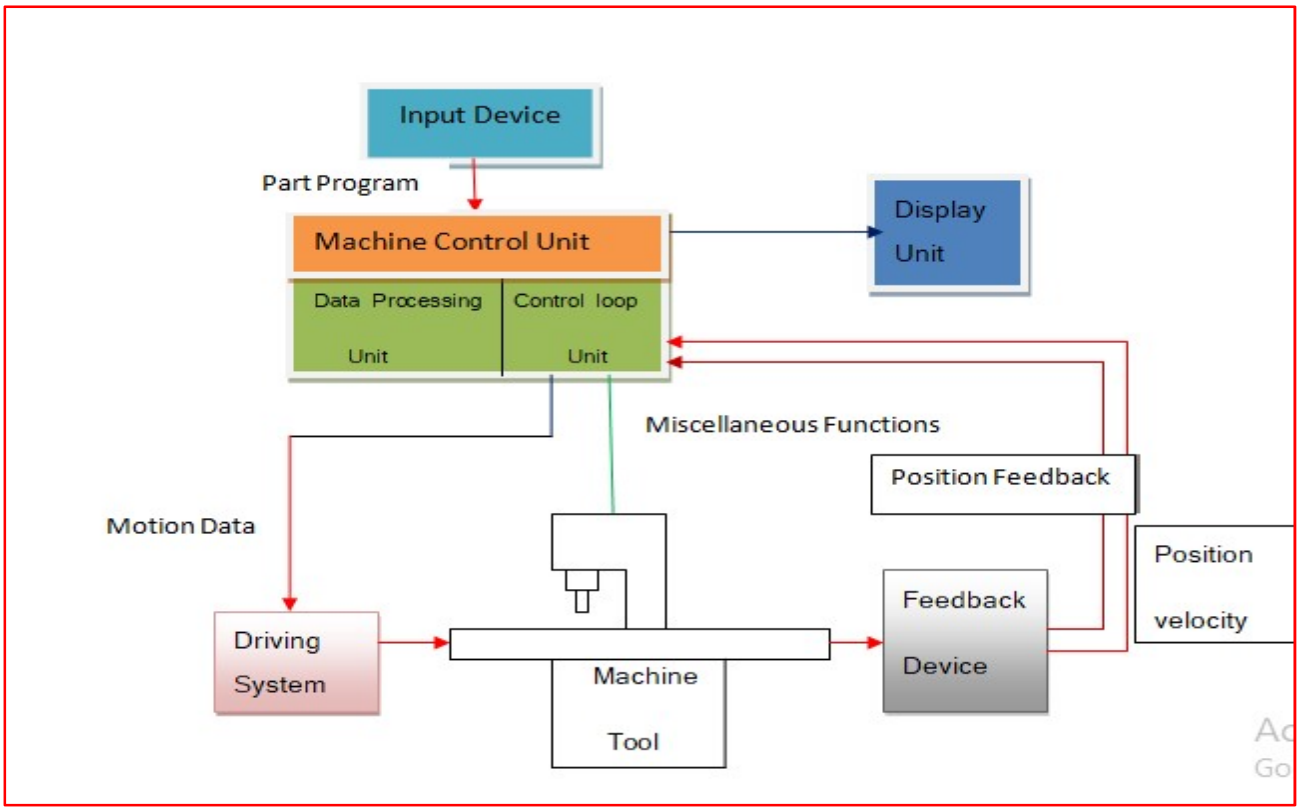

Fig.1: Block diagram of CNC machine

1.2.4 CNC Lathes Machine

Lathes are considered the universal CNC machine tool as they can create all necessary parts for another lathe. They are ideal for symmetrical parts and can drive the cutting tool under G-code control over X and Z axes. Variations include Swiss Lathes. The act of cutting a work-piece is called "Turning."

Advantage of CNC

CNC systems enhance operational flexibility by producing complex shapes with high dimensional accuracy, repeatability, and reduced scrap loss.

They reduce tooling costs by eliminating the need for templates and other fixtures, and enable the downloading and uploading of part programs.

Each setup allows for more operations and reduces lead time for setup and machining compared to conventional methods.

The process of design changes is facilitated, leading to a reduction in inventory.

Microprocessors enable quick program preparation and recall, reducing paper work and facilitating efficient workflow.

The operator’s required skill is lower than that of a qualified machinist, allowing them more time to focus on other work-related tasks.

The simulation option can be used to verify the part program.

Disadvantage of CNC

CNC technology needs relatively high initial investment, as it involves complex systems such as:

- Mechanical
- Hydraulic

- Pneumatic
- Electrical and control systems.
- These systems require special maintenance by trained personnel.
- High preventive maintenance is crucial as system breakdowns can be costly.

1.2.5 Lathe Operations

This text outlines various processes used in metalworking, including **turning, facing, boring, drilling, threading, and knurling.** Turning produces straight, conical, curved, or grooved work-pieces, while facing creates flat surfaces or face grooves. Boring enlarges holes or cylindrical cavities, drilling create holes by fixing a drill in the tailstock, and knurling creates a regularly shaped roughness on cylindrical surfaces.

1.2.6 Cutting tools for CNC turning

This article provides a comprehensive guide to the various types of lathe tools used in CNC turning, emphasizing their importance in producing turned parts and shaping materials to the desired form. It also explains how to select the most suitable lathe tool for different operations, ensuring maximum advantages from these tools.

Types of Cutting Tools

Lathe cutting tools are categorized into four main groups: materials, operations, structure, and feed direction.

Based on Material

Lathe cutting tools are categorized based on the material they are made of.

1. **High-Speed Steel (HSS) Tools**

High-speed steel tools are used for cutting metals like steel, aluminum, and cast iron, providing exceptional results for rough and semi-finish machining, with easy sharpening and long tool life.

2. **Carbide Tools**

Carbide tools are hard and wear-resistant. The lathes that can cut hard metals like stainless steel and titanium, as well as abrasive materials or composites. They can operate at high speeds and have a longer tool life than HSS tools.

3. **Diamond tools**

Diamond tools, made of synthetic diamonds, are used for cutting hard materials like glass or ceramics at high speeds and long tool life. However, their high cost limits their industrial use.

4. **Special Coated Tools**

HSS tools are typically coated with special materials like ceramic, cubic boron nitride (CBN), and tungsten carbide, as their name suggests.

Ceramic tools are hard, wear-resistant tools used for cutting hard metals like cast iron and heat-resistant alloys. They are ideal for high-speed cutting and provide excellent surface finish, making them ideal for high-speed cutting.

Cubic Boron Nitride is a hard, durable tool ideal for rough machining and intermittent cutting, especially when working with cast iron materials, due to its resistance to abrasion.

Based on Operations

1. Turning Tool

Turning cutting tools are categorized into rough turning tools and finish turning tools, each used for varying purposes**.**

Rough turning tools are designed for swift removal of large work-pieces, offering a cutting angle that can withstand high pressure for easy removal.

Finish turning tools are used to remove smaller sections of a work-piece, creating smooth, precise surfaces as the end product, with the angle carefully crafted to achieve the same.

2. Shoulder Turning Tool

A square shoulder is formed using a knife-edge turning tool or facing tool, while a beveled shoulder requires a straight turning tool with zero nose radius and a side cutting edge angle. For filleted shoulders, a straight turning tool is used, considering the work's nose radius.

3. Chamfering Tool

A straight turning tool with chamfer angle cutting edges can also be used as a chamfering tool, with specialized tools used for frequent chamfer work with side cutting edges set at the chamfer angle.

4. Thread Cutting Tool

Thread cutting tools are used to cut threads on lathe work-pieces, with two types: internal and external. External thread cutting uses a chuck to center the work-piece, while internal thread cutting requires a chuck to grip the work-piece and remove chips in a linear pattern.

5. Facing Tool

A facing tool is a machine tool used to cut a surface perpendicular to a work-piece's rotational axis, held by a tool holder on the lathe carriage for perpendicular feed.

6. Grooving Tool

Grooves can be created on cylindrical surfaces using tools like square and V-shaped cutting tools, with the groove's shape determined by the lathe machine tool's shape.

7. Forming Tool

A forming tool is a combination of a turning and grooving tool, enabling the creation of complex shapes in a single pass. A precisely designed tool enhances accuracy and reduces cycle time, while turning tools can also be used.

8. Boring Tool

A bore tool is a tool used to widen the diameter of pre-existing holes to enlarge them.

9. Counter boring Tool

An ordinary boring tool can perform a counter boring operation, leaving a shoulder after turning, while a counter bore with multiple cutting edges is commonly used.

10. Undercutting Tool

The undercutting tool has a cutting edge similar to the groove's form, with clearance angles on all sides, using longitudinal feed for recessing groove cutting edge and front clearance angle based on work bore.

11. Parting off Tool

A parting off tool is a narrow tool used to remove minimal metal from a work-piece, typically forged for use with cemented carbide-tipped tools.

12. Knurling Tool

Knurling tools are metal rollers with embossed patterns, used to create indents on the work-piece to enhance grip.

Cutting Tool Geometry

Turning uses a single point cutting tool, with material selection based on work material type. Cutting speed and feed rate are also considered. The tool's description is provided in Figure2.

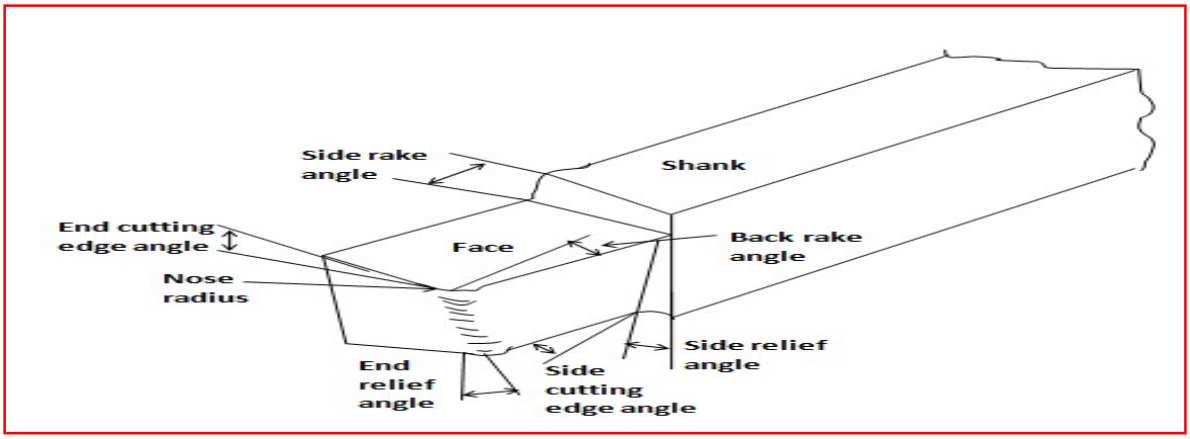

Fig.2: Description of cutting tool

Shear deformation of the work material to generate a chip is the primary cutting action in machining; when the chip is removed, a new surface is revealed. The most common use of machining is to form metals. The procedure is demonstrated in the Figure3.

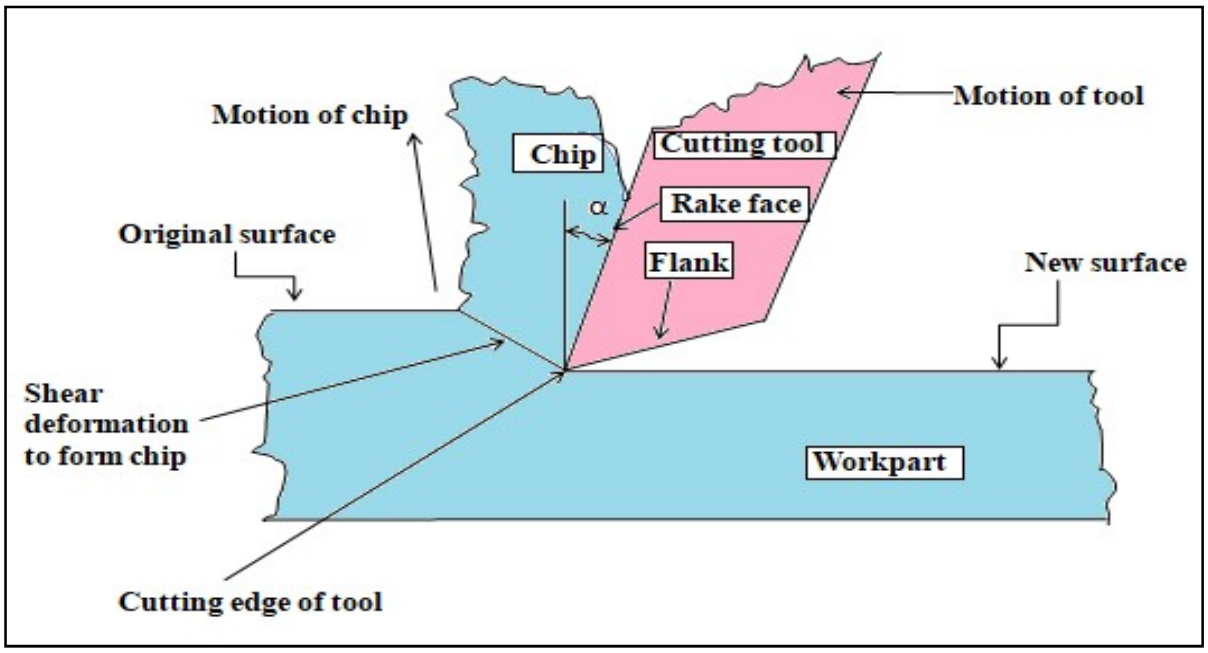

Fig.3: A Cross-Sectional View of the Machining Process

1.3 Tool wear

Cutting tools are subjected to a severe rubbing process, involving metal-to-metal contact and high stress at high temperatures. This situation is exacerbated by extreme stress and temperature gradients near the tool's surface. During cutting, the tools remove work material to achieve desired shape, dimension, and finish. However, wear occurs during the cutting action, leading to tool failure. When tool wear reaches a certain extent, a tool or edge change is necessary to maintain normal cutting action.

1.3.1 Tool wear methodology

Cutting tools experience complex wear appearance under high temperatures, pressure, and sliding velocity, characterized by basic wear types like crater wear, flank wear, thermal

cracks, brittle cracks, fatigue cracks, insert breakage, plastic deformation, and build-up edge, with dominant types varying with cutting conditions.

Crater Wear: Crater wear forms on the rake face in continuous cutting, particularly in turning operations. It conforms to the chip underside and reaches its maximum depth at high temperatures. High cutting speed often determines tool life, as severe catering weakens the tool edge and fractures it. Improvement in crater wear can be achieved by selecting suitable cutting parameters and using coated or ultra-hard material tools.

Flank Wear: Flank wear is a problem caused by friction between the newly machined work-piece surface and the tool flank face, resulting in poor surface finish, decreased tool dimension accuracy, increased cutting force, temperature and vibration. The width of flank wear land (VB) is typically used to measure wear, with a tool reshape criterion defining the threshold value.

Wear mechanism

Research on metal cutting wear mechanisms has revealed that tool wear is not a singular phenomenon but a combination of multiple mechanisms, indicating that a suitable method to slow down the wear process is needed.

Metal cutting tools experience various wear mechanisms, including abrasive, adhesive, delamination, solution, diffusion, oxidation, and electrochemical wear, with abrasive, adhesive, diffusion, and oxidation wear being crucial.

Abrasive wear: Abrasive wear, a mechanical wear primarily caused by impurities like carbon, nitride, and oxide compounds in work-piece material, and built-up fragments, is the primary cause of tool wear at low cutting speed.

Bowden and Tabor's friction and wear mechanism suggests that welded junctions form and are destroyed due to high pressure and temperature. This results in a chemically clean surface, as the chip flows on the rake face, enhancing the overall surface quality.

Diffusion wear: Wear is a process of atomic transfer at contacting asperities, with some workers suggesting it involves chemical action and diffusion. They have demonstrated welding and

preferred chemical attack of tungsten carbide in tungsten-titanium carbides, suggesting wear may depend on diffusion mechanisms.

Oxidation wear: High temperatures and air cause metals to oxidize, which can reduce tool wear by isolating the tool and work-piece. However, at high temperatures, soft oxide layers like $WO_3$and TiO_2 form rapidly and are taken away by the chip and work-piece, resulting in rapid tool material loss, known as oxidation wear.

1.3.2 Prediction of tool wear

Prediction of tool wear is a challenge due to the complexity of machining systems. Tool wear occurs due to contact and sliding between the cutting tool and work-piece, chip under extreme conditions, such as temperatures exceeding 530°C, and pressures exceeding 13.79 N/mm^2. Any element changing contact conditions in the cutting area affects tool wear. Influencing elements come from the entire machining system, including work-piece, tool interface, and machine tool which is shown in Figure4.

Work-piece: The work-piece material's physical properties, including mechanical and thermal properties, microstructure, and hardness, determine the cutting force and energy for the specific cutting conditions.

Tool: The optimal performance of a cutting tool depends on the right combination of tool parameters and cutting conditions, including the choice of tool material, coatings, and geometric design, for different operations like roughing, semi roughing, or finishing.

Interface: Coolants are used in 80% of industrial cutting applications to decrease cutting temperatures and reduce tool wear. New technologies, like minimum liquid lubrication, aim to reduce coolant costs, which account for 16% of total machining costs.

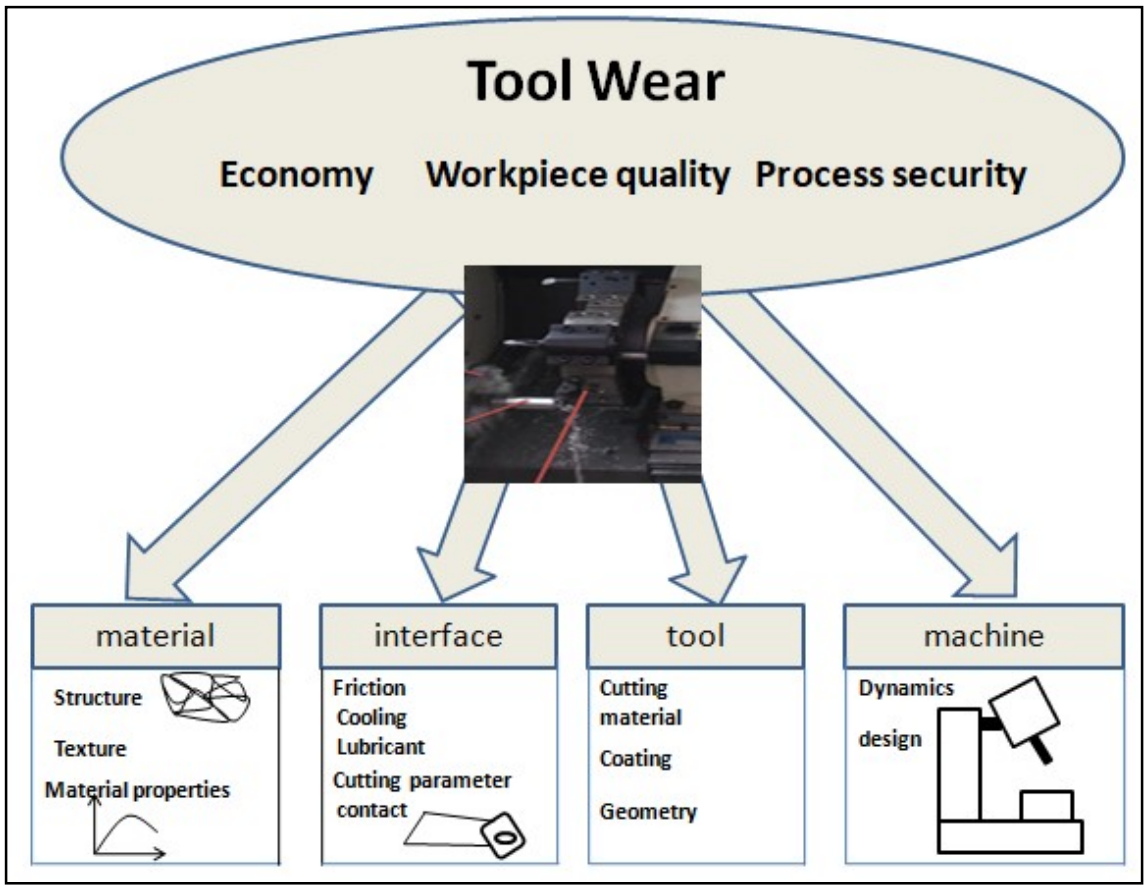

Fig.4: Elements affecting the tool wear

Dynamic: The dynamic characteristics of a machine tool, influenced by its structure and components, are crucial for successful cutting. Unstable processes with large vibrations can cause fluctuating overload, leading to premature edge failure due to tool chipping and excessive tool wear.

The study of tool wear monitoring in machining operations is a significant area of research, as it impacts tool change strategies, product quality, tooling costs, and productivity. Maximizing tool life and increasing tool change times can lead to reduced production costs and increased productivity.

1.4 Cutting Forces

Serope Kalpakjian [4] emphasizes the significance of understanding the forces and power involved in machining operations.

- The machine tool requires power requirements to install a motor of suitable capacity.
- Force data is crucial for designing machine tools for cutting operations, preventing excessive distortion and maintaining desired tolerances for the machined part.
- The work-piece's capacity to withstand cutting forces without excessive distortion must be determined in advance

Cutting force F_z is the component force acting on the tool's rake, normal to the cutting edge and tangential to the revolving work-piece. It represents resistance to rotation and is the highest force in normal operation, accounting for 98% of the total power required.

The feed force (F_f) is a force component that acts parallel to the work-piece's axis and represents the longitudinal feed of the tool. It is typically 50% as large as the cutting force and accounts for only about 1% of the total power required. The force acting in the radial direction from the work-piece's centerline is the smallest force, often 50% as large as the feed force, but its effect on power requirement is minimal due to negligible velocity in the radial direction.

Metal cutting force components are determined in metal cutting dynamometers by measuring deflections or strains in supporting elements. The dynamometer's design should provide large enough strains or displacements for accurate measurement.

Common tool dynamometers include

1.Mechanical dial gauge type,

2. Strain gauge dynamometer,

3.Pneumatic and hydraulic dynamometer,

4. Electrical dynamometers,

5. Piezoelectric dynamometers.

1.5 Cutting Temperature

Cutting temperature in machining is crucial as it impacts tool life, part quality, and chip morphology. Research is ongoing to measure cutting temperatures, as energy dissipated during metal cutting is converted into heat, generating high temperatures in the tool cutting edge region. These temperatures control tool wear rate and chip-tool friction.

When a material is deformed elastically, the energy is stored as strain energy, without generating heat. However, when deformed plastically, most energy is converted into heat. In metal cutting, the material undergoes high strains, with elastic deformation being a small proportion. Therefore, all energy is converted into heat, with heat generated in three distinct regions.

Elastic deformation stores energy as strain energy, while plastic deformation converts most energy into heat. In metal cutting, high strains occur, with elastic deformation being a small proportion. All energy is converted into heat, with heat generated in three distinct regions.

- The shear zone is the heat source where 80-85% of the energy needed to shear
- The chip-tool interface region generates 15-20% heat due to friction energy and plastic deformation, requiring energy to overcome friction. The chip is generated.
- The tool-work interface region generates only 1-3% of heat due to energy needed to overcome frictional rubbing between tool and work-piece flank faces.

The tool-chip interface temperature rises due to three zones, with the maximum temperature slightly away from the cutting edge. This temperature is crucial for tool face crater formation and tool failure due to softening and thermal stresses. Factors influencing tool temperature include cutting speed, feed, and material properties. These variables affect the size of shear zone, chip

tool contact length, and heat distribution. Shorter chip-tool contact length leads to severe temperature rise.

1.5.1 Factors affecting the cutting temperature

- Materials with higher thermal conductivity produce lower temperatures than tools with lower conductivity.
- Rake angle, a key tool geometry factor, significantly influences temperature, with a slight impact on temperature but a significant increase with an increase in approach angle.
- Cutting conditions, including cutting speed, feed rate, and depth of cut, significantly impact the generated cutting temperatures. Cutting speed significantly influences tool-chip interface temperature, controlling the total energy input to the metal cutting operation. Feed rate and depth of cut also influence cutting temperature [4].

1.6 Surface Roughness

Surface roughness measures the fine irregularities on a surface, determining its quality. It is crucial in applications involving friction, lubrication, and wear. Friction increases with average roughness and roughness parameters directly control surface functions like friction, wear, lubricant retention, and load carrying capacity. Roughness also improves fatigue strength, corrosion resistance, and creep life, essential for aerospace components. The effect of roughness on lubrication has been studied to determine its impact on sliding surfaces, compliant surfaces, and roller bearing fatigue.

Surface roughness, often referred to as uneven, irregular, or coarse texture, is a surface property that depends on the scale of measurement and statistical factors like sample size and sampling interval. It can be characterized in two principal planes: right angles to the surface in terms of wave amplitude and parallel to the surface in terms of surface wavelength. However, the technique used to measure roughness in these planes has limitations, as the smallest amplitude and wave length detected correspond to the instrument's vertical and horizontal resolution.

The roughness parameter was initially determined by the vertical distance between the highest peak and lowest valley roughness values. To obtain an average roughness parameter, an AC voltmeter was connected to measure the root mean square (RMS) average of the electrical signal in the U.S., as roughness has statistical implications.

Stylus method is a method used to determine surface roughness of machined surfaces. It involves using standard numerical parameters and surface profiles. Stylus instruments detect variations in height as a function of distance by running a probe across the surface. Early instruments used levers to magnify vertical displacement and recorded the profile on a smoked-glass plate. The next step was the introduction of a transducer, which converted vertical displacement into an electrical signal, which can be processed by an electronics instrument to calculate roughness parameters.

The type of transducer used significantly impacts instrument performance, with piezoelectric crystals being common in less expensive instruments. Other transducer mechanisms include moving coil transducers, capacitance transducers, and linear variable differential transformers. Errors in roughness measurements can be introduced by factors like stylus size, load, speed, and lateral deflection. Controlling variables like stylus tip radius, force, and cut-off length can provide accurate surface information.

The feed rate and cutting speed significantly impact surface finish. As the feed rate increases, the surface finish decreases, while the cutting speed increases. Therefore, choosing the right cutting process parameters for finishing is crucial.

1.7 EN-36C Alloy Steel

This is a nickel-chromium alloy case-hardening steel used in heavy-duty applications like steering worms and aircraft gears. Being carburized and hardened, it can reach core strengths of 850 to 1230 N/mm^2. The chromium content increases hardenability, while the nickel content makes the steel tough and shock-resistant. This type of steel is widely used in various industries.

EN-36C steel, also known as the 832M13grade, is harder when molybdenum is added, and its core strength is significantly improved after heat treatment. Its equivalent grade under the previous BS970:195standard is832M13.Alloy steel manufacturer services typically include

round bar production, with associated standards including UK standard EN-36, European grades 15NiCr13, and SAE/AISI3415.The chemical composition of EN-36C is given below in Table 1 and image is given in Figure5.

Table1: Composition of EN-36C alloy steel

Elements	Carbon, C	Manganese, Mn	Silicon, Si	Nickel, Ni	Molybdenum, Mo	Chromium, Cr	Sulfur, S	Phosphorous, P
Composition %	0.134	0.511	0.23	3.430	0.36	0.786	0.008	0.005

Fig.5: Image of EN-36C alloy steel

1.7.1 Uses of EN-36C Alloy Steel

Carburizing steel grade is suitable for roller and ball bearings, aeroplanes and motor crankshafts, connecting rods with case-hardened ends, highly stressed gudgeon pins, gears, and certain collets. It is used in heat exchangers, power plants, oil and gas industries, chemical industries, and oil and gas pipelines. Its applications include roller paths, connecting rods, highly stressed gudgeon pins, gears, and certain collet.

1.8 Heat Treatment

The heat treatment temperatures of EN-36C steel components, including heating, cooling, and soaking times, are influenced by various factors such as the shape and size of each component, the type of furnace, quenching medium, and work-piece transfer facilities.

1.8.1 Tempering

Steels can be heat treated to achieve high hardness and strength levels, as they are essential for structural components under high stress and tools like dies, knives, cutting devices, and forming devices, which require a hardened structure to resist wear and deformation.

Tempering is a heat treatment that reduces the brittleness of as-quenched hardened steels without significantly lowering their hardness and strength, and is mandatory for all hardened steels before use.

Tempering is the process of heating hardened steel to a temperature below eutectoid, maintaining it for a specified duration to reduce brittleness, followed by air cooling.

The primary objective of tempering is to reduce the brittleness of hardened steel.

After hardening, steel contains accicular martensite, which is brittle and cannot be used as such. Tempering is crucial to reduce its brittleness. During tempering, the martensite hardness may be slightly reduced.

Tempering is the heating of martensitic steel below the eutectoid temperature to make it softer and more ductile. It involves the precipitation of Fe_3C particles from the α' phase→ tempered martensite → spheroidite

Hardening is a process that introduces high internal stresses, resulting in the brittleness of steel.The accicular nature of martensite results in a triaxial stress state, causing brittleness.

Martensite, a meta stable phase, transitions to low carbon martensite and then to equilibrium phases like ferrite and cementite during tempering, reducing brittleness. The reduction of internal stresses in steel results in a decrease in its brittleness.

Austenitizing: It is the process of heating steels to a high temperature until they undergo partial austenite transformation.

Quenching: The process involves quashing using various media such as brine, fresh water, oil, and air.

Tempering: Tempering involves heating the material to 200-550°C, reducing its hardness and restoring its ductility, specifically martensite.

1.8.2 Stages of Tempering

The overlapping changes, which occur when high carbon martensite is tempered, are divided into four stages.

- First stages
- Second stages
- Third stages
- Fourth stages or Secondary hardening

First stage (50-200^{0}C)

In the first stage (50-200°C), a martensite breaks down into a low carbon martension and transition precipitate called ε-carbide (Fe2.4 C) across twins.

Second stage (205-305^{0}C)

The decomposition of retained austenite into bainite leads to a decrease in hardness.

Third stage (250-500^{0}C)

The aggregate of low carbon martensite and ε-carbide is converted into ferrite and cementite, which gradually coarsens to produce visible particles and rapidly softens.

.**Fourth stage (400-700^{0}C)**

Secondary hardening occurs in some steels during tempering, where hardness increases instead of decreasing due to the precipitation of alloy carbides. Steels with carbide-forming alloying

elements exhibit secondary hardening during the fourth stage of tempering. Secondary hardening is observed in steels containing tungsten (W), chromium(Cr), and vanadium(V) with high-speed steel exhibiting secondary hardening at 18% W, 4% Cr, and 1% V. High speed steels are utilized as tool steels due to their ability to retain their hardness for a longer period due to secondary hardening, unlike other steels that may soften during machining.

Secondary hardening occurs during the fourth stage of tempering, which is between 400-700°C.At 400-700°C, alloy steel undergoes carbide changes, with cementite forming first and the alloy diffusing to it. When enriched, Fe_3C transforms into alloy carbide. Transition carbides in chromium steel undergo multiple enrichments, with Fe_3C transitioning from $Cr_7C_3$to $Cr_{23}C_6$ and repeated until equilibrium carbide forms. Steels with multiple carbide-forming elements often have complex reactions, with decomposed carbides not necessarily being followed by carbides from the same alloy elements. Transformation can occur in situ through gradual atom exchange or by resolving existing iron carbides and nucleating coherent carbide with considerable hardening, counteracting the normal softening during tempering.

Secondary hardening, a process where the hardness of alloy steels remains constant upto 500°C, can either peak or gradually drop due to the breakdown of coherence and coalescence of carbide particles. Chromium, for instance, appears to stabilize the size of cementite particles within a temperature range of 200-500°C.Vanadium and molybdenum form a fine dispersion of coherent precipitates (V4C3Mo2C) in a hardened ferrite matrix, growing in grain boundaries and forming a Widmanstätten pattern during over-ageing.

1.9 Optimization Techniques:

The selection of process parameters for tool and work-piece combinations is crucial for effective machining. Optimization techniques like Taguchi Method, Genetic Algorithm, Artificial Neural Network, Fuzzy logic, simulated annealing, gradient search, and finite element method are available. In our research, we plan to use response surface methodology using design of experiment.

1.9.1 Taguchi Method

The Taguchi method, that simplifies the full factorial design process, involves a large number of experiments. To address this, Taguchi introduced the orthogonal array, which allows for a smaller number of experiments. The less function is used to measure performance characteristics that deviate from the target value, which is then converted into the signal-to-noise (S/N) ratio. The S/N ratio is analyzed using three categories: nominal-the-best, larger-the-better, and smaller-the-better.

1.9.2 Response Surface Methodology (RSM):

Response surface methodology (RSM) is a set of mathematical and statistical techniques used for empirical model building. It aims to optimize a response influenced by multiple independent variables through careful experiment design. Experiments consist of runs where changes in input variables are made to identify the reasons for changes in the output response. Methods like Box Benhenken design fall under RSM.

RSM, originally developed for experimental responses, later adapted to numerical experiments. The difference lies in the type of error generated. Physical experiments may cause inaccuracies due to measurement errors, while computer experiments may result in numerical noise due to incomplete convergence, round-off errors, or discrete representation of continuous physical phenomena. RSM assumes random errors.

RSM is being used in design optimization to decrease the cost of expensive analysis methods like finite element method or computational fluid dynamics (CFD) analysis and their associated numerical noise. The engineer optimizes Roman cement calcinations by determining

the optimal temperature and time levels to maximize early age strength (y), which is a function of these factors. The early age strength of the cement is determined by these factors.

$$y = f(x_1, x_2) + \varepsilon$$

The study uses the Central Composite Design (CCD) for experimental investigation, focusing on a response surface design. This design generates a second-order linear regression model, which is better predictive than a first-order linear model. The noise or error observed in the response is represented by ε.

1.9.3 Analysis of Variance

Analysis of variance (ANOVA) is a statistical model developed by statistician and biologist Ronald to analyze differences among group means. It partitions observed variance into components due to different sources of variation. ANOVA tests if the means of several groups are equal, generalizing the t-test to more than two groups. It is useful for comparing three or more means for statistical significance, similar to multiple two-sample t-tests but more conservative, suited to a wide range of practical problems. ANOVAs are more conservative and result in less type I error.

A genetic algorithm (GA) is a search technique used in computing to find true or approximate solutions for optimization and search problems. It is classified as global search heuristics and uses three main types of rules to create the next generation from the current population, making it suitable for a wide range of practical problems.

Selection: The process involves selecting individuals, known as parent, who will contribute to the next generation's population.

Crossover: Combine two parents to form children for the next generation.
Mutation: Apply random changes to individual parents to form children

CHAPTER 2

Literature Review

A comprehensive review of the literature has been discussed on machinability of EN-36C alloy steel with and without tempered on CNC turning. In this section, the effect of various process parameters such as feed rate, depth of cut, cutting speed on output responses like material removal rate, surface finish, residual stress, tool tip temperature are reviewed. Effect of tempering on mechanical properties and microstructural behaviour of hard metals is also reviewed.

Turning is a secondary manufacturing process that involves removing surplus material from work-piece to give the product the desired size, shape, and polish. Typically, turning operations are carried out using both CNC and manual center lathe machines. Preparing a finished product from hard metals with the necessary tight tolerances, surface quality, MRR, and dimensional precision is a significant problem. Numerous machining factors determine the productivity and quality of a machine tool. The cutting parameters, which have a significant impact on the product quality, define the cutting condition. In addition to tool vibration and signature, other tool variables are tool material. The characteristics of work materials include their hardness and softness. The surface roughness is directly impacted by these input process factors. However, it is quite challenging to manage every one of these factors simultaneously for high-quality goods.

The following are the fundamental research trend in the field of Machinability during the turning of hard metals, which can be readily identified.

2.1 Major area of enhancing machinability during turning of hard metals

Poor surface quality during machining, and that result in poor machinability, low productivity. Traditional machining processes are not much efficient to machine hard to cut materials. There are many methods that have been adopted in recent years to overcome these

problems, but the researchers are approaching the combination of conventional and non-conventional machining methods like the laser-assisted machining method and the reason is that laser-helped machining has significantly contributed in the manufacturing field as laser machining market has enhanced by 11% annually. This method has reduced the processing cost by 60–80%, cutting forces 30–50% and tool wear 20–30%. The soft computing methods also help in optimizing the machining process parameters along with the laser-assisted machining process. Artificial neural network (ANN), Genetic algorithm (GA), analysis of variance(ANOVA), Taguchi method, Response surface methodology (RSM) are some of the optimizing methods adopted during the machining process to get the optimum results.

2.1.1 Experimental research: There are various parameters which are affecting the machinability during the turning of hard metals. These affecting parameters are types of work-piece material, tool materials, shape and size of tool, types of machine tool used as well as affected by cutting velocity, depth of cut. In the present research the focus on machinability, reduction in residual stress and tool wear has been analyzed with treatment like tempering on samples of EN-36C alloy steel by optimization using response surface methodology.

2.1.2 Concept of tempering: There is a lot of research being done on tempering. The effect of repeated application of tempering on microstructure and the machinability of hard metal during the turning process has been studied and result has been found significantly improved in microstructure and machinability.

2.1.3 Analytical Research: Mathematical modelling, experimental design, and other variable parameters, optimization techniques are all included in analytical research.

2.2 Literature Review

Rao et al. [5] experimentally analyzed that during turning of metals on CNC lathe, three forces are developed on the cutting tool i.e. cutting force (F_z) as well as thrust force (F_y) and feed force (F_x). Further results reveal that Cutting force has a significant impact on everyone's power consumption. The control of the process that produces the required surface is greatly dependent on the surface finish of machined parts. Controlling friction when sliding is crucial for enhancing a product's appearance, texture, and fit between pieces. In addition to these, it influences heat

conduction, electric currents, paint and coating adhesion on the surface reflectivity. Thus, surface finish and precision have emerged as essential requirements in modern industry. There are numerous approaches and techniques for assessing surface roughness. Techniques can be traditional or nontraditional. When compared to conventional methods, unconventional methods are found faster and more accurate.

Abhang et al. [6] experimentally analyzed the optimization of surface roughness and tool wear during the CNC turning of EN-31steel with using tungsten carbide inserts. Response surface methodology (RSM) was used to conduct experiments at five distinct controllable factors, including speed, feed, depth of cut, tool nose radius and various solid-liquid lubricants. Further results reveal that depth of cut, feed rate and lubricant temperature are more significant parameters for optimizing the surface roughness and cutting forces.

Günay et al. [7] examined the cutting conditions for average surface roughness (R_a) in machining high alloy white cast iron (Ni-Hard) at two different hardness levels (50 HRC and 62 HRC). The study used a CNC lathe using ceramic and Cubic Boron Nitride cutting tools, with parameters such as feed rate, cutting speed, and depth of cut. The Taguchi L18 orthogonal array was used for experimental design and Signalto-Noise (S/N) ratio was calculated for R_a. ANOVA was used to evaluate the effects of cutting variables and tool materials on surface roughness. Further authors showed that feed rate and cutting speed had the most significant effect on R_a for Ni-Hard materials at 62 HRC and 50 HRC.

Zerti O et al. [8] focuses on selecting cutting tool material, geometry, and work tool material, and selecting process and performance parameters for optimization. It uses literature review and industrial surveys to study machining parameters and processes for turning operations on CNC using different grades of Tungsten Carbide tool and varying properties. Surface roughness testing is performed after machining. They compare the effect of cutting parameters on surface roughness of dissimilar geometry on AISI D3 steel using Taguchi analysis using statistical software. Further results reveal that feed rate and nose radius are main influencing factors for surface roughness while tangential force and specific cutting force are affected by depth of cut followed by cutting speed and feed rate.

Zhang et al. [9] introduced Taguchi robust design parameter for optimizing and modeling surface roughness in single-point turning of cold rolled alloy steel 42CrMo4/AISI 4140 using TiN-coated tungsten carbide inserts. Three cutting parameters were used in the experiment: cutting speed, depth of cut, and feed rate. The average surface roughness (R_a) was chosen as a measure of surface quality. The experiment was conducted using the standard L27 Taguchi orthogonal array. Further result showed that the surface roughness was significantly influenced by cutting speed, with feed rate having a smaller impact and depth of cut having the least significant influence. However, the influence of feed rate and depth of cut on surface quality was dissimilar in relation to cutting speed. Increased cutting speed resulted in better surface quality, while increased feed rate and depth of cut led to decreased surface quality.

Kaladhar et al. [10] used AISI 304 austenitic stainless steel and chemical vapour deposition (CVD) coated cemented carbide duratomic cutting insert for experiments. They used the Taguchi technique and ANOVA approach to determine optimal cutting parameters. L16 mixed array was used for data analysis. Furthermore, authors observed that cutting speed was found to be the most significant variable for surface roughness, followed by nose radius. The depth of cut and feed were the most significant for MRR.

Gosai et al. [11] have presented an experimental set up for finding the average temperature of CNMG4325 Grade TN2000 Coated carbide insert cutting tool while turning the EN-36 alloy steel on CNC lathe. An analogue K-type thermocouple sensor placed on the cutting tool allowed for the determination of the tool's average temperature. The cutting parameters were optimized using CCD-based RSM. Further, the results revealed that Optimized values of cutting parameters have minimum temperature with desirability of 98.9 %, which is highly acceptable

Reddy et al. [12] discussed the optimization of CNC turning parameters for EN-16 steel bar using the Grey Taguchi Method. The researchers used Taguchi's L-27 orthogonal array and investigated cutting variables like feed rate, cutting speed, and depth of cut, with responses like material removal rate and surface finish. They also calculated the Taguchi signal-to-noise ratio and created a grey relational grade. The optimum parameters were identified using response tables and graphs, and the significant contributions of controlling parameters were estimated

using ANOVA. Furthermore, authors concluded that lower surface roughness and higher material removal rate are indication of better performance.

Aggarwal et al. [13] revealed that various parameters, including depth of cut, feed rate, cutting speed, nose radius, and cutting environment, impact power consumption in CNC turning of AISI P-20 tool steel. The researchers used L27 orthogonal array and face centered central composite design, response surface methodology (RSM), and Taguchi's technique to conduct experiments. Further, result reveals that the cryogenic environment was found to be the most significant factor in minimizing power consumption, followed by depth of cut and cutting speed.
Işik, et al. [14] examined the turning operation on reinforced glass fiber plastics (GFRP) using a CNC turning machine with a CERMET cutting implement. Further, the results showed that surface roughness decreases with increasing cutting speed, implement radius, and cutting speed, while surface finish increases with rake angle and victual rate. However, an increase in cutting depth does not have a significant impact on surface roughness.

Shetty et al. [15] presented the optimization of machining parameters namely cutting speed and feed rate during the turning of different alloy steels such as EN-47, EN-19, EN-8, EN-24 andSAE8620 on CNC lathe with the use of carbide tip tool. The stylus type SJ-301 was used to measure the surface roughness for each sample. Further, it has been found that the surface roughness was greatly influenced by feed rate and followed by speed.

Abhang et al. [16] presented an experiment set up for measuring temperature between tool and chip during turning of EN-31 alloy steel on CNC lathe machine using tungsten carbide insert. Tool-work thermocouple methods were applied. The response surface methodology is employed in the analysis of the findings. The cutting process parameters used were cutting speed, feed rate, nose radius, and depth of cut. The temperature interface between the tool and the chip grew as the depth of cut, feed rate, and cutting speed increased, but reduced as the nose radius increased. Work material EN-31, tool material tungsten carbide, and two copper plates that clamp the work and tool material were used to prepare the thermocouple junction. A typical thermocouple is an Alumel-chromel. Furthermore, the author’s observed that nose radius was not the most

influential parameter for the tool-chip contact, but rather cutting speed, feed rate, and depth of cut

Routara et al. [17] have experimentally analyzed to optimize the cutting parameters during the CNC turning of EN-8 alloy steel for minimization of surface roughness. Further, the result indicates that surface roughness is found minimum at maximum depth of cut and speed, and maximum at maximum feed rate.

Aslan et al. [18] used L27 Orthogonal array for experimental design planning. ANOVA has been used to evaluate cutting parameters' impact on surface roughness and flank wear, and the S/N ratio of Taguchi method to optimize cutting parameters. Multiple regression analysis predicted surface roughness (R_a) and void (VB) as functions of cutting speed (v), feed (f), and cut depth (d). Further, the results showed that VB value decreases with feed, while surface roughness R_a decreases with higher cutting speed but worsens with feed.

Sahooet al. [19] examined the performance of a TiN/TiCN/Al2O3/TiN multilayer CVD coated carbide insert in hard turning AISI 4340 steel. It used RSM and grey-based-Taguchi methods for mathematical modeling and parametric optimization of tool flank wear and surface roughness. The results showed the economic viability of the coated carbide tool in hard turning, with cost estimation based on total machining cost per part. RSM and Taguchi methods were used for optimizing surface roughness and tool wear. Furthermore, the results revealed that the cutting speed is most significant factor for flank wear while feed rate is for surface roughness.

Suresh et al. [20] conducted hard turning experiments on AISI-4140 steel with TiN coated Al2O3 + TiCN mixed ceramic insert using full factorial design. The study revealed that feed, cutting speed, and depth of cut significantly affect surface roughness, with cutting speed having the most significant impact on flank wear.

Das et al. [21] used ANOVA and RSM to analyze the impact of machining parameters on surface roughness and flank wear in hard turning of AISI H11 (X38CrMoV5-1) steel with a CBN tool. Furthermore, the authors observed that machining time, cutting speed, and feed were the most significant factors controlling flank wear, while feed was crucial for surface roughness.

Aouici et al. [22] experimentally analyzed that a study comparing conventional and wiper ceramic inserts found that wiper geometry provides better surface finish and reduces tool wear. The study was conducted on hot work tool steel AISI H11.Further, results revealed that the tool wear is sensitive to cutting speed and feed, while feed has a predominant effect on surface roughness.

Gaitonde et al. [23] examined the comparison of conventional and wiper ceramic inserts in hard turning through artificial neural network modeling. Further, the results showed that surface roughness is significantly influenced by feed and nose radius, with feed inflating causing maximum roughness and subsiding with increased nose radius, and tool wear becoming predominant with increasing cutting speed.

Horng et al. [24] showed that surface roughness significantly changes with machining parameters like feed, work-piece hardness, and cutting speed, while flank wear is realized with cutting speed and feed, particularly during finish turning of hardened AISI H11 steel with CBN tools.

Hafiz et al. [25] experimentally investigated the Prediction of tool life in end milling of hardened steel AISI D2.They developed a tool life first and second order model in end milling of hardened steel AISI D2 using PVD TiAIN coated carbide cutting tool using RSM. Furthermore, they observed that both models are valid in predicting the tool life of the part machined under specified condition and the prediction of average error is less than 10%.

Slavko et al. [26] investigated that high speed cutting of hardened steel significantly increases the temperature at the contact zone, exceeding the allowed thermal stability of the cutting material. This leads to a drastic reduction in tool life. As feed rate and deformation speed increase, forces, heat generation, and contact zone temperature rise. Furthermore, the results revealed that the tool's flank wear to shift into crater wear due to the higher influence of the diffusion process. The larger cross-section of the chip also increases cutting forces, leading to

chipping of the cutting tool edges. The increased speed and feed rate also contribute to the shift of tool wear into crater wear due to the diffusion process.

Grezik et al. [27] studied simulation models to obtain finite element solutions for cutting forces, cutting energy, and temperature distribution in the turning process with different coated tools. They used tools coated on ISO P20 carbide substrates and AISI 1045 work-piece material. They used third wave advantage and DEFORM 2D software to predict heat intensity, temperature distribution, chip thickness, and cutting forces. Furthermore, they observed that the experimentation and simulation results predicted average steady state temperatures at the tool-chip interface within a 10% difference.

Yigit et al. [28] conducted an experimental study on the impact of cutting speed on turning nodular cast iron using coated and uncoated cutting tools. Furthermore, they found that the wear behavior of multilayered and uncoated tools was similar at cutting speeds of 125-200m/min. The best surface quality was achieved with multilayered coated carbide tools at all speeds, and the force components generated by coated tools were less than uncoated ones.

Aslantas et al. [29] studied the continuous turning of hardened AISI 52100 using coated and uncoated ceramics like Al_2O_3-TiN mixed inserts. They evaluated tool wear, tool life, surface finish, and machinability of hardened steel. Further, the study revealed that TiN coating and crater wear affect chip flow direction, with uncoated ceramic tools causing a decrease in chip up-curl radius. TiN coating ensures tougher cutting tools and maintains surface quality during cutting processes.

Kamdar et al. [30] examined the impact of cutting conditions on EN-36 steel heated with gas flame. They analyzed cutting force, feed force, and surface roughness at various temperatures and depths. Optimum results were achieved using a design of experiments with Taguchi method. Furthermore, the results revealed that varying parameters affected different responses differently, and ANOVA analysis was used to determine the optimum cutting parameters.

Singh et al. [31] used L18 orthogonal array based Taguchi optimization technique to optimize the effect of cutting parameters on surface roughness and material removal rate (MRR) of EN-36 work material in turning operation. The study uses the orthogonal array, signal to noise ratio, and analysis of variance to study performance characteristics in both dry and wet machining

conditions of cylindrical work-pieces using Tin coated tungsten carbide cutting tool on CNC lathe. Five machining parameters, including spindle speed, feed rate, depth of cut, nose radius and cutting environment are optimized considering surface roughness. Further, the results revealed that the optimal cutting parameter, minimum surface roughness (Ra), and maximum material removal rate are obtained, which can be used to increase machine utilization at low production costs in manufacturing environments. The study validates the effectiveness of the Taguchi method through material removal rate and characteristics of a turning product.

Salvi et al. [32] conducted an experiment to determine the optimal cutting conditions for the lowest surface roughness in turning 20MnCr5 casehardening steel of hardness 46 HRC. They used a ceramic-based insert in finish turning. Taguchi L9 orthogonal array was utilized in the experimental design, and variance analysis was employed to determine the significance of cutting parameters. The average surface roughness of 0.91μm was observed at cutting parameters of feed 0.15 mm/rev, cutting speed 232.5 m/min, and depth of cut 0.4 mm. Furthermore, the results revealed that ceramic-based inserts, with lower surface roughness, can be a more efficient alternative to polycrystalline cubic boron nitride (PCBN) inserts for finishing turning.

Suresh et al. [33] conducted a study on the impact of cutting parameters on hard turning of AISI H13 steel at 55 HRC with a Physical vapour deposit (PVD) coated TiCN ceramic tool under dry conditions. They used the Response surface methodology model and ANOVA to identify the most significant parameters. Furthermore, they concluded that abrasion is the primary wear mechanism observed at higher cutting speeds, with feed rate being the most influential parameter. The Response surface methodology model, with a 95% confidence value, measures tool wear and surface roughness. Cutting speed had the most significant effect at 47.4% on tool wear rate, followed by feed rate at 28.15% and depth of cut at 15.8%. Increased cutting speed leads to increased temperature at the contact zone, causing high tool wear. Feed rate was the most influencing factor on surface roughness. Surface finish increased with speed but decreased with feed rate.

Sahoo et al. [34] studied the performance of a multilayer carbide insert in machining AISI D2 steel at 53 HRC using Taguchi L27 orthogonal array. They analyzed S/N ratio and optimum parametric conditions. Further, results showed that a regression model reveals feed as the most influential parameter for surface roughness, followed by cutting speed. High cutting speeds result

in low roughness due to decreased chip-tool contact length, while depth of cut has minimal impact.

Zahia et al. [35] used response surface methodology (RSM) to determine the optimal cutting conditions for AISI 4140 hardened alloy steel at 56 HRC. Taguchi L27 orthogonal array was utilized in experiments and a regression model was developed for surface roughness. Furthermore, they observed that work material hardness enhances machining force, while feed rate and depth of cut significantly impact on surface roughness and cutting parameters. Feed rate was the main contributor at 77.92%, followed by cutting speed at 15.47%. The optimal cutting parameters for turning AISI 4140 steel were cutting speed of 180 m/min, feed rate of 0.08 mm/rev, depth of cut 0.15 mm, for surface roughness of 0.23 micron.

Lawrence et al. [36] studied the impact of machining parameters on surface roughness and material removal rate in hard turning of EN-36 steel. They used Taguchi L9 orthogonal array and Grey relational analysis to design experiments. Further, results revealed that feed rate was found to be the most influential factor, followed by cutting speed. The optimal machining parameters were found to be 650 rpm, 0.2 mm/rev, and 0.4 mm depth of cut.

Rashid et al. [37] investigated the influence of machining conditions and parameters on the surface roughness of AISI 4340 steel at 69 HRC. The experiment was designed using a Taguchi L16 orthogonal array and a multiple regression model. The study revealed that cubic boron nitride-based cutting tools can achieve desirable surface finishes without additional tools for work-pieces as hard as 69 HRC. The cutting parameters were optimized to be feed rate of 0.02 mm/rev, cutting speed of 250 m/min, and depth of cut of 0.3 mm. Furthermore, the result revealed that a very low feed rate is the most significant (99.16%) factor in affecting surface roughness.

Aouici et al. [38] compared surface roughness between ceramics and Cubic boron nitride (CBN) inserts in hard turning of AISI H11 hot work steel at 50 HRC. They utilized Taguchi L18 orthogonal arrays and Response surface methodology-based mathematical models to examine the impact of cutting speed, feed rate, and cut depth on the work-piece's surface roughness. They utilized three ceramic inserts: reinforced ceramic insert (CC670), mixed ceramic insert (CC650), and Cubic boron nitride insert (CBN7020). Furthermore, they concluded that feed rate

significantly influenced hard turning with ceramic inserts, and surface roughness increased with cutting speed. CBN inserts showed better performance compared to ceramic inserts. The average value of surface roughness was observed as 0.180μm and 0.300 μm on surface machined by a CBN and ceramic insert respectively.

Lister et al. [39] showed that temperature at the chip-tool interface is crucial for analyzing and controlling machining processes due to high shear and friction energies. Primary and secondary shear zones affect tool wear and mechanical properties. Heat generation occurs at three zones: primary shear zone, chip tool interface, and tool work-piece interface. Total tool wear rate and crater wear on the rake face are strongly influenced by temperature. Experimental methods have been developed to measure tool temperature at the interface. Research on cutting operations temperatures has focused on tool-chip thermocouple, embedded thermocouple, and thermal radiation methods. Further, these methods evaluate cutting temperatures based on the thermocouple principle, highlighting the validity of assumptions and potential errors in experimental techniques.

Shaw [40] experimentally analyzed that the tool-work thermocouple is a popular tool for measuring temperature during metal cutting, indicating the impact of cutting speed, feed rate, depth of cut, and tool parameters on the temperature. The chip-tool interface forms the hot junction, while the tool end forms the cold junction. Electrical insulation is required between the tool and work-piece. This technique is easy to apply and measures the chip-tool interface temperature over the entire contact area. The thermocouple method is used to measure the average emf at the tool work-piece interface. However, this method requires accurate calibration of the tool and work piece materials. Two methods can be used to fix the hot junction close to the cutting edge: clamping the thermocouple in a recess ground off the tool's rake face, or inserting the thermocouple in a grooved carbide chip breaker. Both methods yield the same results, but the second method is considered better due to the change in temperature distribution along the rake face and its ease of implementation. He uses the tool-work thermo couple technique to measure the chip-tool interface temperature during machining of EN-31 steel alloy. The comparison has been made on the obtained results. It was suggested that the second method is better due to the recess in the cutting tool and its ease of implementation.

Honeycombe [41] studied that Cutting tools are made of high-speed steels, which are advanced materials on iron-base matrix. These steels are complex alloys of carbon, tungsten, molybdenum, vanadium, chromium, and cobalt. Their typical as-quenched microstructure consists of twinned plate martensite, retained austenite, and undissolved carbides. To modify their mechanical properties, they must be thermal tempering resistant, as tool points can be heated up to 650°C during cutting. Further study reveals that martensite is a very strong phase but since it is normally very brittle, it is necessary to modify its mechanical properties by tempering in a temperature range of 150-700°C.

Dobrzański et al. [42] studied the heating as-quenched martensite tempers unalloyed, medium, and high carbon steels through three stages: precipitation of carbide, transformation of retained austenite into lower bainite, and precipitation of cementite. In steels with alloying elements contributing to secondary hardening, a fourth stage occurs: precipitation of MC and M2C-type alloy carbides.

Taylor et al. [43] studied the transformation of supersaturated martensite into metastable carbide (Fe2.4C) occurs at 100-200°C, enhancing steel strengthening. This transformation occurs during tempering at 200-320°C, forming a non-homogeneous mixture of supersaturated ferrite and cementite, or lower bainite. Further the study indicate that cementite is formed during tempering at 200-420°C, decarbonizing the matrix and dissolving metastable carbides, allowing for steel matrix recovery. This process is believed to enhance steel strength.

Gianfrancesco et al. [44] stated that the nucleation mechanism of cementite is not fully understood, but it can nucleate independently on carbide particles. It mainly nucleates on grain boundaries of the former austenite or subgrain boundaries of the newly formed cell structure. Above 400°C, the diffusion of alloying elements occurs, and cementite dissolves, allowing the nucleation of MC and M2C carbides coherent with the alloy matrix. This leads to an increase in the hardness of tempered steel, known as secondary hardening. The microstructure of correctly heat-treated high-speed steel should consist of a hard and homogeneous matrix with a high volume fraction of fine and uniformly distributed carbides. The research aimed to evaluate the influence of phase transformation kinetics during tempering on the properties of high-speed steels.

Wang et al. [45] developed an empirical model to predict surface roughness in turning operations using various parameters like work-piece hardness, feed rate, cutting tool point angle, depth of cut, spindle speed, and cutting time. The study employed data processing techniques and non-linear regression analysis, incorporating logarithmic data transformation. Furthermore, the authors observed that smaller error were produced during cutting experiments by existing model as compared to some other models.

Suresh et al. [46] developed a surface roughness prediction model using response surface methodology (RSM) and genetic algorithms (GA) for machining mild steel and TiN-coated tungsten carbide cutting tools. Furthermore, the results reveal that the GA program provided optimal machining conditions and minimum and maximum surface roughness values.

Neşeli et al. [47] used response surface methodology (RSM) to optimize tool geometry parameters on surface roughness during hard turning of AISI 1040 with P25 tool. Their experimental contribution focuses on predicting and optimizing surface roughness and cutting force components during hard turning of AISI H11 steel with a cubic boron nitride (CBN 7020) cutting tool, using an ANOVA study that considers cutting parameters and work-piece hardness. Furthermore, the results revealed that the tool nose radius was the dominant factors for the surface roughness.

Attanasio et al. [48] explained that the machining of heat-treated hardened steel components with a hardness of 50±1 HRC has gained popularity as a cost-benefit and malleable machining process for metal components containing ferrous elements. Superior cutting tool materials and distinctive coating technology have made turning hard to cut materials easier, producing cutting inserts with superior hardness value, resistance to wear, and chemical balance. Further results showed that machining in a dry environment is suitable for hard turning operations, as maximum heat is generated, making machining easier. However, controlling heat produced at the insert and work material interaction zone is crucial to minimize wear and protect the work- piece surface from residual stress. Divergent lubricating techniques have been introduced to reduce overall machining costs and create an environment-friendly machining condition. Minimum quantity lubrication (MQL) is one of these techniques, with researchers investigating its impact on hard machining. Studies have shown that reducing the use of cutting fluid in machining provides worker safety, environmental, and cost-effective benefits. Applying minimum quality lubrication

to the tool surface enhances tool life. Standard lubricants in turning have better results than traditional fluids, improving overall process achievement by reducing machining forces and wears at the tool surface and providing better surface finish.

Dhar et al. [49] conducted an experiment on the mechanical output of dry lubrication and minimum quantity lubrication (MQL) for turning 1040 grade steel. They measured machining forces, tool wears, chip reduction efficiency, machining temperature, surface roughness, and dimension deviation, finding near dry lubrication improved these factors. Further, the results revealed that the use of dry lubrication causes reduced in tool wear, cutting temperature, cutting forces, surface roughness and dimensional deviation.

Dhar et al. [50] conducted a study on the impact of minimum quantity lubrication (MQL) on the temperature of the cutting zone, product quality, and chip formation in turning 1040 grade steel using an uncoated carbide tool. Furthermore, they found improved in cutting performance, decreased cutting temperature, and improved chip tool interaction.

Autretet al. [51] studied the mechanical performance of minimum quantity lubrication (MQL) for turning hardened bearing grade steel materials using a completely dry lubrication method. Further, they found that MQL decreased surface roughness, temperature, tool flank wear, and had minimal impact on machining forces.

Khan et al. [52] studied the impact of minimum quantity lubrication (MQL) on the finish hard turning of low alloy, comparing dry and wet cutting with vegetable oil-based cutting lubricant. Further, they found a 10% reduction in average chip-tool interface temperature, brighter as well as smoother chips, reduced tool wear and improved surface finish.

Vyas et al. [53] discussed the formation of saw tooth chips in metal cutting, which result from high-speed and feed milling of hard and brittle materials due to thermal origin and cyclic cracking in the original surface, involving both gross and micro cracks. Further, the results revealed that the main cause for saw-tooth chip formation is cyclic cracking.

Jena et al. [54] explained that the heat treatment is a common method for developing desired properties in steels, with martensite being the strongest microstructure. However, due to internal stresses, it is rarely used in untempered condition. Tempering increases ductility and toughness

in steels, which are crucial for impact energy absorption. Temperature and time play vital roles in determining steel's mechanical properties, and much research has been conducted to understand the effect of tempering temperature on steel's properties.

Yang et al. [55] have found that high-carbon stainless steels typically have an as-quenched structure consisting of twinned plate martensite and retained austenite. Treatment conditions can alter these distributions, and residual austenite transformation tempering occurs through heterogeneous nucleation and growth processes at grain boundaries, causing stacking faults and defects. Research on retained austenite and lath martensite in low-carbon alloy steels has been extensive, but little has been done on the mixture of twinned plate martensite and retained austenite in high-carbon alloy steels. This study compares microstructural variation with tempering temperature in an ultra-high strength metal alloy with high carbon content, focusing on the effect of tempering temperature on experimental extra-high carbon steels. The study examines the typical microstructure of two structures tempered at 650°C for 2 hours and 250°C for 5 hours. Furthermore, the results revealed that the complete transformation of retained austenite can be easily achieved by multiple tempering cycles rather than single long-time cycle.

Bhat, T. B. [56] have studied Armour on combat vehicles is increasingly being developed to provide greater ballistic protection without increasing weight. Ultra high strength (UHS) steels are the most widely used metallic armour due to their high strength, hardness, toughness, weldability, and ease of heat treatment. Quenching and tempering are well-established methods for strengthening UHS steels while retaining or increasing impact toughness. Martensite, the highest strength structure, is rarely used in untempered conditions due to large internal stresses associated with the martensitic transformation. Furthermore, they observed that tempering increases ductility and toughness, which are essential for impact energy absorption. Tempered martensite lath structure also provides the best dynamic strength in steel.

Ulutan et al. [57] found that nickel and titanium alloys are widely used in the aerospace industry due to their superior mechanical strength, chemical resistance, and thermal conductivity compared to steels. However, these alloys are challenging to machine due to their excellent properties, potentially affecting the final surface integrity of a machined component. Furthermore, it has been observed that over the past decade, numerous research studies have focused on work-piece surface integrity and functional performance.

Zhuanget al. [58] developed a finite element method-based analytical model to predict residual stress relaxation under cyclic mechanical loads. Further, they analyzed stress relaxation from shot peening, laser shock peening, and low plasticity burnishing, revealing that it depends on initial residual stress state, cold work amount, cyclic load amplitude, mean value, cycle number, and material strain-stress behavior.

Hoffmeister et al. [59] conducted a study on residual stress relaxation of shot peened Inconel 718 specimens after isothermal static and cyclic loading. Further, the authors found that compressive residual stresses relaxed under static loading until tensile residual stresses were built, and during cyclic loading, residual stresses relaxed almost completely in the first cycle. The study aimed to analyze the stability of residual stresses generated by machining in Inconel 718 under mechanical static loading at room temperature. An Inconel 718 disc was face turned and specimens were loaded at different stress levels. Initial and final residual stresses were measured using X-ray diffraction. A finite element model was fitted to the experimental results, and the study was extended for more loading conditions.

Cullity, B. D [60] studied the aerospace, automotive, and power industries are continuously seeking ways to enhance fatigue life through surface-treatment processes like laser peening or shot peening. These processes introduce near-surface compressive residual stresses, which can delay crack nucleation and propagation. As a result, residual stresses are increasingly accounted for in fatigue life prediction models. To accurately assess these stresses, various characterization techniques have been developed, including hole-drilling, X-ray diffraction (XRD), and ultrasonics. X-ray diffraction is widely used in industries and laboratories for residual stresses measurement, as it measures crystallographic lattice deformation. A change in lattice spacing induces a shift in the diffracted X-ray angle, according to Bragg conditions.

Noyan et al. [61] used the traditional $\sin^2 \psi$ method for stress calculation, with a diffractometer using Line Sensitive Scintillation Detectors (PSSD) to capture scattered X-rays in stress-free isotropic polycrystalline material. X-rays are diffracted in all directions by grains, forming a cone. In stress-free isotropic polycrystalline material, X-rays are diffracted in all directions by grains, creating a cone. Line detectors capture a limited part of scattered X-rays, corresponding to two diffraction cone radii. For strain measurements in plane-stress state, a minimum of two sample orientations is required.

Prevey, P. S [62] developed cos α method in Japan in 1978, is a stress calculation method that captures the diffraction cone of a single incident X-ray beam via a 2D detector. The method is enhanced with the introduction of new 2D photosensitive detectors like image plate (IP) and advanced calculation algorithms. Further, they observed that the portable apparatus with IP enables quick residual stress measurements using the cos α method. The two XRD methods presented measure the elastic strain for a specific diffraction peak corresponding to specific atom planes in the crystal structure. The material's chosen peak is subjected to X-ray residual stress measurement, necessitating determination of X-ray elastic constants (XEC).

Noyan et al. [63] performed residual stress measurements using XRD techniques in 1925, with significant improvements in 1970s and 1980s. Today, numerous RS measurement techniques based on XRD are widely used in industry and academia. Single exposure technique (SET) was commonly used in 1950s but had limited accuracy and was not effective on materials with near random grain orientation distribution. Single exposure technique (SET) relied on precise knowledge of unstressed lattice spacing, which was challenging to experimentally determine. This made it difficult to assess the quality of data due to non-linear relationships. Further, they concluded that to address these limitations, Multiple exposure technique (MET) was developed, which uses more data points and provides high-confidence RS measurement results without relying on unstressed lattice spacing.

Pineault et al. [64] assessed various XRD techniques for measuring RS, including Cosα and Multiple exposure technique (MET), which are applicable in Psi, Omega, or Modified Psi modes, with the generalized technique applicable in either mode. The technique is applicable to MET when used in either Omega or Psi mode. XRD employs d-spacing as a strain gage and is exclusively applicable to crystalline, polycrystalline, and semi-crystalline materials. Furthermore, the results revealed that the d-spacing of a material increases when it is in tension, while it decreases when it is compressed. The presence of RS in the material results in a shift in the XRD peak angular position, which is directly measured by the detector.

Wojciechowski et al. [65] have experimentally developed the models to describe force and wear-time relationships during the turning process. The study found that the ratio between force components is a reliable indicator for the wear process compared to absolute force values.

Zębala et al. [66] experimentally analyzed the interaction between cutting forces and tool wear during machining of sintered nickel-cobalt alloy with CBN tools. Additional findings showed that tool wear was seen when the sintered nickel-cobalt alloy was turned longitudinally. On the worn side of the rake side, there are visible cracks and material that looks like chipping.

Tu et al. [67] have investigated the crater wear of ceramic inserts due to the effect of tool tip temperature during machining of Inconel 718. Furthermore, they deduced from the data that while cutting speed has a smaller interaction influence, the hardness of the work-piece is a major factor in temperature generation at the tool tips and wear. Additionally, they discovered that whereas cutting speed and material hardness both have a major impact on crater wear, contact condition and cutting speed are the primary causes of flank wear.

Poulachon et al. [68] investigated the formation of white layer due to the successive tool flank wear in turning of hard metal with cubic boron nitride tools and to correlate this with surface integrity of machined surface. Furthermore, compared to coarse microstructure materials, fine microstructure materials have a higher rate of white layer generation, according to the study.

Lescano et al. [69] analyzed the influence of hardening and tempering process on the mechanical and microstructural behavior of commercial IRAM-IAS15B41 boron steel. Additional they came to the conclusion that in the microstructure of the material under investigation, low tempering circumstances result in extremely small carbides whereas high tempering conditions result in bigger carbides.

Jian et al. [70] studied in an experimental setting how heat treatment procedures affected the die steel H13MOD's microstructure and mechanical characteristics in comparison to H13 steel. Furthermore, at the same tempering temperature, the findings showed that H13MOD had greater impact toughness and ductility than H13. Furthermore, at the tempering temperature below -540 ^{0}C, H13 showed greater hardness and tensile strength than H13MOD steel.

Stoicanescu et al. [71] experimentally analyzed the effect of heat treatment on high speed steel which consists of 1.3343residual austenite. They also came to the conclusion that as the number of tempering procedures increases, the remaining austenite concentration decreases.

Deng et al. [72] presented the numerical investigation on the structural evolution and hardness distribution of steels after application of combined effect of tempering and quenching.

Additionally, simulation findings showed that residual stresses created by the quenching process may be eliminated by the tempering process.

Sasaki et al. [73] have designed and manufactured a new X-ray stress analyzer of portable type for measuring the residual stresses in rails. The residual stress is measured using the Cosα technique.

Sasaki et al. [74] have evaluated the tri-axial residual stress with the help of Debye-Scherrer ring formed on two-dimensional imaging plate on X-ray stress analyzer. Additionally, it was contrasted with the tri-axial stress generated by Dolle and Hauk's traditional approach.

Savaria et al. [75] have experimentally investigated the effect of microstructure, hardness and residual stress on the bending fatigue strength of induction hardened aeronautical gears. Further, the results revealed that residual stresses can have a significant impact on bending fatigue.

Arrazola et al. [76] presented the comparative results of residual stress of turned specimen of IN718 nickel-based alloy using two different techniques; 3-D finite element (FE) based simulation and using diffraction method. Furthermore, they observed that the stress predictions have significant variations with respect to the FE simulation model, these variations can be captured, and the resultant surface integrity can be better represented in an interval.

Hua et al. [77] have focuses on the magnitude and direction of principle residual stress and their effect on fatigue strength of turned Inconel 718. The outcome demonstrates that principle residual stress has a substantially larger magnitude than surface residual stress.

Reddy et al. [78] conducted an experimental study on cutting tools and cutting conditions using the Taguchi method. They used four TiAlN-coated carbide end milling cutters and developed a mathematical model to simulate surface roughness in machining parameters. The model was then optimized using genetic algorithms, ensuring accurate and efficient cutting.

Jain et al. [79] analyzed the impact of surface roughness machining parameters on AISI 1045. A mathematical surface roughness prediction model (RSMT) was developed using surface response

methodology. Furthermore, they observed the model assessed the effect of drilling parameters on surface roughness, and optimum machining conditions were determined using RSM and a genetic algorithm. The model accurately predicted surface roughness, indicating its effectiveness.

Jain et al. [80] focused on optimizing performance composites like real energy, metal removal rate, and superficial ruggedness by grinding Al-SiC35P. It uses a non-dominated genetic sorting algorithm (NSGA-II) and Al-SiC specimens with 8 volumes. Process variables include silicon carbide particle percentage, feed, and cutting depth. A predictive prediction model (RSM) is developed using surface response methodology. An improved NSGA-II algorithm is used to optimize the model. The results are comparable to consensus, indicating the model can be effectively used for predictive purposes. The study identifies the optimal values for three parameters.

Hou et al. [81] introduced a technique for minimizing surface roughness using nonlinear regression and KPCA hybridization. It uses GAs to approximate optimal three-dimensional values, aiming to minimize surface roughness calculations. The method uses KPCA-based regression to prevent multi-collinearity in the predictive model. Furthermore, the results revealed that the proposed approach offers a more precise model than linear regression, reducing surface roughness by 45.3%, and 54.2%, respectively, according to experimental results and RSM.

Kilickap et al. [82] conducted experiments on the AL6063 high-speed end mill cutter using a central rotatable composite design. They determined temperature increases using a K-type thermocouple and used a genetic algorithm to optimize machining process parameters, ensuring minimum temperature rise and analyzing the direct effects of temperature increase.

Pai et al. [83] studied the impact of three input variables on the micro-wire electric discharge machine (MDS), kerf width, and rugged surfaces in titanium alloy. They conducted experiments and used ANOVA to evaluate the effects. The model developed uses a genetic algorithm to determine the optimal machining conditions. The study demonstrated optimal machining efficiency in removal rate, bracket width, and surface ruggedness under optimal conditions.

Wibowo et al. [84] developed the models, including the core composite structure and box-Behnken design, to study surface roughness and stiffness reactions in cross-sectional cylindrical

grinding of stainless steel products. The central composite design showed better efficiency and better response to porosity than the Box-Behnken design. The critical deviation values for surface roughness, durability, and porosity in central composite designs were 5.95, 1.29, and 63.94, respectively. The associated Box-Behnken design values were equivalent to 14.19, 3, and 4.94. The study also focused on optimizing the hardness of the die-cast part and achieving taste and surface ruggedness. The study investigated the impact of machining parameters on friction and surface roughness in the cross-sectional cylindrical grinding process through experiments and analyzes the results. The Response Surface Method (RSM) was utilized for mathematical simulation to establish connections between various output response processes. Contour and surface plots were utilized to illustrate controller performance changes with machining parameter variations, while a multi-objective genetic algorithm (MOGA) was employed to simultaneously enhance vibration and surface roughness. RSM cum MOGA is a valuable tool for assessing and optimizing development processes where multiple input parameters impact a critical output response.

Davis, J. R [85] studied that the stainless steel materials have gained significant popularity in engineering due to their corrosion resistance, strength range, formability, and aesthetic appeal. Duplex stainless steel (DSS) is a blend of ferritic and austenitic stainless steel, enhancing stress-corrosion cracking resistance, toughness, and ductility compared to ferritic stainless steel (FSS), despite its challenges like low thermal conductivity and high deformation hardening.

Snis et al. [86] studied that Duplex stainless steel (DSS) is widely used in industrial sectors like desalination, chemical tankers, pressure vessels, storage tanks, pulp and paper machinery, and civil engineering due to their high chromium content and low nickel and molybdenum content, making them excellent engineering materials.

Agrawal et al. [87] studied the machining characteristics of cast austenitic stainless steel(ASS), focusing on cutting force requirements, tool rake-face wear, and chip characteristics. They found that the composition of stainless steel affects machinability, with high cutting forces and sharp edge chipping leading to catastrophic failure at the tool nose. Nitrogen addition increases strength but decreases machinability.

Kumar et al.[88] studied on the tool life of alumina-based ceramic cutting tools for machining hardened martensitic stainless steel and found that flank wear affects tool life at lower cutting speeds, while crater or notch wear affects tool life at higher speeds.

Noordin et al. [89] suggested higher insert radius, low feed rate, and low cut depth for better surface finish in dry turning operations. Cubic Boron Nitride tool wear rate is higher than PCBN tool due to abrasion and diffusion.

Saï et al. [90] studied on residual stresses, microstructure, surface roughness, and micro hardness of carbon steels and DSS materials during milling operations found that high cutting speed with reduced feed rate enhances surface quality, with depth of cut having less impact.

Mandal et al. [91] used Taguchi method and regression analysis to evaluate the machinability of AISI 4340 steel with zirconia toughened alumina ceramic inserts. Furthermore, the results revealed that the depth of cut and cutting speed are key factors causing tool flank wear, with feed rate having less influence.

Asiltürk et al. [92] conducted dry turning tests on hardened AISI4140 steel using coated carbide cutting tools. Further, they used the Taguchi method to optimize cutting parameters, finding that feed rate significantly affects surface roughness. Limited research has been conducted on the machining characteristics of nitrogen alloyed DSS, so this work aims to optimize cutting parameters to minimize surface roughness, cutting force, and tool wear during dry turning operations.

Matsumoto et al. [93] found that as work-piece hardness increases, residual stresses in the facing of case hardened AISI4340 steel become more compressive without phase transformations. Further, the results revealed that the residual stress near the machined surface or hardened steel is a compressive stress, and it changes to tensile stress as the hardness decreases.

Thiele et al. [94] studied surface residual stresses in hardened materials with different feed rates. Furthermore, they found that the results did not agree with each other, possibly due to measurement errors caused by X-ray beam scattering on the specimen surface. This discrepancy could be attributed to different feed rates and tool edge preparation.

Thiele et al. [95] conducted a study on subsurface residual stresses in orthogonal machining of hardened AISI52100 steel. The study revealed that the hone edge geometry produced more compressive residual stresses than the chamfer edge geometry after machining a work-piece hardened to HRC 57. The study found that harder materials induced more compressive residual stress in the subsurface, with the maximum compressive hoof residual stress increasing from 700MPa to 1150MPa with an increase in work-piece hardness from HRC 41 to HRC 57.

.Matsumoto et al. [96] studied the impact of finishing processes and parameters on residual stress in case carburized steel, focusing on the depth of residual stress. They found that residual stresses after hard turning and superfinishing are more compressive and reach deeper to the machined surface than after grinding and superfinishing. Furthermore, the results revealed that the depth of cut and feed rate did not significantly impact the subsurface residual stresses. The primary cutting zone's size was secondary, while the size of the plastic zone near the tool edge significantly influenced its size. To increase the plastic deformation zone, several tool geometries were investigated, with the hone edge and double chamfer geometries offering greater subsurface penetration and larger maximum compressive stress values. The study revealed that the double chamfer geometry yielded a maximum compressive circumferential stress of 800MPa at 20m depth, 780MPa using the 20m hone edge preparation, and only 250MPa using a sharp edge.

Abrão et al. [97] studied the impact of tool wear on hard turning of AISI 52100 steel and compared the fatigue life of hard turned and grounded specimens with the same surface roughness. Furthermore, they found that hard turning produced microstructural alterations, including a white surface layer of untempered martensite and a deeper dark layer of over tempered martensite. The residual stresses in the subsurface were compressive, and the fatigue life of hard turned specimens was longer.

Agha et al. [98] experimentally studied on super finish hard turned AISI 52100 steel and revealed compressive residual stress distributions in both circumferential and axial directions. Results showed that the flank wear significantly influenced distributions, causing axial tensile surface stresses and reduced residual stress penetration in the circumferential direction.

Mittal et al. [99] developed an empirical model to predict residual stresses in hard turning based on cutting conditions. This model was used to select process parameters that maximize the

fatigue life of rolling contact surfaces. Previous research indicates that residual stress profile in hard turning is influenced by cutting edge geometry, work-piece material properties, and cutting conditions. Despite numerous experimental studies, these are primarily empirical and valid for the case investigated. A more fundamental model is needed that considers work-piece hardness, cutting edge geometry effects, and cutting conditions simultaneously to predict residual stress profiles in hard machining. This model should also be used for cutting tool design and process parameter selection.

Ozel et al. [100] have studied the impact of tool nose design on surface finish and productivity in finish hard turning processes. The study explores surface finishing and tool flank wear in AISI D2 steels using ceramic inserts, using multiple linear regression and neural network models for prediction. The study reveals that wiper tools can achieve surface roughness R_a values as low as 0.18–0.20μm, and tool flank wear reaches a tool life criterion value of VBC = 0.15mm before or around 15 minutes of cutting time at high speeds. The study demonstrates that neural network models are effective in predicting tool wear and surface roughness patterns across various cutting conditions.

Thamizhmnaii et al. [101] showed that the wear pattern of CBN tools in hard turning depends on the tool and work-piece material composition, cutting conditions, and the combination of CBN tools and work materials. Adhesion, abrasion, and diffusion are the main tool wear mechanisms, with individual effects depending on these factors. Some of the main mechanisms include diffusion wear, oxidation wear, fatigue wear, adhesive wear, and abrasive wear. Further, the results revealed that the chemical loading on tools and cutting materials causes diffusion wear, oxidation wear causes gaps in the film, fatigue wear breaks tool edges, adhesive wear forms at low machining temperatures, and abrasive wear is influenced by work material hardness and cutting material content.

Lin et al. [102] revealed that tool life increases with cutting speed until it starts to decrease. In low-speed cutting, abrasion is the main form of wear. Further, the results revealed that as cutting speed increases, a sticking layer forms on the tool face, protecting it from wear. At high speeds, the chip transitions from continuous to saw-tooth type, increasing friction force and gradually abrading the layer. The bond between hard particles weakens, leading to increased wear on the rake face and flank wear.

Thamizhmanii et al. [103] showed that the flank wear in ceramic cutting tools is mechanically activated wear caused by the abrasive action of hard work-piece material with the ceramic tools. Furthermore, they concluded that the wear is characterized by grooves and ridges on the flank face and significantly affects the quality of the machined surface. It also affects surface finish, residual stress, micro structural changes, tool shape, and cutting conditions. High temperatures between the cutting face and work-piece cause abrasive and adhesive wear, which affect tool material properties and work-piece surface. Increased temperature at the cutting edge can lead to loss of hardness and wear. Lower cutting speed results in lower flank wear, but as these parameters increase, flank wear also increases.

Mahfoudi et al. [104] explained that the most known wear mechanisms are activated during machining hard materials with PCBN tools, such as mechanical, thermal, or chemical damage. Further, the results revealed that the mechanical damage, including fractures, is caused by the material's brittleness and toughness, and tool failure often results from other damage mechanisms. Mechanical abrasive wear is common when hard turning is performed at cutting speeds ranging from 100 to 250 m/min, caused by hard martensite elements in the work material. Chemical and diffusion wears have been more discussed in literature, but they are increasingly being considered important for the damage mechanisms of CBN inserts.

Arsecularatne et al. [105] studied that most known wear mechanisms are activated during machining hard materials with PCBN tools, such as mechanical, thermal, or chemical damage. Mechanical damage, such as fractures, is related to the brittleness and toughness of the material and its weakness to resist shear solicitation. Furthermore, the authors observed that the tool failure often results from other damage mechanisms. Mechanical abrasive wear is commonly observed when hard turning is performed at cutting speeds ranging from 100 to 250 m/min. Abrasive wear is caused by hard elements of martensite in the work material. Chemical and diffusion wears have been more discussed in literature, but they are increasingly being considered important for the damage mechanisms of CBN inserts.

Huang et al. [106] studied that abrasive wear is the damage to surfaces caused by the motion of harder asperities or trapped hard particles. Hardened steel has two-phase microstructure, consisting of cubic ferrite and small cementite particles. Further, the results revealed that the cementite particles are not as tightly constrained by the ferrite matrix phase as in pearlite. Free

cementite particles are easily generated during hard turning, forcing them against tool surfaces, causing three-body abrasive wear. This is considered the dominant abrasive wear mechanism in hard turning.

Xie et al. [107] showed that the tool failures in turning operations include progressive wear, chipping, partial fracture, plastic deformation, and thermal crack. Currently, experimental and analytical methods are the main methods for investigating tool wear. The advancement of advanced computers and numerical methods has enabled the study of metal machining phenomena like cutting force, temperature, and progressive tool wear. These methods are expected to become effective tools for tool wear study and partially replace time and cost consuming experimental methods.

Lorentzon et al. [108] has estimated that the high stress at tool-chip interface, work hardening, and high temperature in nickel alloy machining contribute to tool wear. Understanding the wear process is crucial for predicting wear rates and improving tool life. Historically, experimentation was the main method, but the finite element method and powerful computers have enabled simulation of complex contact problems. This method has been effective in analyzing chip formation and predicting variables like temperatures, forces, and stresses. However, the approach for simulating tool wear in nickel-based super alloys has shown significant discrepancies between simulated and measured geometry, particularly around the tool tip. More work is needed to enable accurate tool wear simulations, which must also consider modeling wear and friction at the tool-chip interface, as these phenomena are strongly related.

Wang et al. [109] explored the wear of tool inserts in hard turning with cubic boron nitride (CBN) tools. The tool's cutting edge is subjected to high stresses, temperatures, and chemical reactions, causing tool wear through various mechanisms. The mechanisms are influenced by various factors such as the material combination, cutting geometry, environment, and mechanical and thermal loadings. The progression of tool wear is influenced by five wear mechanisms: abrasion, adhesion, fatigue, dissolution/diffusion, and tribochemical process. It is widely accepted that tool wear mechanisms in machining involve multiple mechanisms, making it difficult to predict their relative importance. Crater and flank wear are prevalent machining wear patterns, primarily resulting from interactions between the insert and the hot metal chip.

Mamalis et al. [110] had worked on the finite element method used for modeling various machining operations over the last three decades. The first models, which appeared in the 1970s, used the Eulerian formulation for orthogonal cutting, which involves a finite element mesh spatially fixed and material flowing through it to simulate chip formation. This approach minimizes computational time by minimizing the number of elements needed to model the work-piece and chip, primarily used for simulating the steady state condition of the cutting process. However, this formulation requires complex programming and experimental data to determine chip geometry. The updated Lagrangian formulation, widely used today, attaches elements to the material, allowing the undeformed tool to advance towards the work-piece. A chip separation criterion is applied, which can be geometric or physical and may involve a critical distance between the tool and the work-piece. The separation criteria include critical stress or strain values for chip formation and crack propagation criteria. The method has a disadvantage as it results in significant mesh deformation during the simulation, which is attributed to plastic deformation in the cutting zone. Continuous remeshing and adaptive meshing are usually applied to overcome this disadvantage, but advances in computers have made it possible to reduce the time needed for analysis. An arbitrary Lagrangian-Eulerian formulation has also been proposed to combine the advantages of both methods, but it is not as widely used.

Bouzid et al. [111] focused on measuring flank wear in relation to cutting time to determine tool life. It found that an increase in cutting speed leads to a higher decrease in the second gradual stage of wear due to the rapid removal of the thin coat layer during high-speed turning. An empirical model was developed for tool life determination in relation to cutting speed. Furthermore, the results suggested that optimal cutting speed can be set to achieve maximum tool life based on the findings.

Sharma et al. [112] has estimated that the tool wear is the most critical factor for successful manufacturing process maximization and automation in metal cutting processes. Monitoring tool wear is essential for automated manufacturing. Predicting tool wear is challenging due to its nonlinear and stochastic nature. Initial efforts focused on mathematical models of the cutting process, which relied on large amounts of experimental data. These methods did not consider the complex nature of metal cutting operations. Researchers sought other sensor integration methods to operate without human assistance and estimate most or all forms of tool wear in metal cutting.

Astakhov et al. [113] studied that despite numerous investigations, the nature of tool wear remains unclear due to the complexity of physical, chemical and thermo mechanical phenomena in the cutting zone. The dominant mechanism of wear is difficult to identify due to the simultaneous influence of various mechanisms, such as adhesion, abrasion, diffusion, and oxidation. Interpretations of these mechanisms are subjective and based on various factors, making experimental methods dominant in tool wear studies as optimal cutting temperature, minimum tool wear rate, minimum stabilized cutting force, and highest machined surface quality. This temperature is invariant to the method of achieving it, such as cooling or pre-heating the work-piece. Furthermore, they observed that the specific contact stresses at tool chip interfaces, chip compression ratio, and average contact temperature remain unchanged when the depth of cut increases and uncut chip thickness remains constant. If the machining is performed at the optimal cutting regime, an increase in the depth of cut should not alter the tool wear rate.

Maranhão et al. [114] found that the AISI 316 is a challenging material to machine due to its high tensile strength, ductility, work-hardening rate, low thermal conductivity, and abrasive behavior. High cutting forces, high cutting temperature, fast tool wear rates, notch wear, chip breakability issues, BUE formation, and poor surface finish are common consequences of these properties. The issues are addressed by using a coated tool with a chip breaker. Work hardening can lead to unstable chip formation, vibrations, mechanical modifications, and heterogeneity on the machined surface. Low thermal conductivity hinders heat conduction at tool tips, potentially causing heat-concentrated areas in the working material, affecting the piece's integrity and causing residual stressed layers. Residual stresses are crucial in machining materials, as the energy used to plastically deform the work-piece during a turning operation is converted into heat. Temperatures during machining operations are influenced by tool-chip contact, cutting force levels, and friction between the tool and chip. Further, results revealed that the shear zone is subject to the majority of heat, and the contact length between the chip and tool influences cutting forces, cutting conditions, tool performance, and tool life.

Coelho et al. [115] studied that wear minimization in metal cutting has been achieved through various methods, including tool steels, heat treatments, new tool materials, and coatings. The first significant improvement occurred with HSS, but its use in metal cutting has been significantly reduced since the mid-20th century. Recent developments include sintered carbides

with submicron and ultra-fine grains, PCD and PCBN, which are suitable only for nonferrous materials and can compete with ceramic materials and grinding processes. Ceramics, PCBN, and PCD are expensive compared to carbide, necessitating careful analysis for their application. No material has ever demonstrated all the properties of an ideal cutting material, including high hardness, wear resistance, toughness, and chemical stability. Further, results revealed that the coating materials can be used to withstand cutting conditions at the interface tool chip, offering higher hardness at high temperatures, lubricant properties, good chemical stability, and good thermal properties.

Baker et al. [116] studied that uses a finite element model of a two-dimensional metal-cutting process to investigate the impact of cutting speed on cutting force and chip formation. The model employs a generic flow stress law, disregarding friction due to its limited speed dependence. Furthermore, they concluded that the simulation reproduces the observed decrease in cutting force with speed and plateau at high speeds, primarily due to thermal softening changes. Large cutting speeds produce segmented chips, which are more energetically favorable than continuous chips.

Shi et al. [117] found that despite significant progress in modeling metal cutting processes, several fundamental issues remain unresolved. These include the frictional behavior along the tool-chip interface and its impact on thermo mechanical quantities. Additionally, understanding tool wear and its correlation with thermo mechanical quantities in metal cutting is complex and depends on various factors. Research has primarily focused on the physics of wear, without quantifying wear and tool life through combining experimental observations with numerical simulation solutions of thermo mechanical quantities in metal cutting.

Umbrello et al. [118] stated that the machining generates a significant amount of heat due to heavy deformations on the material. This is due to the development of tool materials and machines that allow for high cutting speeds. Today, mandrel rotation speeds exceed 18,000 rpm and cutting speeds are hundreds of m/min. The use of lubricants and coolants is discouraged due to environmental impact and industrial costs. Traditional chip formation theory suggests that a significant portion of the heat generated is due to deformation work on the shear plane. The rake face is a secondary source of heat generation due to friction between the work-piece surface and the tool.

Arunachalam et al. [119] showed that mixed ceramic cutting tools induced higher tensile residual stresses than CBN cutting tools. The study found that cutting speeds were more sensitive to residual stresses and surface roughness than the depth of cut. As the cutting speed increased, the residual stress values shifted from compressive to tensile. Coolant use either increased or decreased tensile residual stresses, while dry cutting always resulted in tensile stresses. Further, the study suggests that round CBN cutting tools should be used at slow speeds and with coolant for optimal compressive or minimal residual stresses and excellent surface finish.

Gunnberg et al. [120] found that increasing feed led to higher compressive stresses, while cutting did not affect residual stresses. Both models showed increased compressive stress when the rake angle was negative. Controlling cutting parameters allowed for tailor-made stresses in the product, extending the machined component's service life. Furthermore, they showed that the depth of cut had less impact on residual stresses and surface roughness than cutting speed and feed.

Attanasio et al. [121] studied that an increase in cutting velocity or feed rate leads to deeper craters, while feed rate primarily influences crater position and extension. Tool life is influenced by factors such as material composition, cutting conditions, and geometry. Cutting conditions like feed rate, depth of cut, and cutting speed affect tool wear, while tool geometry parameters like rake angle, chamfer length, hone radius, and tool nose radius affect tool wear. Cutting speed has a greater impact on tool wear, as the temperature of the cutting edge increases as the speed increases.

Caruso et al. [122] found that surface residual stresses increase with increasing cutting speed, width of cut, and feed rate. The results revealed that the developed FE model successfully reproduced experimentally observed stresses in orthogonal machining of AISI H13 tool steel, demonstrating the ability to simulate complex machining processes.

Ulutan et al. [123] found that the maximum value of compressive stresses along the feed direction beneath the surface decreases with an increase in nose radius. This trend was closely matched by simulations. Furthermore, they observed that the stresses die out at depths closer to the machined surface, while simulations predicted residual stresses at deeper levels. Tensile residual stresses at the surface decreased consistently with increasing depth of cut. However,

increasing nose radius led to a shift in tensile direction, unlike simulation results. For a maximum nose radius of 1.2 mm, stress became compressive at 0.2 mm depth.

Outeiro et al. [124] found that residual stresses were tensile at the surface and gradually shifted to compressive values beneath it before stabilizing at around zero MPa. The residual stresses generated by turning AISI 316L were tensile and high at the machined surface, but not as high as those obtained by turning Inconel 718. Furthermore, they concluded that the higher surface residual stresses were generated with uncoated tools than coated tools, and higher stress values were obtained on the transient surface.

Rizzuti et al. [125] found that tensile residual stresses were on the machined surface, while compressive residual stresses were below it. The reliability of FE numerical models for predicting residual stresses depends on accurate predictions of mechanical and thermal aspects. Further, the results revealed that the experimental residual stresses increased with edge radius upto 30 microns, but decreased for edge radii of 55 and 75μm.

The literature mentioned above revealed that information about the tempered and untempered EN-36C alloy steel's mechanical performance, microstructural characteristics, machining characteristics, and residual stresses is just not readily available.

The current study aims to examine the impact of tempering on the mechanical characteristics, microstructural development, and residual stresses of EN-36C alloy steel following CNC turning. Additionally, a comparative analysis of the mechanical characteristics of tempered and untempered EN-36C alloy steel, including hardness, impact resistance, and tensile strength, has been done.

Energy dispersive X-ray analysis (EDAX) has also been used to do a microstructural examination on the material under investigation. To assess several reactions, including residual stresses, material removal rate (MRR), surface roughness, and tool tip temperature for test specimens, an experimental examination using CNC turning has been conducted. In the X-ray residual stress measurement system (μ-X360), residual stresses were measured using the cosα technique with the use of image plates (IPs).Enhancing the machinability of EN-36C alloy steel while maintaining a fairly stable hardness is the main goal of the tempering procedure.

2.3 Research Gap

After thorough literature survey on CNC turning of hard metals like EN series steel, Metal Matrix composites, aluminium alloys and their matrix, the following observations are found.

- A thorough literature is available on CNC turning of hard metals but very limited literature is available on tempered EN-36C steel and yet to be explored.
- Machinability and residual stress of tempered EN-36C alloy steel in CNC turning process has to be explored.

2.4 Research Objectives

Based on thorough literature survey, the following research objectives are drawn.

1. To temper EN-36C steel bars with preserving their properties.
2. Statistical modeling for surface roughness using response surface methodology.
3. To study the surface integrity.
4. To study the tool wear while turning EN-36C tempered steel bar.

CHAPTER 3

Material and Experimental Works

In this chapter, the sample preparation of EN-36C alloy steel, chemical composition, tempering of prepared samples, testing of samples for mechanical and microstructural properties were carried out. A brief discussion was made on sequence of experimental processes.

3.1 Preparation of Samples and Testing

In the present work, the specimens of EN-36C alloy steel have been prepared from cylindrical bar of 32mm diameter and 150mm in length for experimentation. The specimens were tempered at 200ºC, 300ºC, 500ºC and 700ºC respectively for two hours in an electronically controlled box type muffle electric furnace as shown in Figure6. The specimens were allowed to cool in the furnace. Optical emission spectroscopy (OES) is carried out to check the authentication of their chemical compositions. The chemical compositions of EN-36C were ascertained using a specimen size of 25x25x3 mm and shown in Table 2. Three samples were evaluated in each instance to guarantee uniformity and repeatability.

Fig.6: Tempering of EN-36C alloy steel in Muffle Electric furnace

Table2: Chemical composition of EN-36C alloy steel after OES testing

Elements	Carbon, C	Manganese, Mn	Silicon, Si	Nickel, Ni	Molybdenum, Mo	Chromium,Cr	Sulfur, S	Phosphorous, P
Composition %	0.133	0.510	0.23	3.450	0.37	0.787	0.009	0.006

The experiments were conducted on cylindrical bars of EN-36C alloy steel with a diameter of 32 mm and a length of 150 mm, both tempered and untempered using a tungsten carbide cutting tool on CNC turning at same cutting conditions. The cutting speed of 650 rpm, the depth of cut of 1.7 mm, and the feed rate of 0.20 mm/rev were selected as the turning parameters.CNC machine used for turning the samples is given in Figure7. The complete flow of work conduct process is shown in Figure8.

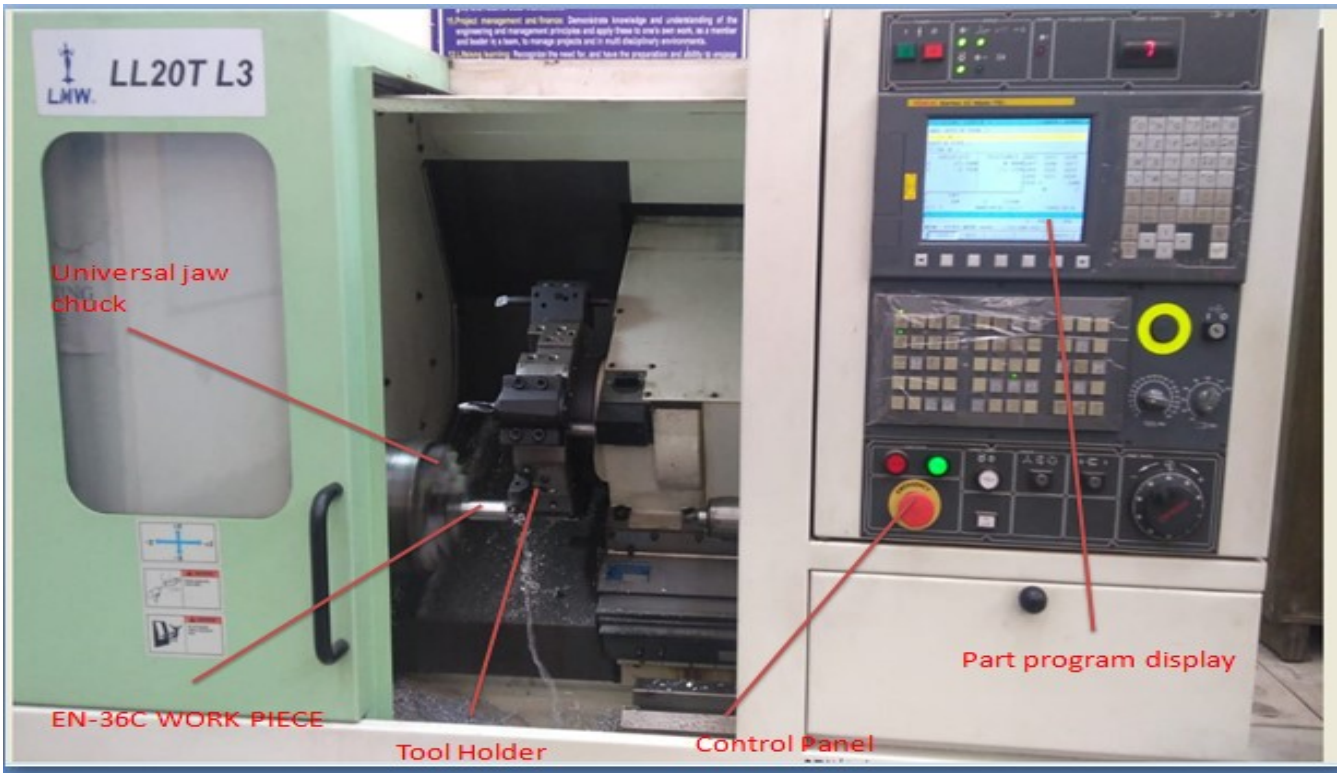

Fig.7: Work-piece setup on CNC machine

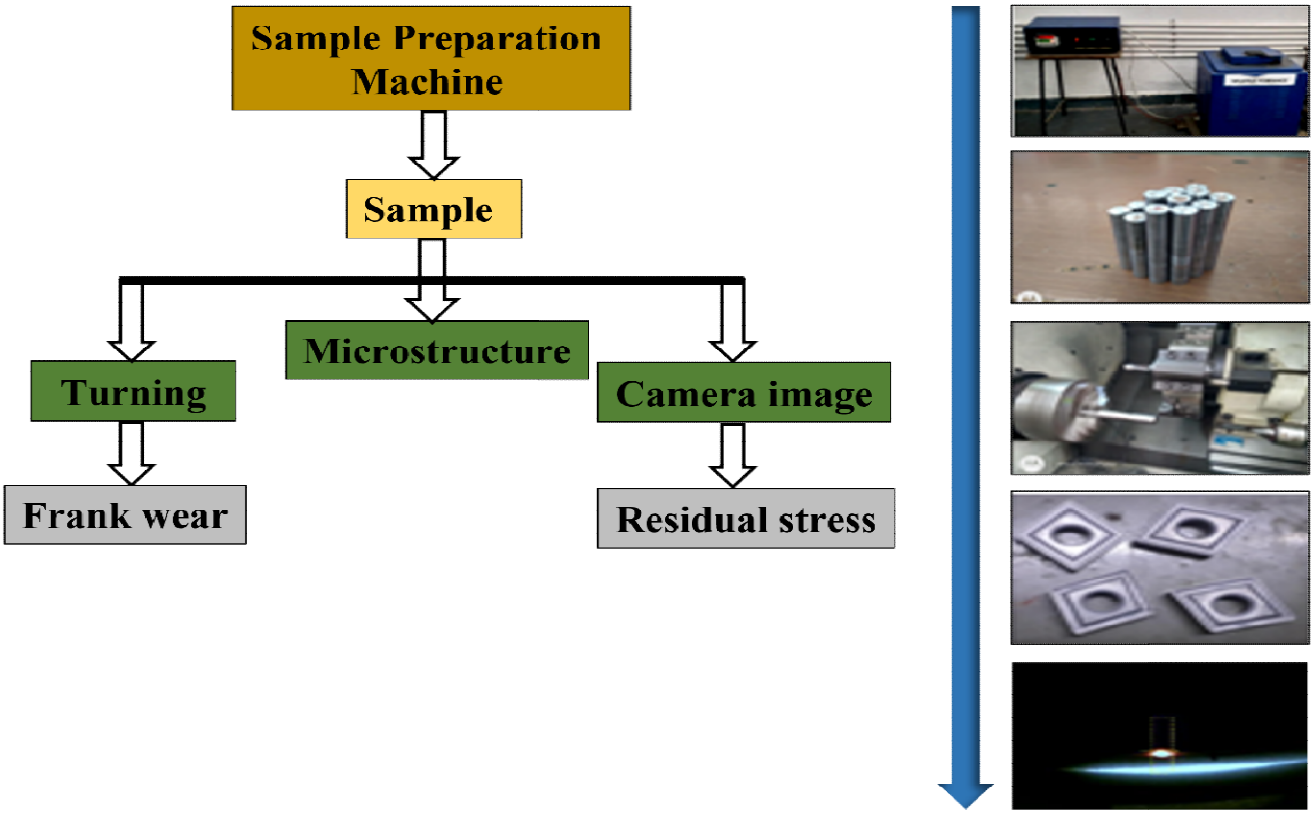

Fig.8: Experimental procedure

3.1.1 Tensile Testing

To examine the mechanical properties of EN-36C alloy steel, a standard test procedure was adopted with standard test specimen. The specimens were prepared as per ASTM E-8 standard from tempered and untempered EN-36C alloy steel which is shown in Figure9. [118,126]. Tensile tests were performed at room temperature on computerized universal testing machine (UTM). Calibration and measurement of specimen's strain upon loading have been done using extensometer. Tensile test was performed under constant and continuous application of load at room temperature with gauge length and diameter of 40 mm and 10 mm respectively for all specimens at tempered and untempered. During testing, the cross head velocity and strain rate were observed as 1.5 mm/min and $10^{3}s^{-1}$ respectively [126]. Broken parts of specimens are shown in Figure10.

Fig.9: Tensile test specimens (a) Untempered(b)Tempered at 200ºC (c)Tempered at 300ºC (d) Tempered at 500ºC (e) Tempered at 700ºC

Fig.10: Broken test specimens (a) Untempered (b)Tempered at 200ºC (c)Tempered at 300ºC (d) Tempered at 500ºC (e) Tempered at 700ºC

Each specimen underwent a tensile test utilizing a UTM with a 20 kN capacity in order to determine the ultimate tensile strength, yield stress, gauge elongation, and percentage reduction, all of which are listed in Table 3.For every specimen, a stress vs strain curve was drawn at constant loading until the fracture point. Following the test, different output responses were measured, and cracked surfaces were analyzed using SEM and EDAX. Tensile characteristics were found to be significantly influenced by the tempering temperature, as evidenced by current experimental investigations and literature reviews.

Table3: Tensile test data of EN-36C alloy steel

Sr. No	Specimen conditions	Load P (kN)	Tensile Strength (UTS) Mpa	Stress at Yield (YS) MPa.	Gauge Elongation (mm)	%Elongation
1	Untempered	55.521	1024.001	814.680	8.57	21.425%
2	Tempered at 200^0C	58.64	706.914	422.434	4.57	11.425 %
3	Tempered at 300^0C	53.44	746.626	453.845	8.73	21.825 %
4	Tempered at 500^0C	80.425	680.418	449.643	11.17	27.925 %
5	Tempered at 700^0C	58.006	738.554	613.520	9.46	23.65%

3.1.2 Hardness test

The hardness of the test specimens was examined using a Rockwell hardness tester. The preparation of the hardness test specimens followed ASTM E18-07 guidelines. The test specimens had a diameter and heights of 10 mm. Specimens were appropriately polished to eliminate surface blemishes before the hardness test. Every specimen's hardness was assessed in four distinct places because the experimental findings were unknown; three samples were generated for every test condition. In scale B, a diamond cone with an indenter diameter of 1/16" was employed to measure hardness under an applied load of 100 kg-f. The hardness was calculated by equation1.The values of hardness of each specimen on Rockwell hardness tester are tabulated in Table 4.

$$HRX = M - \frac{(h_2 - h_1)}{0.002} \quad (1)$$

Where M = 100 for A, C and D scales and 130 for B, E, M, R scales

h_1= Indentation depth produced by the preliminary test force

h_2 = indentation depth produced by the test force.

Table4: Hardness (HRB) of the specimen

Sr. N.	Specimen condition	Trail I	Trail II	Trail III	Average HRB
1	Untempered	93	92	94	93
2	Tempered at 200^0C	98	97	99	98
3	Tempered at 300^0C	100	101	102	101
4	Tempered at 500^0C	93	92	91	92
5	Tempered at 700^0C	97	98	99	98

3.1.3 Impact test

Charpy test was conducted to measure the toughness of the test specimens. The material for the impact test required a special preparation of specimens as per the ASTM (E23-02a) standards [118]. Due to unpredictability in the experimental results, three specimens were prepared for each test condition from EN-36C alloy steel which is shown in Figure11. Three were untempered and twelve were tempered at 200ºC, 300ºC, 500ºC and 700ºC. All specimens were prepared in the dimensions of 10 mm×10 mm×55 mm with V notches at the distance of 27.5 mm at one end of the specimen which is shown in Figure10. The specimen notches are of 2 mm in depth and have the angle of 45°. All prepared specimens were tested on Charpy impact test machine with the capacity of 300 Joule. The specimen was kept on anvil as a simple supported beam. The broken specimens after impact testing are shown in Figure12. The test readings were noted down of each specimen from Charpy energy scale. The value of impact energy of specimens is mentioned in Table 5.

Table 5: Impact values of each specimen of EN-36C alloy steel in KVC (J)

Sr. No.	1	2	3	4	5
Specimen condition	Untempered	Tempered at 200°C	Tempered at 300°C	Tempered at 500°C	Tempered at 700°C
Impact KVC (J)	35	139	161	187	69

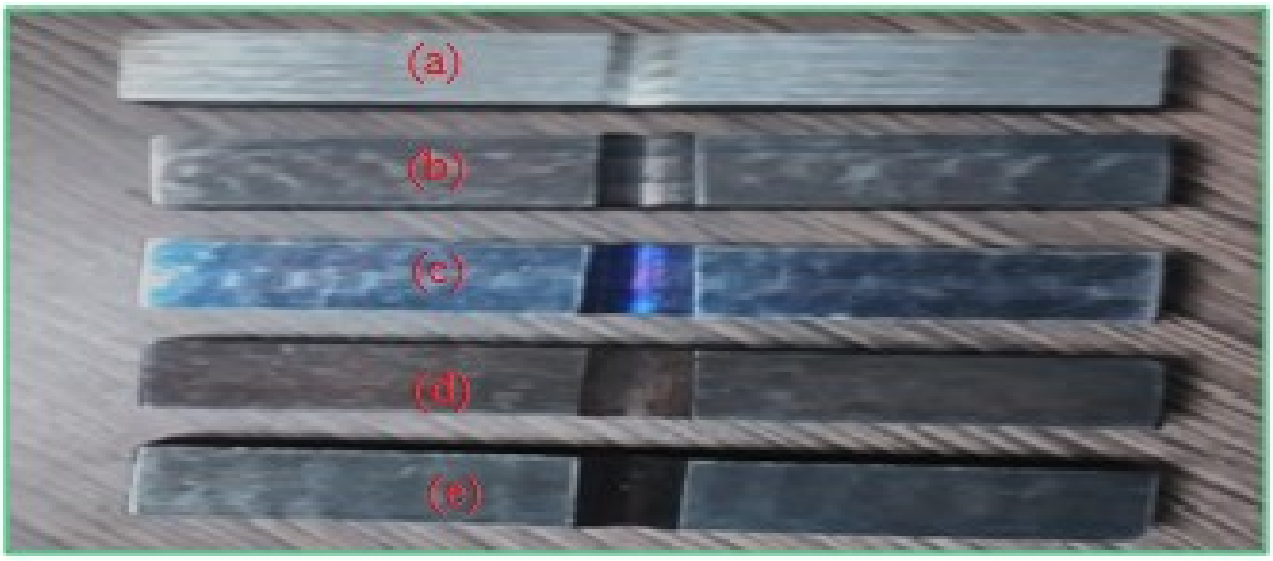

Fig.11: Impact test of EN-36C alloy steel (a) Untempered(b)Tempered at 200ºC (c)Tempered at 300ºC(d) Tempered at 500ºC (e) Tempered at 700ºC

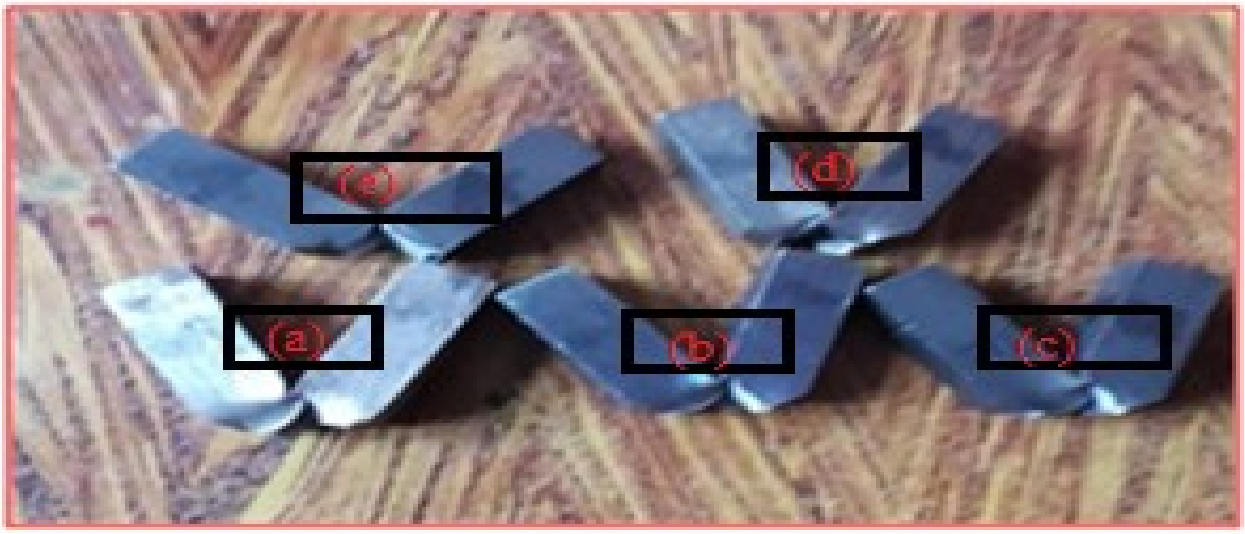

Fig.12: Broken specimens of EN-36C alloy steel (a) Untempered(b)Tempered at 200ºC (c)Tempered at 300ºC (d) Tempered at 500ºC (e) Tempered at 700ºC

3.2 Surface roughness measurement

Surface roughness of tempered and untempered specimens was measured with the help of a portable stylus-type profilometer, talysurf which is shown in Figure13. Turning was carried out at the same process parameter (cutting speed, depth of cut, feed rate) for each specimen. Cut off length 0.8 mm and Gaussian filter with a ratio of 2.5 μm was used. All the roughness parameters

such as average value of surface roughness (R_a), root mean square value of surface roughness (R_q), and peak to valley height value of surface roughness (R_z) were measured on the specimens repeatedly at five places in the transverse direction. The average value of surface roughness is presented in Table6.The results were depicted that specimens tempered at 500°C have lowest surface roughness.

Fig.13: Setup of surface roughness tester

Table 6: Surface roughness of specimens after experimentation

S. No.	Specimen condition	CLA (R_a)	RMS (R_q)	Peak to valley (R_z)
1.	Untempered	2.33	2.81	12.90
2.	Tempered at 200 °C	2.09	2.46	10.20
3.	Tempered at 300°C	3.09	3.82	17.60
4.	Tempered at 500°C	1.93	2.36	10.30
5.	Tempered at 700°C	2.40	2.91	12.4

3.3 Tool wears measuring method

Total twenty set of combinations of machining parameters were applied to coated tool inserts, revealing tool wear that was detected using a toolmaker's microscope during the machining process. The toolmaker microscope was used to measure flank and crater wear, illuminated using two LEDs on a measuring bench. The study involved magnification using a

lens and distance measurements using micrometers. The cutting tool insert was placed on a measuring bench, visible in the microscope eyepiece. The bench was translated to X and Y axes using two-micrometer screws. The geometry of the cutting tool insert was observed using micrometer screws. The tool insert was placed horizontally for flank wear and vertically for crater wear. The geometrical change was inferred for all tool inserts. Identification marks were given to all coated cutting tool inserts for 20 trials of experiments. The tool maker microscope was used to identify the insert geometry. The CNMG-120408-THM inserts are double-sided 80^0 rhombic inserts with positive rake angle that varies along the edge to negative in order to prevent chipping were used for cutting each specimen. The images of some inserts are shown in Figure14.

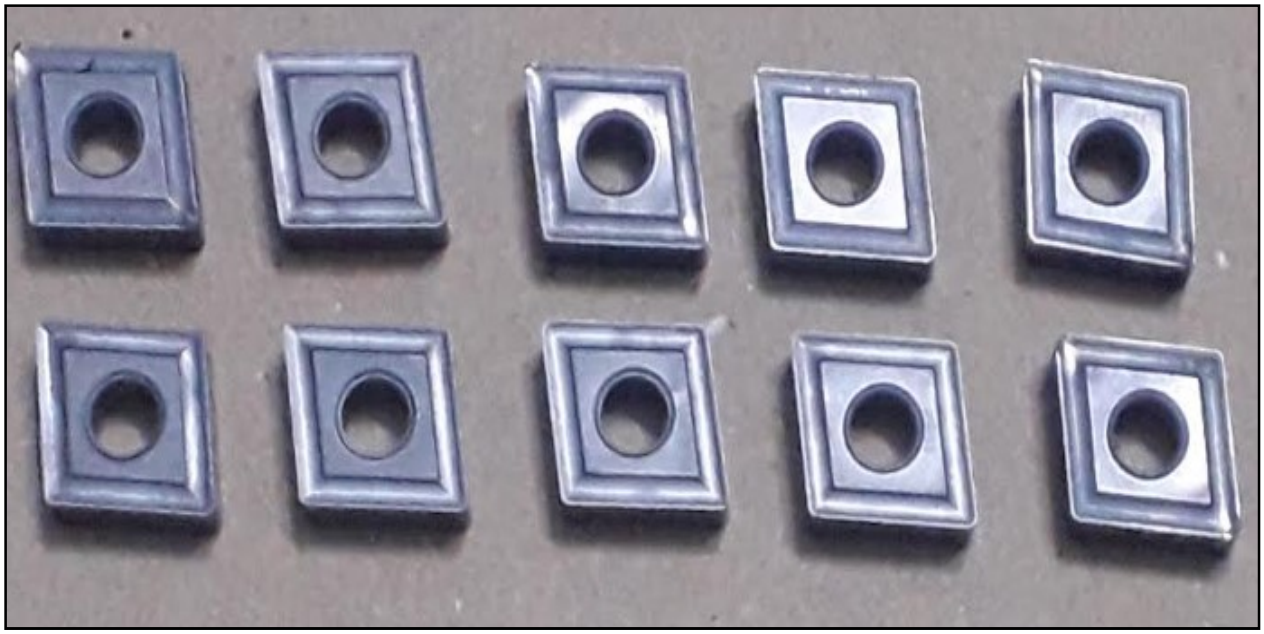

Fig.14: CNMG-120408-THM cutting inserts

3.4 Measurement of cutting tool tip temperature

The recording of thermal processes in the tool/work-piece contact zone is challenging due to its small spatial dimensions, necessitating extensive experimental efforts. In view of this, the cutting tool tip temperatures were measured with the help of highly sensitive electronic device

(FLUKE thermal imager) which is shown in Figure 16.For measuring the tool tip temperature of each specimen, the infrared gun was shooted exactly in the contact point of cutting tool and work-piece during turning process. The gun was pointed at four places in each specimen during turning process. The average value of tool tip temperature is shown in Table 7 and the bar graph is shown in Figure15.

Table 7: Average tool tip temperature of all specimens during experiment

Tempering temperature	**Average tool tip temp. in** ^{0}C
Untempered	65
Tempered at 200°C	63
Tempered at 300°C	62
Tempered at 500°C	61
Tempered at 700°C	67

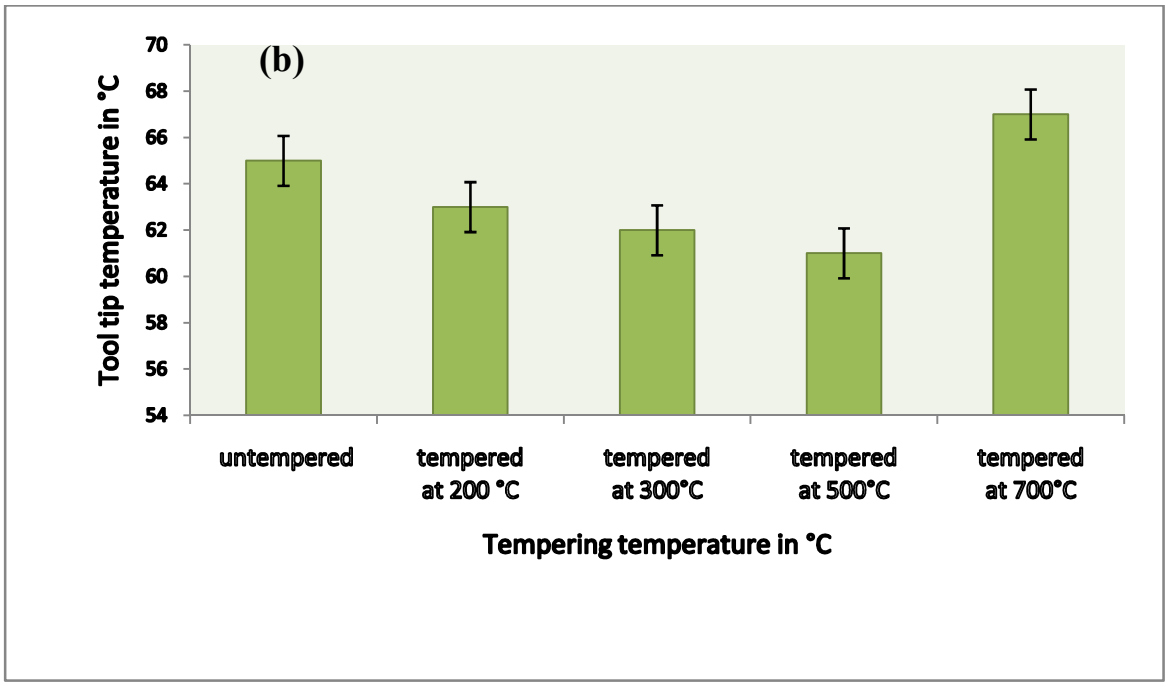

Fig.15: Bar chart for average tool tip temperature of untempered and tempered specimens

Fig.16: Measurement of tool tip temperature by FLUKE thermal imager

CHAPTER 4

Machinability and mechanical properties of tempered and untempered EN-36 C

In this chapter, the discussion is made on Machinability and related factors which affect on it. Apart from this, a comparative study on mechanical properties of EN-36C alloy steel tempered and untempered has been carried out. The comparative study on surface roughness has also been carried out after conducting the experiments on CNC lathe at same process parameters using cylindrical bar of tempered and untempered EN-36C alloy steel.

4.1 Machinability

Machinability refers to a metal's ability to remove material with a satisfactory finish at the lowest cost. The most machinable metal is one that can be efficiently remove the most material per tool grind with a satisfactory finish, characterized by its machinability, which includes tool life, surface finish, and cutting power required.

4.1.1 Factors Affecting Machinability:

Factors influencing the machinability of metals include

i. The type of work-piece refers to the material used to create the work-piece.

ii. Types of cutting tool material

iii. Shape and Size of cutting tool

iv. The type of machining operation.

v. The size, shape, and velocity of the cut.

vi. The machine type and quality used.

vii. The quality of the lubricant used during the machining operation.

viii. The coefficient of friction between a chip and a tool

ix. The shearing strength of the work-piece material

To machine metal, the tool must first penetrate the surface, and the formed chip should break easily. The ideal method is to have a built-in breaker, as it's incorrect to assume that soft metal is easy to machine.

Toughness is often inversely related to softness, making chip separation difficult. In steel, a spheroidized structure is considered the easiest to machine.

Machinability refers to the ease with which a material can be machined, influenced by machine variables such as cutting speed, feed and depth of cut, tool form, material, cutting fluid, rigidity of tools, shape and size of work, and tool engagement nature.

The ease of machining is influenced by various factors such as the work material's hardness, tensile strength, chemical composition, microstructure, degree of cold work and strain hardenability.

The ease of machining can be accessed through factors such as tool life, cutting forces, power consumption, surface finish and chip disposal ease.

4.1.2 Variables Affecting Machinability:

Machinability is influenced by the following variables:

i. Machine Variables:

Machine variables like power, torque, accuracy, and rigidity indirectly impact machinability. A rigid machine with sufficient power to withstand cutting forces and minimize deflections is crucial for tool life and surface finish. Limiting cutting forces requires limiting speed, feed, and depth of cut [127].

ii. Tool Variables:

The optimization of a cutting tool involves factors such as tool material, geometry and engagement with the work. Proper cutting tool geometry is crucial for efficient machining, ensuring a reasonable tool life and maximum material removal, based on work material and machining conditions.

Surface finish is significantly influenced by cutting tool geometry, with rake angle and nose radius enhancing it, while tool rigidity impacts tool life, surface finish and dimensional accuracy.

iii. Cutting Conditions:

Cutting speed significantly impacts tool life, improving surface finish through continuous reduction of built-up edge. Dimensions of cut and cutting fluids also impact the tool life.

iv. Work Material Variables:

Machinability is influenced by various factors such as hardness, tensile strength, chemical composition, microstructure and the method of production of the work material.

4.1.3 Merits of Machinability

Outputs of good Machinability are listed below:

- High cutting speed can be used
- High material removal rate
- Low power consumption
- Good life of tool and wear rate is very low
- Good surface finish
- Minimum idle time

4.2 Mechanical Properties

4.2.1 Tensile strength

The stress-strain graphs of tempered and untempered specimens as shown in Figure17 (c) indicate that the values of tensile strength of tempered specimens had significantly reduced as compared to untempered specimen. Results depicted that the peak value of tensile strength specimen tempered at 500°C was observed as 680.42 MPa. Further it was noticed that the tensile strength was minimum in the specimens tempered at 700°C. However, percentage elongation was found to be maximum in the specimen tempered at 700°C. From archival literature it was observed that the grain size of the specimens tempered at higher temperature become large [118,128].

4.2.2 Hardness Properties

The hardness tests were performed on each specimen of EN-36C alloy steel of tempered and untempered specimens. The average hardness values of untempered and tempered specimens with respect to temperatures were represented in Figure17 (a). It can be seen from the bar chart graph that values of hardness get increased slightly at tempering temperature of 300ºC and 700°C [129].Causes of this variation was due to the change in the microstructures of the alloy steel during the tempering [118,136]

4.2.3 Toughness Properties

The Impact tests of each specimen of EN-36C alloy steel were evaluated and tabulated in the Table 5.It has been seen that there is a less significant effect of tempering temperature on the hardness, but has a more significant effect on the toughness properties of EN-36C alloy steel.

From Figure17 (b), it can be seen clearly that the values of toughness of tempered specimens get increased first and reached to the maximum value and again reached to minimum values of toughness at tempering temperature of 700ºC [129].The effect of tempering causes the change in microstructure in the specimen as well as little bit change in hardness. But its dominating effect has been seen on specimen tempered at 500°C.

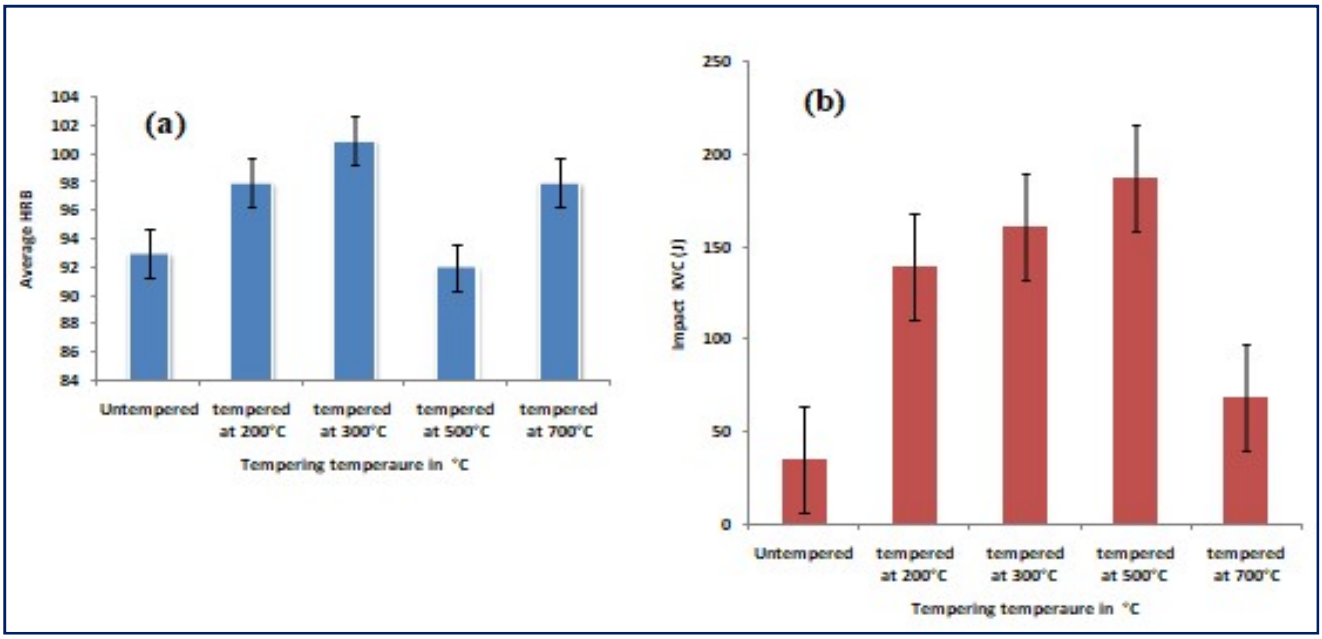

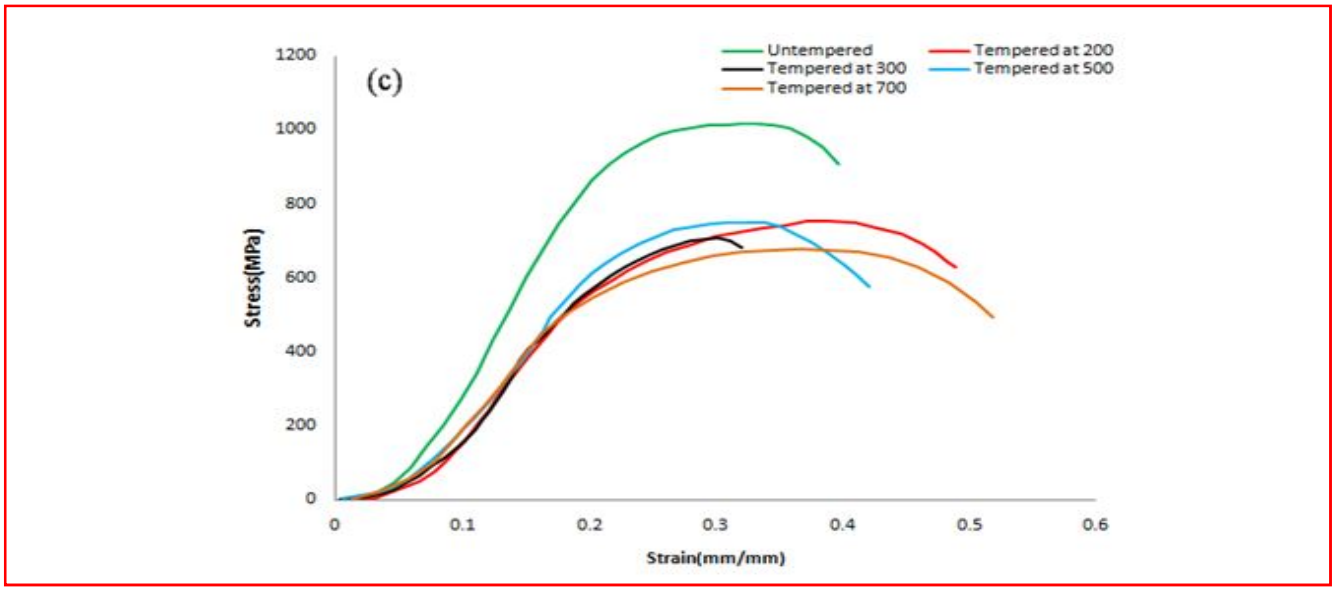

Fig.17: The graph of Mechanical properties of tempered and untempered steel alloy of EN-36C
(a) Hardness test bar chart (b) Impact test bar chart(c) Tensile test

4.3 Surface Roughness

The average surface roughness (R_a), root mean square value of surface roughness (R_q), and peak to valley height value of surface roughness (R_z) of all turned specimens which is shown in Table 6 is represented in the form of bar chart shown in Figure 18, Figure 19 and Figure 20 respectively. It could be seen from bar graph that the surface roughness Ra, R_q and R_z of turned specimen tempered at 500°C has minimum values 1.93µm, 2.36µm and 10.30µm respectively as compared to other all tempered and untempered specimens. The surface roughness profiles of untempered and tempered specimens are shown in Figure21 (a) and (b) respectively.

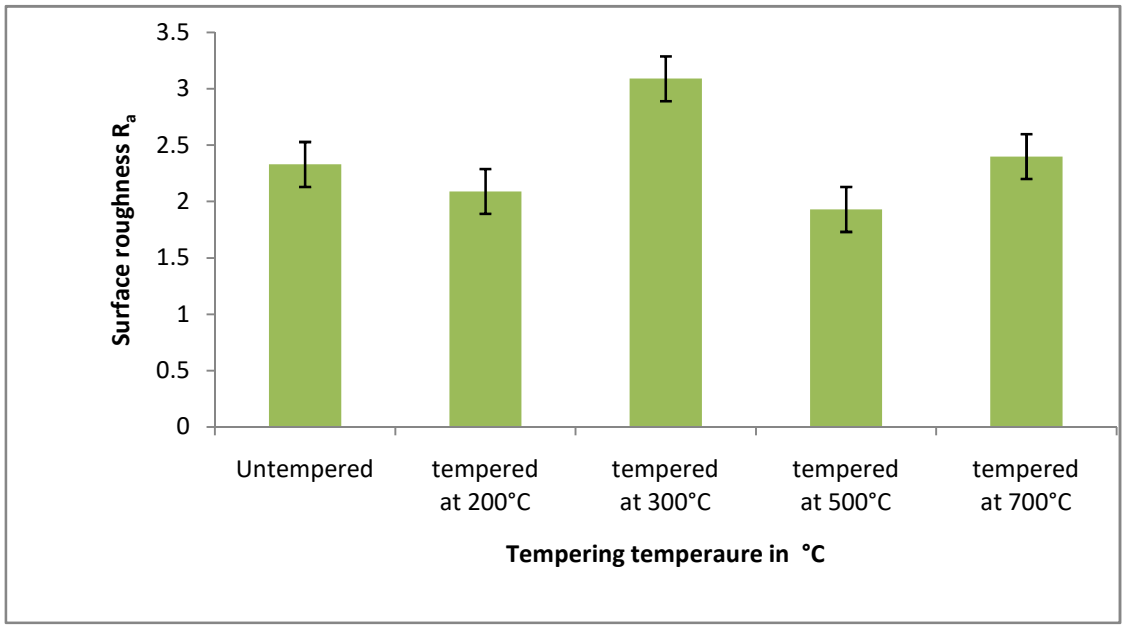

Fig.18: Surface roughness (R_a) of untempered and tempered specimens

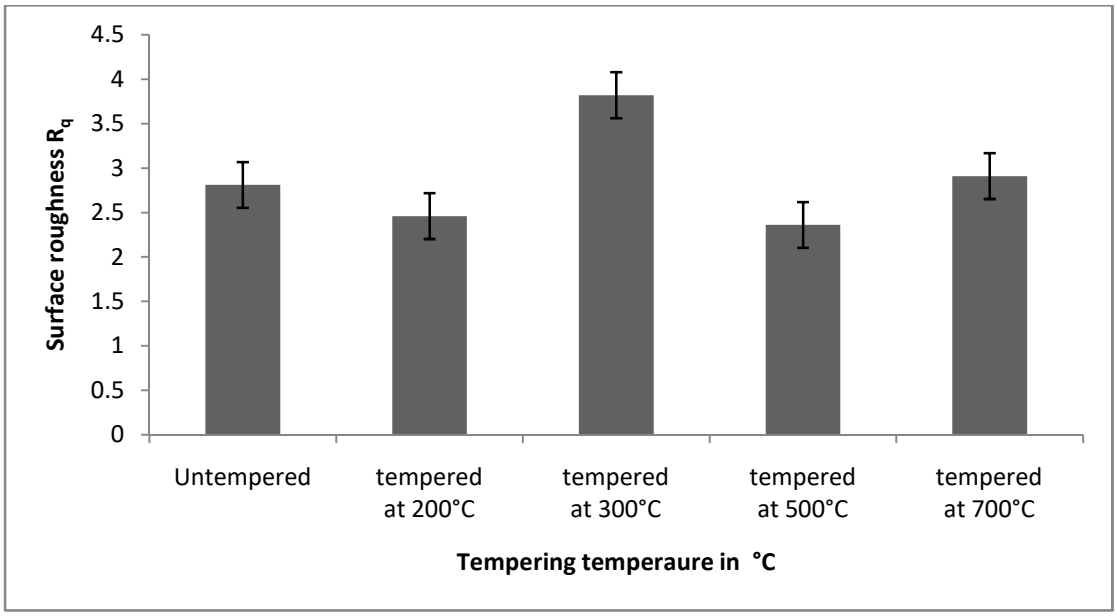

Fig.19: Surface roughness (R_q) of untempered and tempered specimens

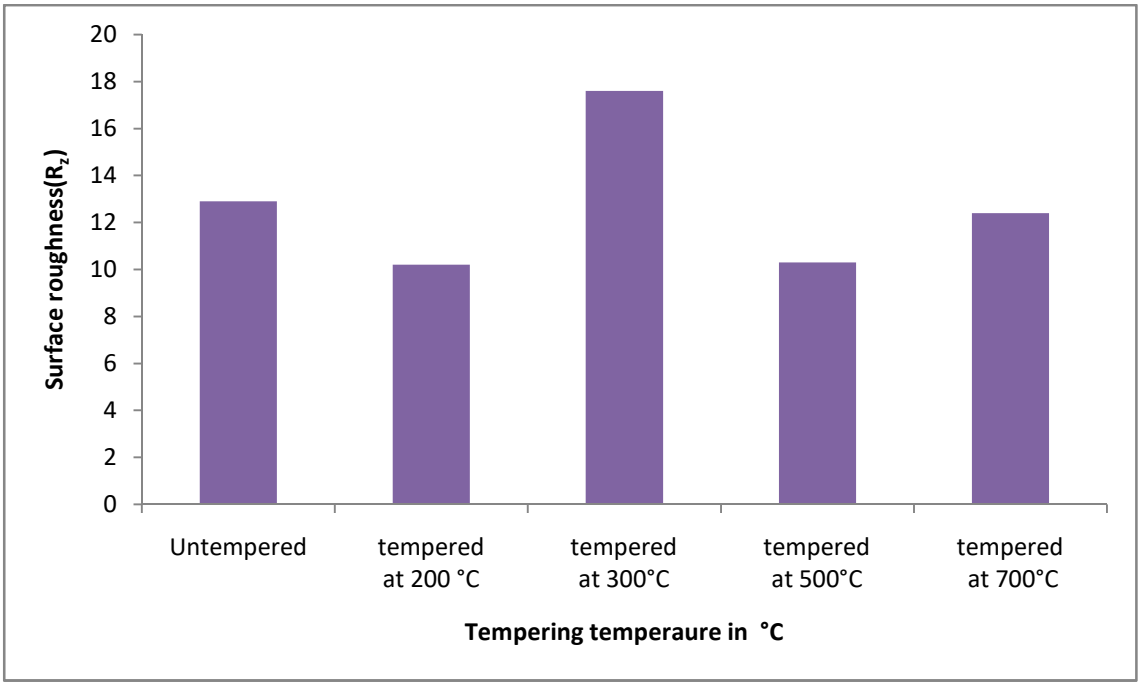

Fig.20: Surface roughness (R_z) of untempered and tempered specimens

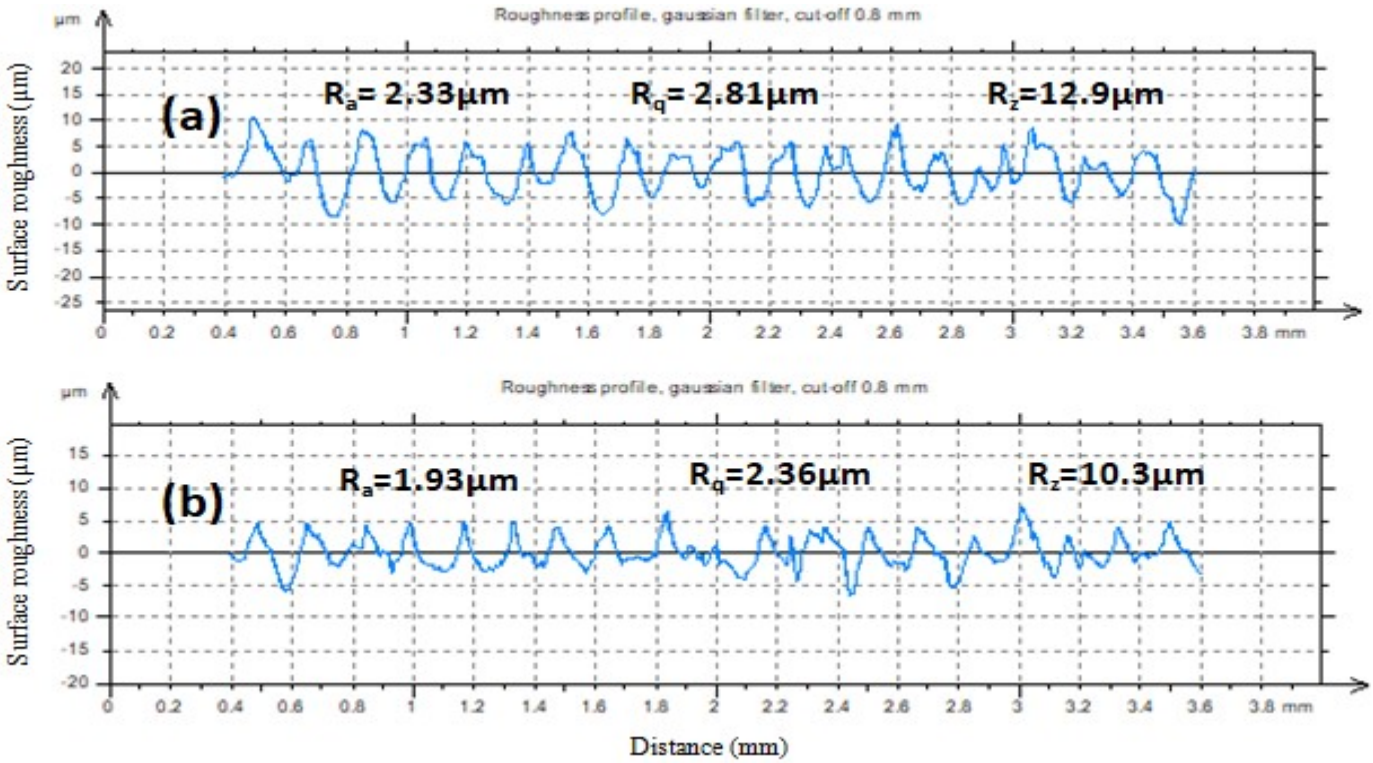

Fig.21: Roughness profile for specimen (a) Untempered (b) Temperedat 500ºC

CHAPTER 5

Statistical Analysis

This chapter discusses the design of experiments using Response Surface Methodology (RSM), utilizing statistical analysis and ANOVA to understand the process. The optimum process parameters were selected for minimum surface roughness, residual stress and tool wear and maximum material removal rate for demonstrating the effectiveness of the method in achieving desired results.

5.1 Design of Experiments

A well-planned experimentation is crucial for clear and accurate conclusions from preliminary observations. The experimental design is an effective method for inferring conclusions from variable observations, guiding data collection, and developing accurate findings and interpretations. Response surface methodology (RSM) was used for the current experiments, resulting in the best response. Organization of trials according to the experimental design offers several benefits, including improved accuracy, better results, and improved interpretation.

(a)The process involves identifying key decision factors that significantly influence and enhance the effectiveness of a product or process.

(b) There have been significantly fewer trials conducted.

(c)The text focuses on determining the ideal configuration parameters.

(d) The task involves determining the experimental error.

(e) The impact of parameters on the process's features can be analysed and conclusions have been drawn.

5.2 Response Surface Methodology

Response surface methodology (RSM) is a group of mathematical and statistical methods that can be used to analyze issues when various independent factors have an impact on a dependent variable or response. The response will be optimized as a result. The independent variables, which are continuous and subject to negligible error control by the experimenter, are considered to be y_1, y_2, y_3,...,y_k. It is assumed that the response "x" is a random variable. This method explains how a specific response is impacted by a particular set of input factors and what level the input variables should be regulated to give the product the intended specifications. The following diagram illustrates the relationship between the dependent and independent variables:

$$X = f(y_1, y_2, y_3, \ldots\ldots\ldots, y_k) + \varepsilon \quad (2)$$

Where ε displays the noise or error that was seen in the response "x."

If the anticipated response is indicated by:

$$E(x) = f(y_1, y_2, y_3, \ldots\ldots\ldots, yk) = \eta \quad (3)$$

Thereafter, the surface symbolized by:

$$H = f(y_1, y_2, y_3, \ldots\ldots\ldots, y_k) \quad (4)$$

The surface is formed by factors and responses with levels "m" indicated by variables y_1, y_2, y_3,..., y_k. The surface characteristic with the most interest is x_1, where m is the maximum or minimum. ε represents the noise or error in response "x."

The response surface methodology begins by determining the functional connection between y and independent variables using a low order polynomial. The first order model is used as the approximation function if the answer can be accurately predicted using the equation

$$x = \alpha_0 y_0 + \alpha_1 y_1 + \alpha_2 y_2 + \ldots + \alpha_k x_k + \varepsilon. \quad (5)$$

If the system is curved, a higher degree polynomial, like a second order model, must be used.

$$x = \alpha_0 y_0 + \sum_{i=1}^{k} \alpha_i y_i + \sum_{i=1}^{k} \alpha_i y_i^2 + \sum_{i<j} \alpha_{ij} y_i y_j + \varepsilon \quad (6)$$

The majority of issues with response surface methodology are related to one of these models, specifically response surface design, which refers to designs for fitted response surfaces.

5.3 First order design

The response surface is fitted using first-degree polynomials in this particular case.

$\eta=\alpha_0 y_0+\alpha_1 y_1+\alpha_2 y_2+\ldots\ldots\ldots\ldots\ldots+\alpha_k y_k$ (7)

The 2k factorial design in single or fractional replication is useful for fitting a linear relationship between response and variables in exploratory work, as fractional designs do not estimate experimental error variance. This can be obtained as

a) The experiments will be conducted again.

b) If there is strong evidence that error variance remains constant over time, using a prior experiment's estimate can be used.

c) The 2k factorial is increased by adding multiple tests at the point where all 'x' values are '0' on the coded scale.

5.4 Second order design

Second degree polynomials typically have the following form as

$x = (a_0 y_0 + a_1 y_1 + a_2 y_2 + \ldots\ldots + a_k y_k) + (a_{12} y_1 y_2 + a_{13} y_1 y_3 + \ldots\ldots\ldots + a_{K-1} y_{K-1} y_k) + (a_{11} y_1^2 + a_{22} y_2^2 + \ldots\ldots + a_{kk} y_k^2)$ (8)

The equation outlines linear, squared, and cross product terms for regression coefficient estimation. A 3k factorial design is required for each variable, but it necessitates extensive testing when using more than three variables, despite its potential drawback.

5.5 Non Central composite design

This design style has k extra points for each element, and can be used when 2k factorial trials show the point of highest reaction is near one of the factor combinations.

5.6 Rotatable Second order design

The design ensures that the standard error remains constant for all locations within a region's centre, irrespective of the distance from the region's centre. If the study centre is (0, 0, 0), any point on the fitted surface can specify the standard errors of Y from any experimental result. The error value remains constant for all k distances from the region's centre due to rotatability requirements.

$$y_1^2 + y_2^2 + y_3^2 + \ldots + y_k^2 = k^2 = \text{constant} \quad (9)$$

5.7 Analysis of Variance

Analysis of variance (ANOVA) is a crucial technique used in various fields to analyse the variance between two samples. It is used when multiple samples mean need to be examined simultaneously, making it a valuable analytical tool. ANOVA was first used by Professor R.A. Fisher, who developed a complex theory explaining its practical application. Later, Professor Snedecor and others contributed to its development. ANOVA is primarily used to evaluate the homogeneity of differences between different sets of data, with the fundamental idea being to separate the entire variation. This method is essential for determining if samples came from populations with the same mean.

ANOVA is a statistical technique used to analyse variations within and between samples. It divides variance into subsets for analytical purposes, breaking down components of variance into distinct components. This method is used to determine which cutting input factors have the greatest influence on machined surface quality and tool wear. Developed by Professor Snedecor, ANOVA primarily evaluates the homogeneity of differences between data sets, aiming to separate the entire variation.

Present work utilizes central composite design (CCD) under response surface methodology to design the experiments based on the preliminary study. In this regression analysis, the significance of process parameters such as cutting speed (V), depth of cut (d) and feed rate (f) on output responses like material removal rate (MRR), tool wear and residual stresses are investigated. The level and ranges of the selected process parameters are given in Table 8. The

effects of machining parameters on various responses were tested with the use of a central composite design (CCD). According to RSM, parameters and their levels, along with 20 numbers of run orders with responses, were reported in Table 9.

Table 8: Design of experimentation for Process parameters

Parameters	Units	-2 Lowest	-1 Low	0 Center	+1 high	+2 highest
cutting speed(V)	rpm	250	400	550	700	850
feed rate *(f)*	mm/rev	0.08	0.12	0.16	0.20	0.24
depth of cut (d)	mm	0.5	1.0	1.5	2.0	2.5

Table 9: Design matrix layout and experimental results

Run order	Process Parameters			Responses		
	Cutting speed (rpm)	Feed rate (mm/rev)	Depth of cut(mm)	Residual stress(σ_r) MPa	Tool wear, $T_{w\,(}$mm)	MRR g/min
1	550	0.16	1.5	275	0.075	54.3
2	550	0.16	1.5	275	0.076	54.3
3	250	0.16	1.5	180	0.04	26.3
4	700	0.12	2	350	0.097	66.7
5	550	0.08	1.5	200	0.055	45
6	550	0.16	1.5	270	0.079	54.3
7	550	0.16	1.5	270	0.075	54.3
8	550	0.16	1.5	269	0.075	54.3
9	850	0.16	1.5	435	0.165	97.3
10	700	0.20	2	360	0.145	112.3
11	550	0.16	2.5	295	0.11	84.3
12	400	0.12	2	230	0.043	37.1
13	700	0.20	1	360	0.112	55.5
14	400	0.12	1	210	0.044	25

15	700	0.12	1	300	0.097	38.5
16	550	0.24	1.5	325	0.097	84.3
17	550	0.16	0.5	240	0.069	24.8
18	400	0.20	1	219	0.065	34.6
19	400	0.20	2	280	0.084	59.6
20	550	0.16	1.5	239	0.067	43.9

5.8 Analysis of residual stress

As shown in Tables 10 and 11, respectively, the residual stress data are analyzed using ANOVA both before and after insignificant factors are removed. Using RSM as a backward elimination technique, all of the insignificant terms are removed as shown in Table 11. Terms are significant if $p < 0.05$; otherwise, they are insignificant. Fits are not significant because ($p > 0.05$). The responses of each factor at a particular level are predicted using an equation based on real factors.

Table 10**:** Analysis of variance for residual stresses

Source	Sum of Squares	D_f	Mean Square	F-value	p-value	
Model	71532.53	9	7948.06	19.87	< 0.0001	Significant
V	55342.56	1	55342.56	138.38	< 0.0001	
f	8977.56	1	8977.56	22.45	0.0008	
d	3630.06	1	3630.06	9.08	0.0131	
V*f	15.12	1	15.12	0.0378	0.8497	
V*d	120.12	1	120.12	0.3004	0.5957	
f*d	10.12	1	10.12	0.0253	0.8767	
V^2	3292.37	1	3292.37	8.23	0.0167	
f^2	0.9383	1	0.9383	0.0023	0.9623	
d^2	52.37	1	52.37	0.1309	0.7250	
Residual	3999.27	10	399.93			

Lack of Fit	3067.93	5	613.59	3.29	0.1084	Insignificant
Pure Error	931.33	5	186.27			
Cor Total	75531.80	19				
Std. Dev	20.00		R^2 = 0.9471			
Mean	279.10		Adjusted R^2 = 0.8994			
C.V. %	7.17		Predicted R^2 = 0.6670			
			Adeq precision = 17.7858			

In Table10 sources likeV*f, V*d, f*d, f^2 and d^2 are found insignificant. After backward elimination method, these insignificant terms get reduced as shown in Table 11.Table 11 of the ANOVA indicates that cutting speed significantly contribute (77.58%) and feed rate (12.58%) to residual stresses, whereas depth of cut (5.08%) respectively. It was discovered that the residual stress value anticipated by this model was 180.528 MPa.

Table11: ANOVA for reduced quadratic model of residual stresses after backward elimination

Source	Seq SS	D_f	Adj MS	F-value	p-value	Cont. (%)	
Model	71334.44	4	17833.61	63.73	< 0.0001	-	Significant
V	55342.56	1	55342.56	197.78	< 0.0001	77.58	
f	8977.56	1	8977.56	32.08	< 0.0001	12.58	
d	3630.06	1	3630.06	12.97	0.0026	5.08	
V^2	3384.25	1	3384.25	12.09	0.0034	4.74	
Residual	4197.36	15	279.82			-	
Lack of Fit	3266.03	10	326.60	1.75	0.2781	-	Insignificant
Pure Error	931.33	5	186.27			-	
Cor Total	75531.80	19	R^2 = 0.9444				
Std. Dev	16.73		Adjusted R^2 =0.9296				
Mean	279.10		Predicted R^2 = 0.8767				
C.V. %	5.99		Adeq precision= 29.7288				

The final equation after the backward elimination process is given in Eq. (10).

Residual stress (σ_r) = +64.55801-0.153243 V+592.18750 f+30.12500 d+0.000496V^2 (10)

5.9 Analysis of Tool wears

Table 12 displays the ANOVA results for tool wear generated by the RSM with all significant and insignificant terms. Table 13 displays the modified ANOVA results for tool wear after insignificant terms were removed using the backward elimination method. It is evident that terms such as V, f, d, V*f, V*d, V^2, and d^2 are significant ($p < 0.05$) and that the lack of fits, f*d, f^2 are insignificant since ($P > 0.05$). The values of Predicted R^2 (0.9513) and Adjusted R^2 (0.9785) are fairly close to each other, and less than 0.2 indicates good agreement between them.

Table 12: Analysis of variance for tool wear

Source	Sum of Squares	D_f	Mean Square	F-value	p-value	
Model	0.0214	9	0.0024	100.41	< 0.0001	Significant
V	0.0156	1	0.0156	660.42	< 0.0001	
f	0.0019	1	0.0019	79.98	< 0.0001	
d	0.0018	1	0.0018	74.56	< 0.0001	
V*f	0.0001	1	0.0001	6.11	0.0330	
V*d	0.0003	1	0.0003	13.21	0.0046	
f*d	0.0000	1	0.0000	1.71	0.2200	
V^2	0.0014	1	0.0014	58.52	< 0.0001	
f^2	0.0000	1	0.0000	0.6724	0.4313	
d^2	0.0004	1	0.0004	18.48	0.0016	
Residual	0.0002	10	0.0000			
Lack of Fit	0.0002	5	0.0000	1.98	0.2363	Insignificant

Pure Error	0.0001	5	0.0000
Cor Total	0.0216	19	R^2 = 0.9891
Std. Dev	0.0049		Adjusted R^2 =0.9792
Mean	0.0853		Predicted R^2 = 0.9402
C.V. %			Adeq precision= 37.2652

Table 13: ANOVA for quadratic model of tool wear after backward elimination regression

Source	Seq SS	D_f	Adj MS	F-value	p-value	Cont. (%)	
Model	0.021	7	0.0030	138.77	< 0.0001	-	Significant
V	0.0156	1	0.0156	687.89	< 0.0001	74.28	
f	0.0019	1	0.0019	106.50	< 0.0001	9.04	
d	0.0018	1	0.0018	98.25	< 0.0001	8.57	
V*f	0.0001	1	0.0001	8.64	0.0316	0.47	
V*d	0.0003	1	0.0003	14.80	0.0038	1.42	
V^2	0.0014	1	0.0014	62.73	< 0.0001	6.66	
d^2	0.0004	1	0.0004	19.52	0.0013	1.90	
Residual	0.0003	12	0.0000			-	
Lack of Fit	0.0002	7	0.0000	1.99	0.2455	-	Insignificant
Pure Error	0.0001	5	0.0000			-	
Cor Total	0.0216	19	R^2 = 0.9864				
Std. Dev	0.0049		Adjusted R^2 =0.9785				
Mean	0.0853		Predicted R^2 =0.9513				
C.V. %	5.80		Adeq precision= 41.8778				

Final regression equation after backward elimination is given by Eq. (11).The equation based on actual factors is used for predicting the responses of each factor for given levels.

Tool wear (T_w) = +0.026556-0.000158V+0.661458f-0.072833d-0.000708V*f +0.000083V*d+ 3.22222E-07 V^2+0.016000 d^2 (11)

5.10 Exposition of material removal rate (MRR)

Tables 14 and 15 represent the ANOVA results of MRR before and after eliminating the insignificant terms like V*f, V^2, d^2 by the backward elimination method, respectively. The terms in Table 15 are significant, and lack of fit is found to be insignificant, which is desired for the adequacy test. The values of $R^2 = 0.9553$ and Adjusted $R^2 = 0.9347$ are quite close to each other, which shows good agreement between turning parameters and response MRR.

Table 14: Analysis of variance for material removal rate

Source	Sum of Squares	D_f	Mean Square	F-value	p-value	
Model	10540.48	9	1171.16	42.53	< 0.0001	Significant
V	4182.86	1	4182.86	151.91	< 0.0001	
f	1877.06	1	1877.06	68.17	< 0.0001	
d	3633.08	1	3633.08	131.95	< 0.0001	
V*f	116.28	1	116.28	4.22	0.0669	
V*d	286.80	1	286.80	10.42	0.0091	
f*d	215.28	1	215.28	7.82	0.0189	
V^2	88.71	1	88.71	3.22	0.1029	
f^2	168.78	1	168.78	6.13	0.0328	
d^2	0.1092	1	0.1092	0.0040	0.9510	
Residual	275.34	10	27.53			
Lack of Fit	185.21	5	37.04	2.05	0.2241	Insignificant
Pure Error	90.13	5	18.03			
Cor Total	10815.83	19	$R^2 = 0.9745$			
Std. Dev	5.25		Adjusted R^2 =0.9516			
Mean	55.33		Predicted R^2 =0.8535			
C.V. %	9.48		Adeq precision= 24.6509			

Table 15: ANOVA for reduced quadratic model of MRR after backward elimination

Source	Seq SS	D_f	Adj MS	F-value	p-value	Cont.(%)	
Model	10332.5	6	1722.08	66.32	< 0.0001	-	Significant
V	4182.86	1	4182.86	192.57	< 0.0001	40.48	
f	1877.06	1	1877.06	88.69	< 0.0001	18.16	
d	3633.08	1	3633.08	163.72	< 0.0001	35.16	
V*d	286.80	1	286.80	15.71	0.0157	2.77	
f*d	215.28	1	215.28	9.79	0.0317	2.08	
f^2	137.43	1	137.43	9.77	0.0267	1.33	
Residual	483.33	13	37.18			-	
Lack of Fit	393.19	8	49.15	2.73	0.1421	-	Insignificant
Pure Error	90.13	5	18.03			-	
Cor Total	10815.8	19					
Std. Dev	3		$R^2 = 0.9553$				
Mean	6.10		Adjusted $R^2 = 0.9347$				
C.V. %	55.33		Predicted $R^2 = 0.8676$				
	11.02		Adeq precision= 24.3476				

Final equation after backward elimination regression is given in Eq. (12). The equation based on actual factors is used for predicting the responses of each factor for given levels.

$$MRR=+69.79730-0.011958V-567.84007f-55.27083d+0.079833V*d+259.37500\ f*d+1404.87132\ f^2 \quad (12)$$

CHAPTER-6

Microstructural Analysis of tempered and untempered EN-36C

This chapter elaborates scanning electron micrographs (SEM) and optical microscope obtained with CNC turned surfaces of tempered and non-tempered work piece of EN-36C alloy steel at optimum process parameters have been studied.

6.1 SEM Analysis

The composition and microstructural analysis of EN-36C have been done by Energy Dispersive X-ray Analysis (EDAX) using a scanning electron microscope (SEM). Figure 22(c) shows the microstructure of the specimens tempered at 500ºC (for 2h). The martensite and retained austenite microstructure has been obtained after tempering process at 300°C and 500°C (for 2h). It was observed that untempered specimens have ferrite (white) and pearlite (black) as the two major constituents in their microstructure as shown in Figure 22 (a). Further, optical micrographs show that the specimen tempered at 200°C has needle (like bainite) microstructure having good mechanical properties.

The specimens tempered at 300 and 500°C (for 2h) show better mechanical properties than the specimen tempered at 200°C [4, 34].

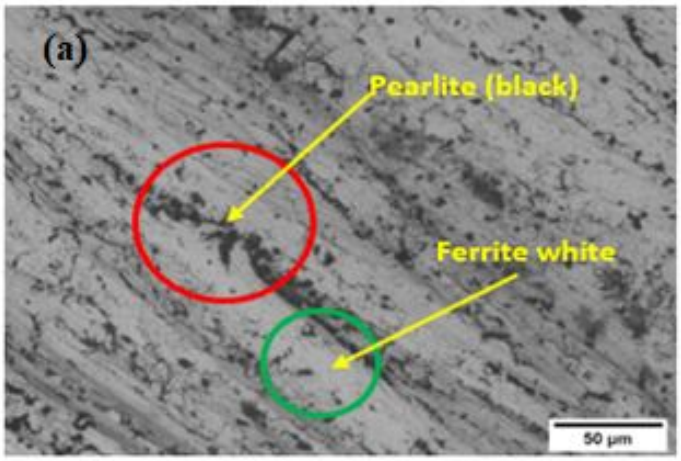

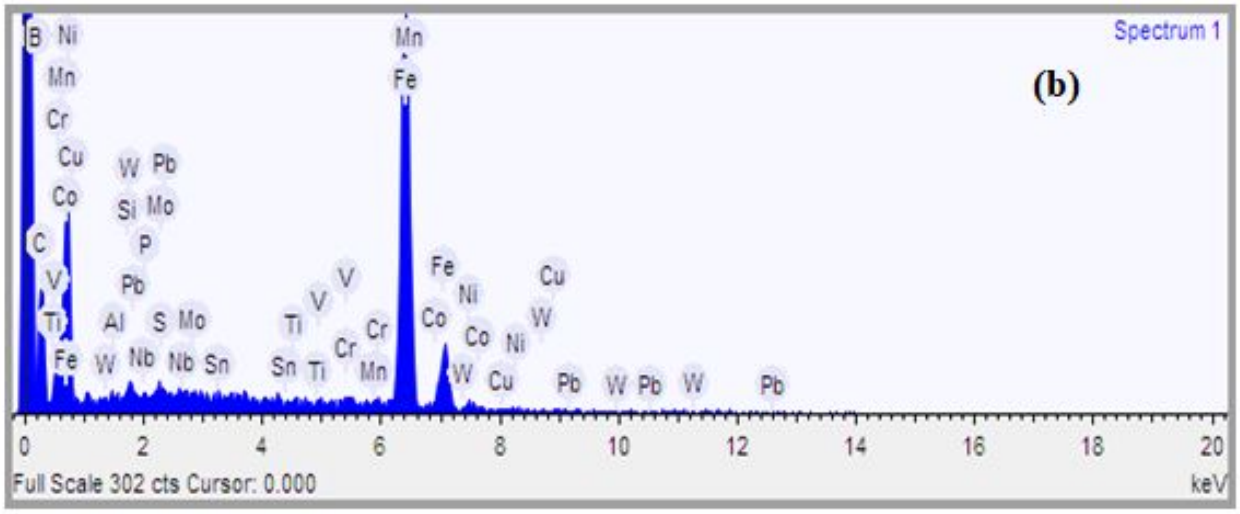

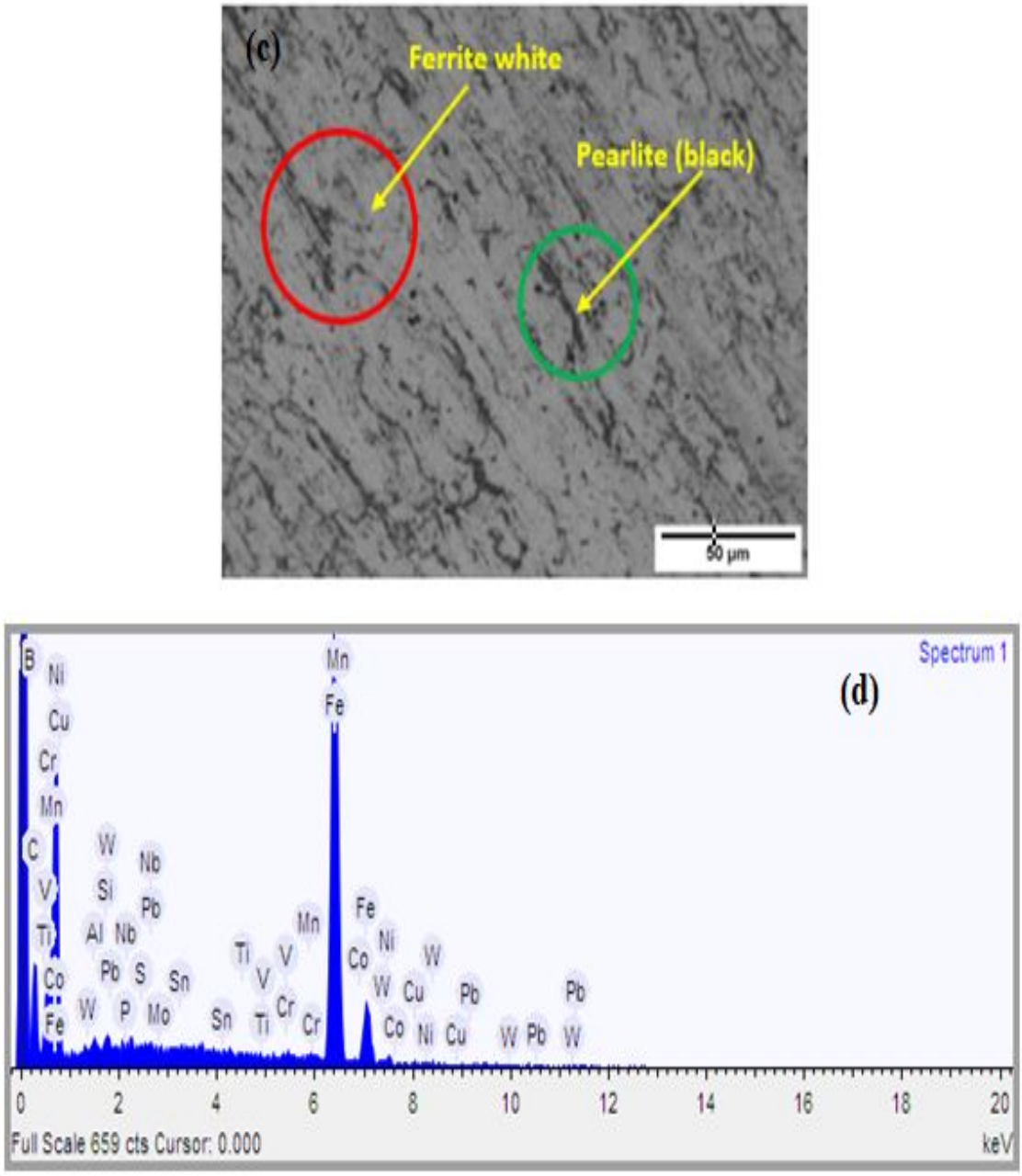

Fig.22: SEM of untempered EN-36C (a) Microstructure (b) EDAX (c) Microstructure of tempered EN-36C (d) EDAX of tempered EN-36C

6.2 Optical Microscope Analysis

In order to examine the microstructures of alloy steel (EN-36C), a tiny piece with a diameter of 30 mm was created using the conventional procedures of sanding, polishing, and etching. The microstructures were captured on camera using an optical microscope set to 100X magnification. Figure 23(a) and (b) display images. From a literature survey, it was found that the behavior of mechanical and microstructural properties changes significantly after tempering the sample in a controlled manner [132]. It has been observed prickly martensite structure from microstructural image. The white parts seen in the images are partial ferrite and residual austenite [132]. Tempering, often called "drawing," is the process of applying a regulated heat treatment to normalized and hardened steels to increase their ductility and toughness while reducing their hardness and improving their dimensional stability. The previously quenched martensite changes into tempered martensite by solid-state reactions during the tempering process. Tempered martensite is made up of soft ferrite matrix with finely scattered cementite (carbides) spheroids at higher tempering temperatures. As a result of this change, toughness increases and hardness decreases. The main objective is to ensure that carbides precipitate by progressively reducing the hardness to the required level and then chilling to stop the solid-state processes. The degree of tempering effects depends on the temperature and duration of the process [133,134].The tempering process can be carried out at temperatures below the lower critical temperature (Ac1). Tempering takes place for at least one hour on average. For a variety of carbon and alloy steels, SAE AMS 2759 offers recommended tempering conditions and heat-treating cycles. To attain a tangential compressive residual stress condition on the component's surface while maintaining allowable levels of distortion, quick cooling techniques may be used in some production scenarios after tempering. The white portion of the tempered sample's microstructure can be plainly observed to be much larger than that of the untempered sample. The reason for the increase in toughness and ductility, which improve machinability, is the microstructure that is left behind from the tempering process.

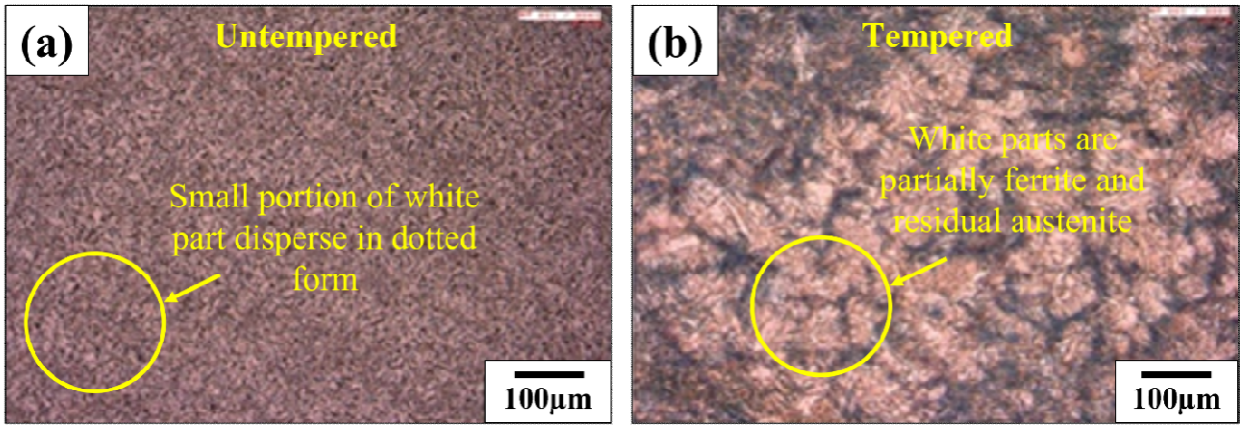

Fig.23: Microstructure of (a) Untempered EN-36C (b) Tempered EN-36C

CHAPTER 7

Study of residual stresses

This chapter explains the residual stress of CNC turned surfaces of tempered and untempered EN-36C alloy steel using an X-ray residual stress analyzer. The process is analyzed using response surface methodology and ANOVA. The optimal process parameters are obtained for the response percentage reduction in residual stress.The regression analysis investigates the significance of process parameters like cutting speed (V), feed rate (f) and depth of cut (d) and tempering temperature on the output response percentage reduction in residual stress (%ΔRS).

7.1 Study of Residual stresses

Residual stress on the work-piece surface, caused by various machining techniques, negatively impacts manufactured components due to factors like temperature changes, volume changes, resolidification, melting, and phase transformations. This reduces product reliability and increases the likelihood of product failure. Research on residual stress is crucial to improve product reliability, and various categories of residual stress measurement methodologies (NDT) have been used to categorize these tests.

7.2 Destructive and non destructive technique

Residual stress measurements can be done using destructive and non-destructive methods. Destructive methods involve removing a small portion of a part to understand stress relaxation, such as hole drilling, core drilling, stripping, and contour method. These methods are easy to execute and provide accurate results, but can cause unacceptable surface damage when assessing critical components. Non-destructive methods, such as X-ray, neutrons, synchrotron radiation, and magnetic strain, have been developed to prevent such damage [138]. X-ray diffraction (XRD) is preferred for measuring residual stress near surfaces due to its low penetration depth, while neutron diffraction provides volumetric stress fields due to its high penetration depth.

X-ray diffraction (XRD) is a method used to calculate stresses in materials. The sin 2Ψ method involves scanning along defined incident angles over a pre-determined diffraction angle,

requiring accurate verification of the selected diffraction peak position. The obtained 2θ values are then used in linear regression to obtain slope and intercept values for stress calculation. Line detectors are typically used in sin 2Ψ method, which captures a small part of the Debye-Scherrer (D-S) ring at every incident angle. However, the cos α method, where α represents the azimuthal angle, has gained attention as a new method to measure residual stress. This method uses the entire D-S ring from a single exposure of X-rays at a single incident X-ray beam angle, offering advantages such as simpler optical setup and faster in-plane normal and shear stress calculations [139].

7.3 X-ray residual stress measurement system

The measurements of residual stress were done by μX-360 pulstec machine (Japanese built) as shown in Figure24.

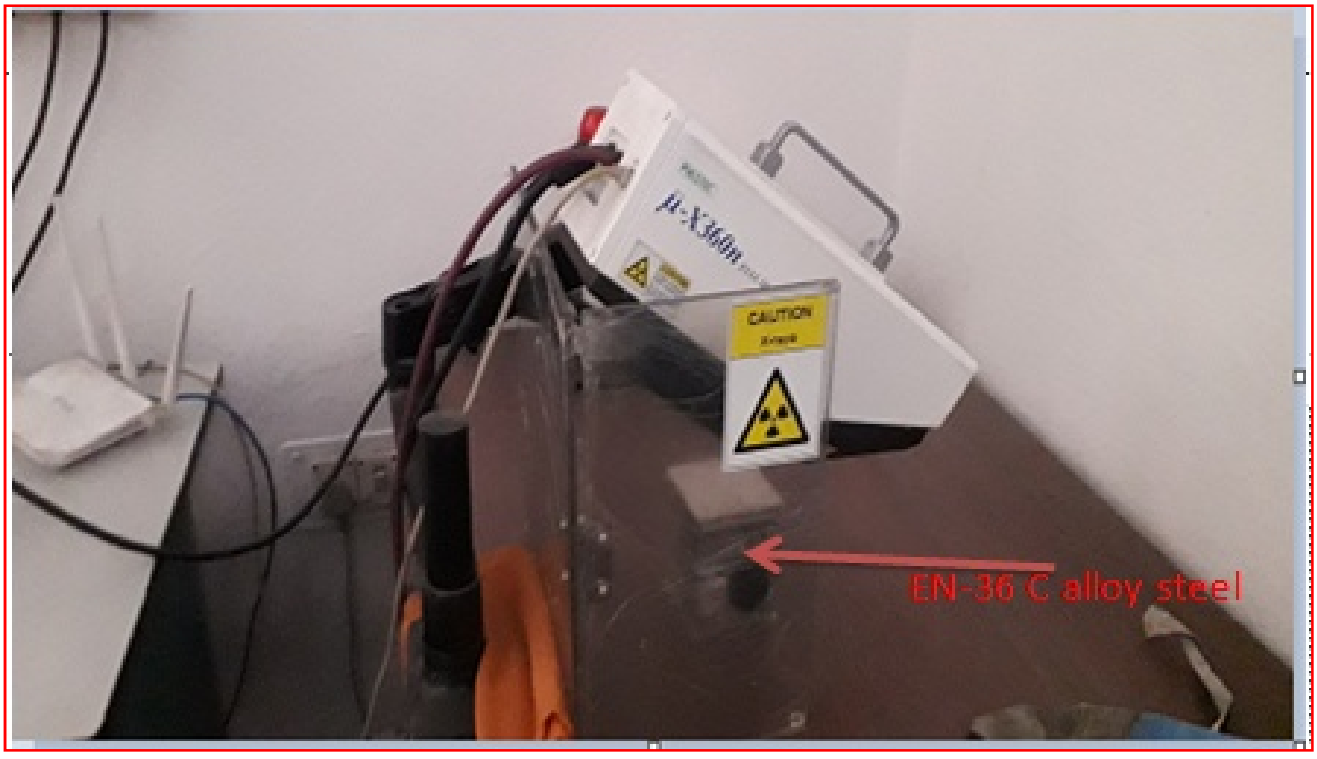

Fig.24: Residual stress measurement system with position of EN-36C

The machine consists of a computer, sensor unit and power unit, generating X-rays in 90 seconds. It uses a 30KV X-ray tube, a 2-D X-ray sensor, and a power supply unit to measure

residual stress. The machine has an air conditioning element for efficient operation. The sample is 38mm away from X-ray focusing lens, and the X-ray tube current is 1mA. The specimen is studied for its lattice constant, inter-planar spacing, diffraction planes, crystal structure, poison's ratio, and Young's modulus. The incidence angle for X-rays is fixed at 35 degrees. The machine requires an AC supply with specifications of 240V and 50/60Hz, but can be powered by a battery powered 24 V source. The machine has four stages for measuring residual stress as sample location and picture capturing, incidence of X-rays and detection by a 2-D sensor, residual stress computation, and output data results. The output reading also computes the standard deviation in the acquired reading to ensure repeatability.

7.4 X-ray Diffraction

Residual stress is calculated using X-ray diffraction scattering according to Bragg's law. As per Bragg's law equation is given below

$$n\lambda = 2h \sin\theta \quad (13)$$

The integer 'n' in this equation represents the order of reflection rays Wavelength coming from the source is denoted by λ, inter planar spacing in the crystal is denoted by h and θ represent angle of incidence as shown in Figure25.

The equation involves the order of reflection, incoming X-wavelength rays, crystal's inter-planar spacing, and angle of incidence. The difference in crystal orientation causes the

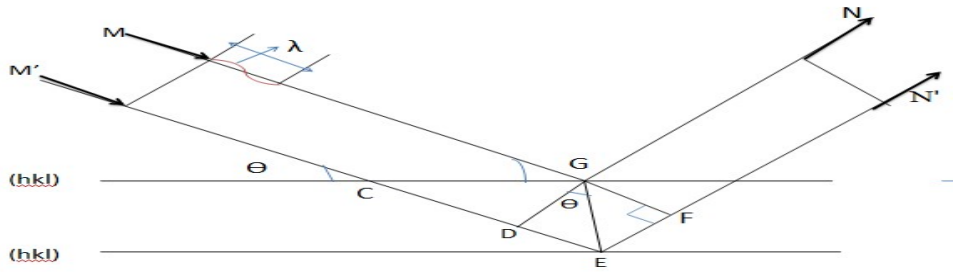

Fig.25: Diffraction of X-ray from work-piece surface

diffracted X-ray to form a cone around the incident X-ray axis, resulting in the Debye-Scherrer ring of residual stress which is shown in Figure26. This ring is produced by a single, brief X-ray

irradiation. The residual stress can be calculated by precisely measuring the Debye-Scherrer rings, which are a direct indicator of strain.

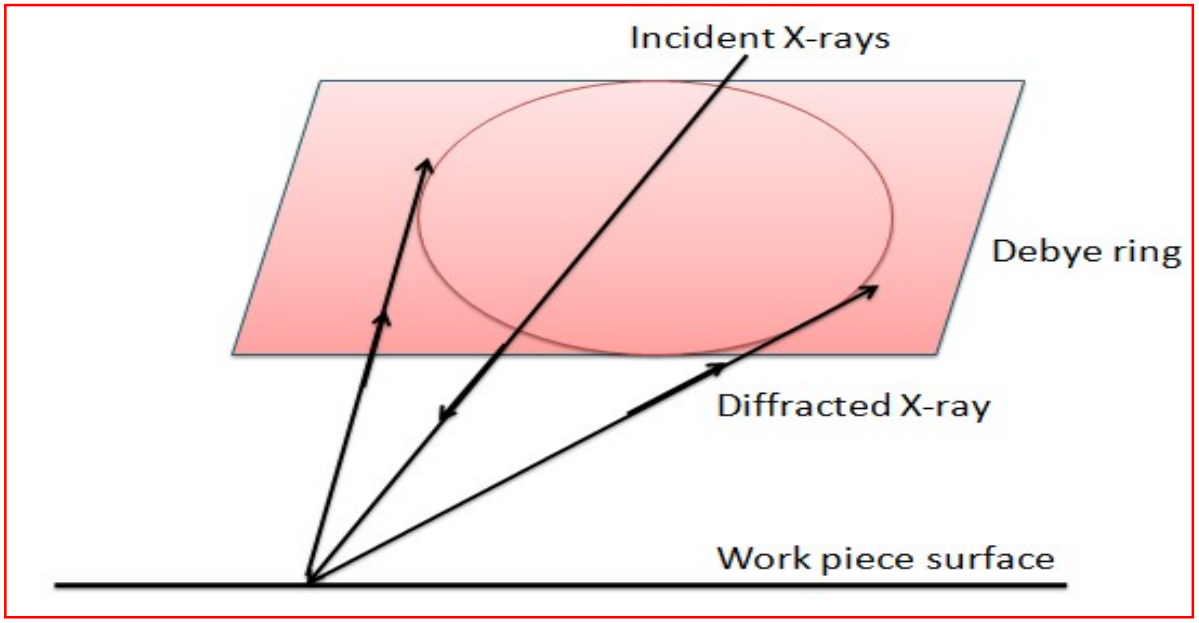

Fig.26: Formation of Debye-Scherer ring

7.5 Preliminary experimentation for residual Stress

Residual stresses may be tensile or compressive in nature. Further, it causes severe risks such as surface cracks and fatigue failure. It is very difficult to measure and model the characteristics of residual stresses of any machined parts. In various studies it has been found that many surfaces exhibit the compressive residual stresses [121,128] and too rare information is available for tensile residual stresses. The surface residual stresses of turned (tempered and untempered) specimens have been measured with the help of X-ray residual stress measurement system (μ-X360 Ver. 2. 3. 0. 1). The best experimental values of residual stresses are tabulated in Table 4. The residual stress behaviour, and Debye –scherrer rings for untempered and tempered at 500^{o}C specimens have been mentioned in Figure 27 (a-d) and 28 (a-d) respectively

Figure 27(a) and (b) shows the cosα and sinα diagrams respectively for untempered specimens. Further Figure 27(a) shows that the normal stresses which are compressive in nature. It can be further seen that the value of $\varepsilon_{\alpha 1}$is zero at cosα = 0 and minimum at cosα = 1.Figure 27(b) also shows the negative values of residual shear stresses of all specimens. Further, the value of strain$\varepsilon_{\alpha 2}$ is zero at sin α = 0 and minimum at sin α = 1.

Figure 27(c) and (d) shows the cosα and sinα diagrams respectively for tempered specimens. Further the Figure 27 (c) and (d) reveals that the values of normal and shear stresses are also negative for tempered specimens.

It is found that the value of normal residual stress of specimen tempered at 500°C has much lower value than the untempered specimen. It is also observed that other specimens tempered at 200°C, 300°C, 700°C have less residual stresses as compared to un tempered but more than the specimen tempered at 500°C. The experimental measured values of normal stresses are mentioned in Table4.

Figure28 (a) and (b) shows the Debye-Scherrer (D-S) rings of untempered specimen for 3-Dimensional (3-D) and 2-Dimensional (2-D) respectively by cosα methods. Further, Figure39 (c) and (d) shows the Debye-Scherrer (D-S) rings of tempered (at 500°C) specimen for 3-Dimensional (3-D) and 2-Dimensional (2-D) respectively by cosα methods. The full-width at half-maximum (FWHM) averaged values around the whole circumference of rings is indicated in each 2-D graph of D-S rings for both the cases Figure 28 (b) and Figure 28 (d). As shown in Figure 28 (b), the value of FWHM of untempered specimen was found to be 4.18°. The Figure 28(d), shows the FWHM of specimens tempered at500°C was measured as4.12°.TheFWHM confirmed the grain size of tempered and untempered specimens microstructure. The D-S ring of

untempered specimens has higher intensity irregularities than tempered specimens because untempered specimens have higher value of FWHM. Furthermore, it can also be seen explicitly in Figure 28(a-d) that the uniformity in D-S rings increases with tempering temperature [137].

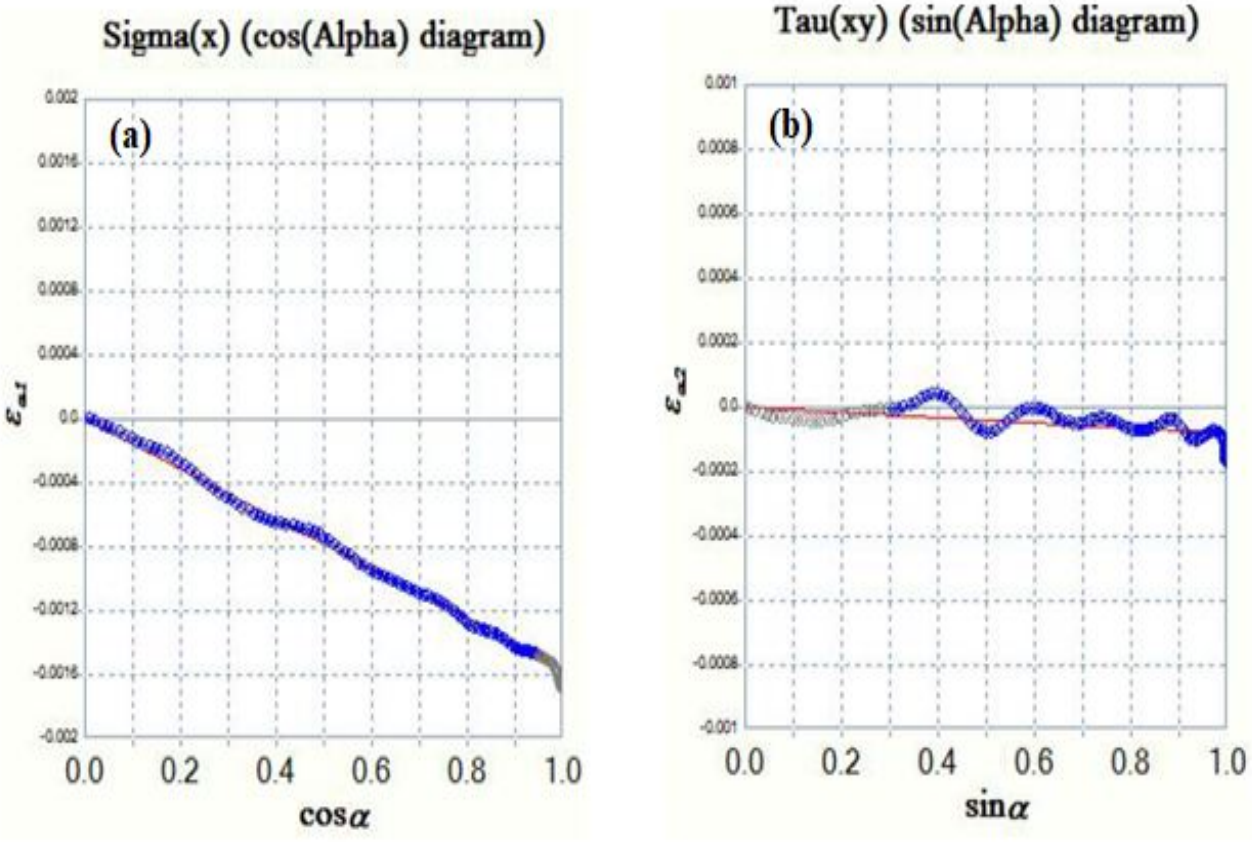

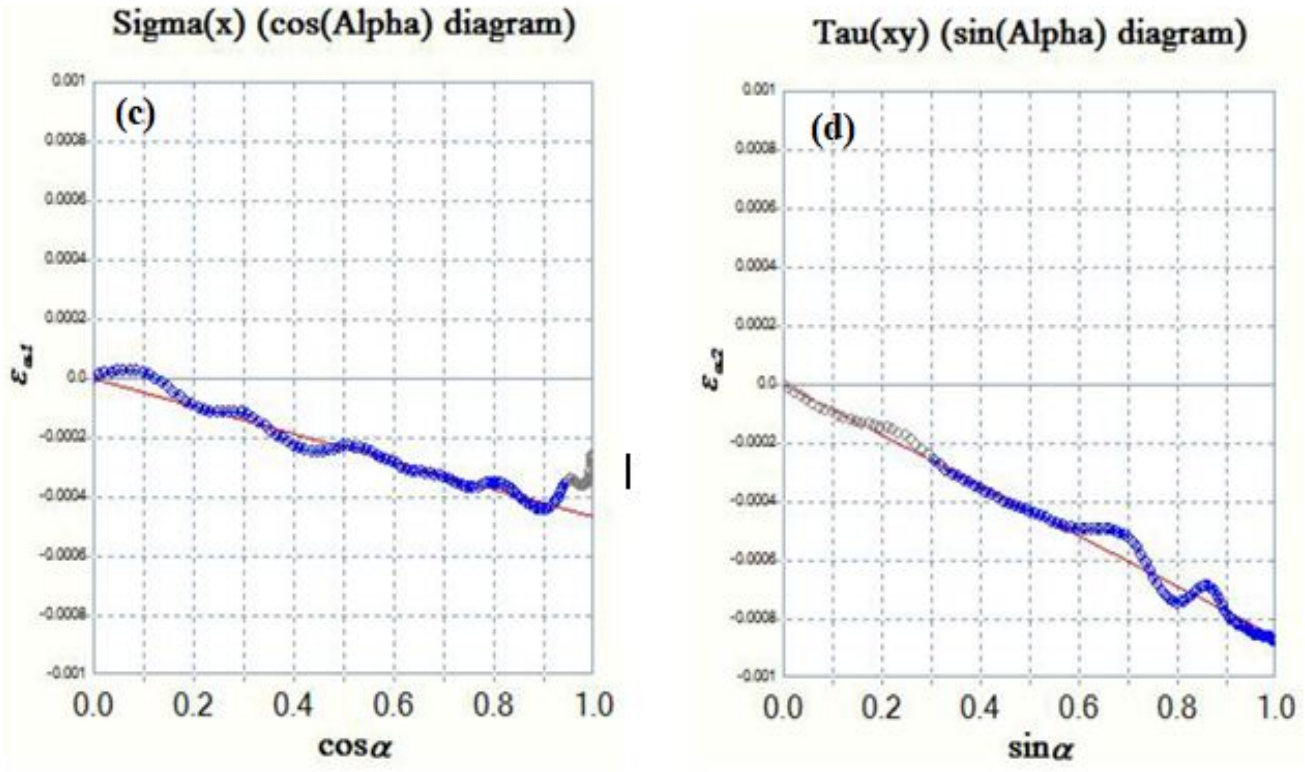

Fig.27: EN-36C alloy steel (a) Untempered cosα diagram (b) Untempered sin α diagram, (c) Tempered cosα diagram at 500ºC, (d) Tempered sinα diagramat 500ºC

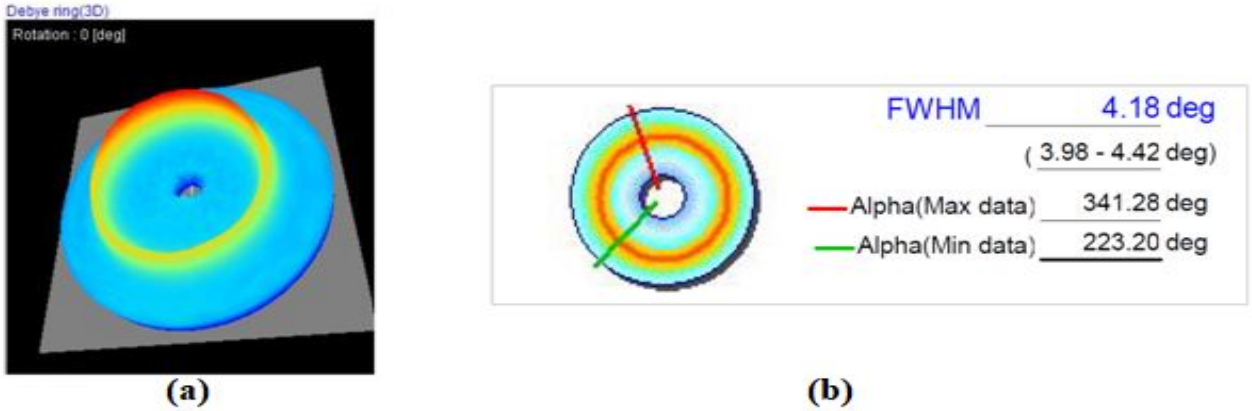

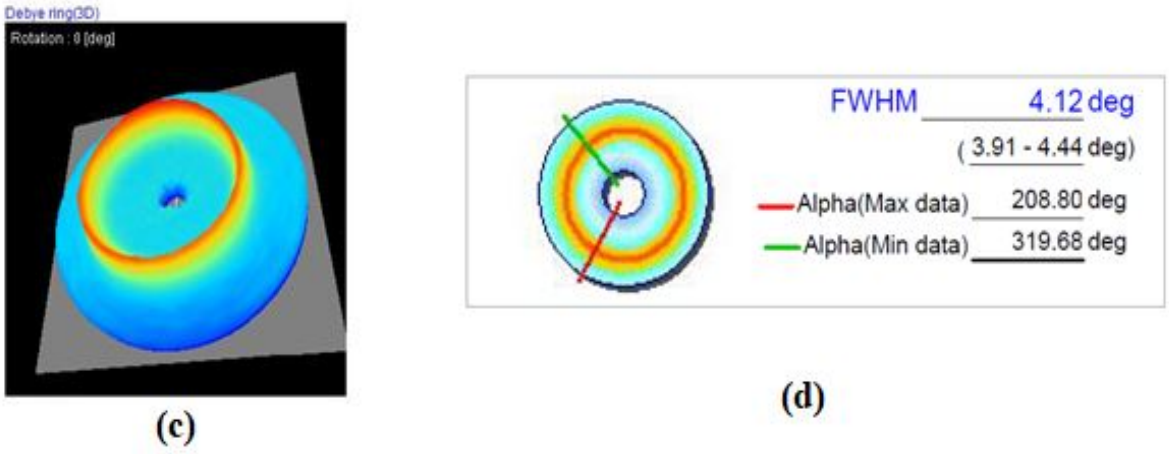

Fig.28: Untempered EN-36C (a) Debye-Scherrer (D-S) rings in 3D (b) Debye-Scherrer (D-S) rings in 2D, Tempered at 500ºC (c) Debye-Scherrer (D-S) rings in 3D (d) Debye-Scherrer (D-S) rings in 2D.

Figure 29 (a-e) shows comparative distributions of FWHM of entire Debye Scherrer ring of all the turned samples at the same process parameters with and without tempering. It has been seen from Figure 29 (a) that the machining of untempered sample has the value of FWHM is 4.2° the variation lies between (3.975-4.425 degree) and from graph it is found that α_{max} 18° and α_{min} 222°with peak strength (average) 175k. The FWHM of samples tempered at 200°C, 300°C, 400°C and 700°C are shown in Figure 29 (b),(c),(d) and (e) respectively. The value of FWHM of sample tempered at 200ºC is 4.14°, the variation lies between (3.96-4.33 degree) and α_{max} 24° and α_{min} 144°with peak strength (average) 161.5k. At 300°C, FWHM was found as 3.96°the variation lies between (3.74-4.18) and α_{max} 162° and α_{min} 312°.with peak strength (average) 152.5k.In similar way at 500°C FWHM was found as 4.175° the variation lies between (3.9-4.45 degree) and α_{max} 204° and α_{min} 322°with peak strength (average) 149k.In last at 700°C, FWHM was observed as 4.05º the variation lies between (3.8-4.3) and α_{max} 156° and α_{min} 240° with peak strength (average) 151.5k. It has been observed that the peak strength was maximum i.e. 175k of untempered sample and minimum i.e. 149k of sample tempered at 500ºC. Whereas samples tempered at 200ºC, 300ºC and 700ºC were observed peak strength as 161.5 k, 152.5k and 151.5 respectively. All these peak strength shows the intensity of residual stresses. It is concluded that the residual stress is maximum for turned sample at without tempering and minimum at the tempering temperature of 500ºC.

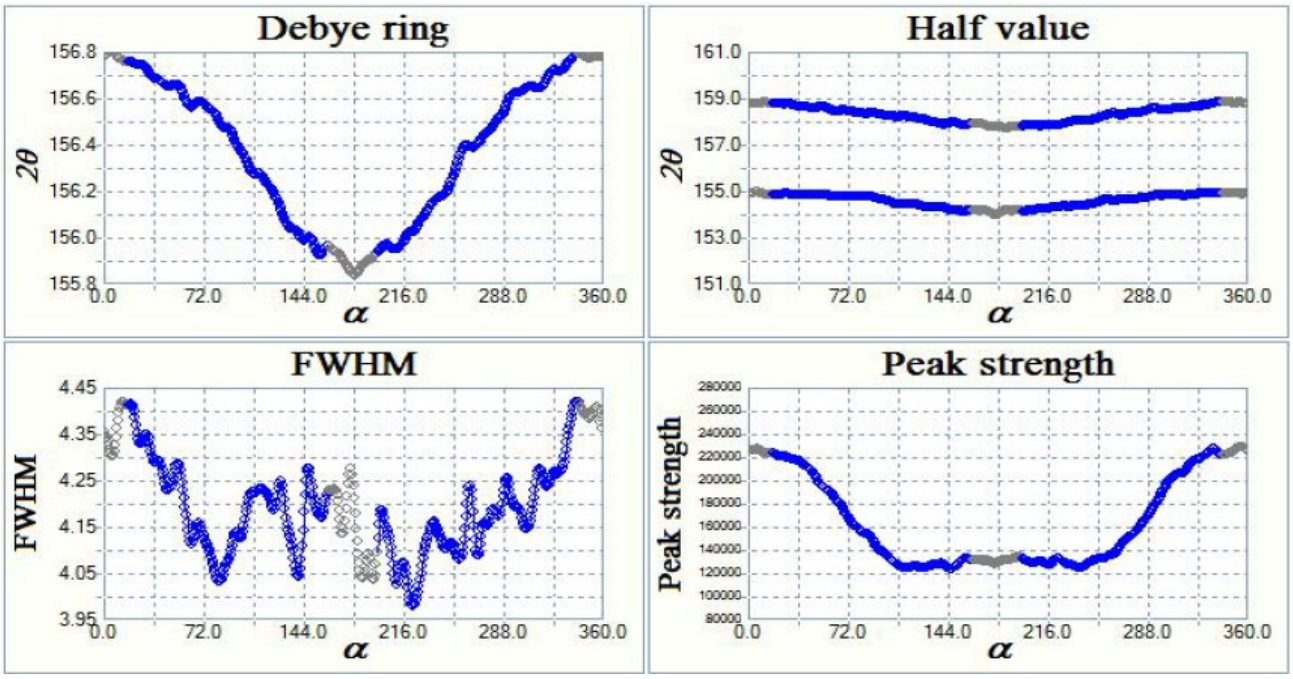

(a) FWHM graph of untempered EN-36C

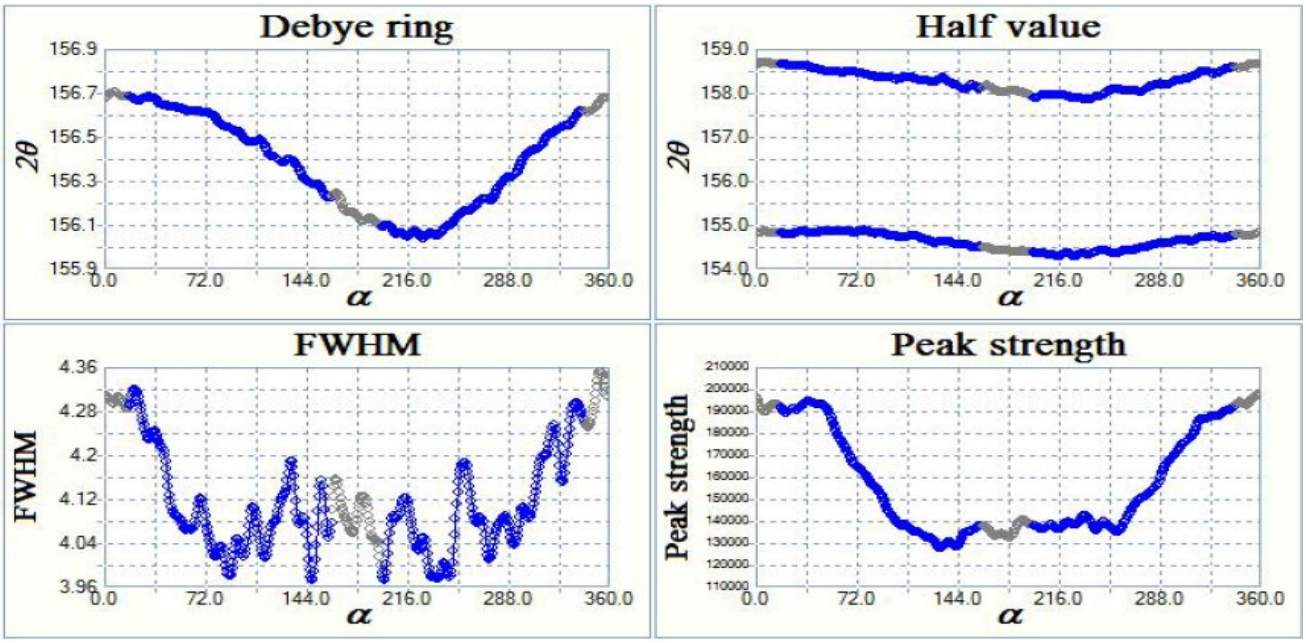

(b)FWHM graph of EN-36C tempered at 200ºC

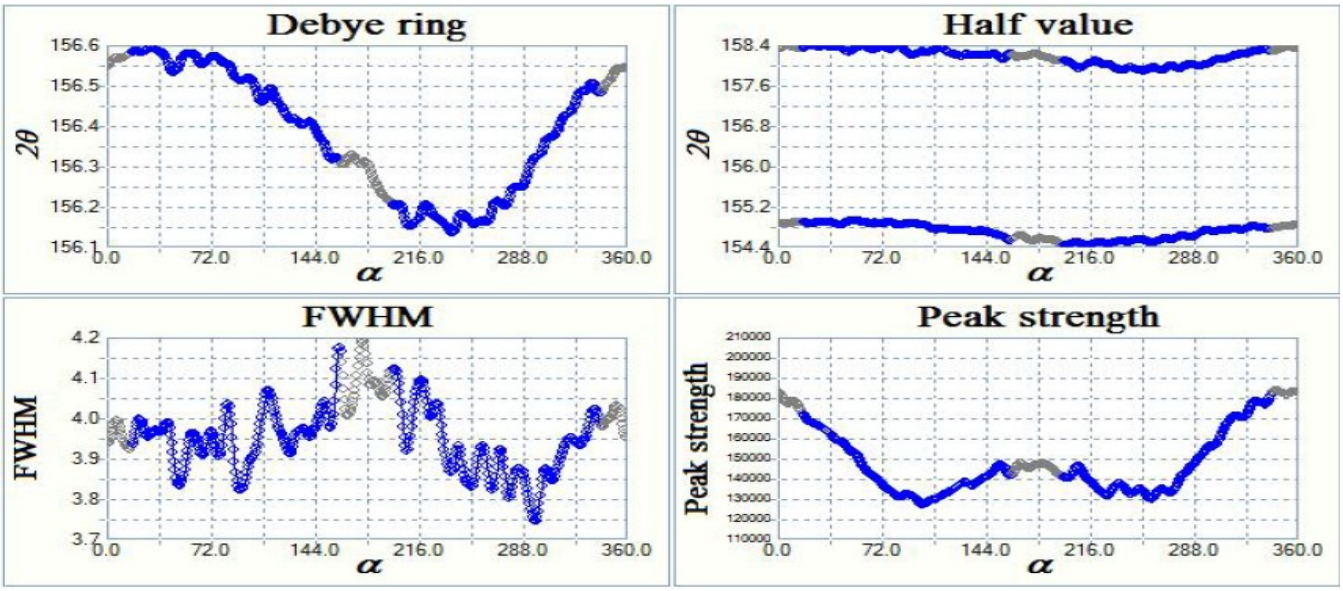

(c) FWHM graph of EN-36C tempered at 300ºC

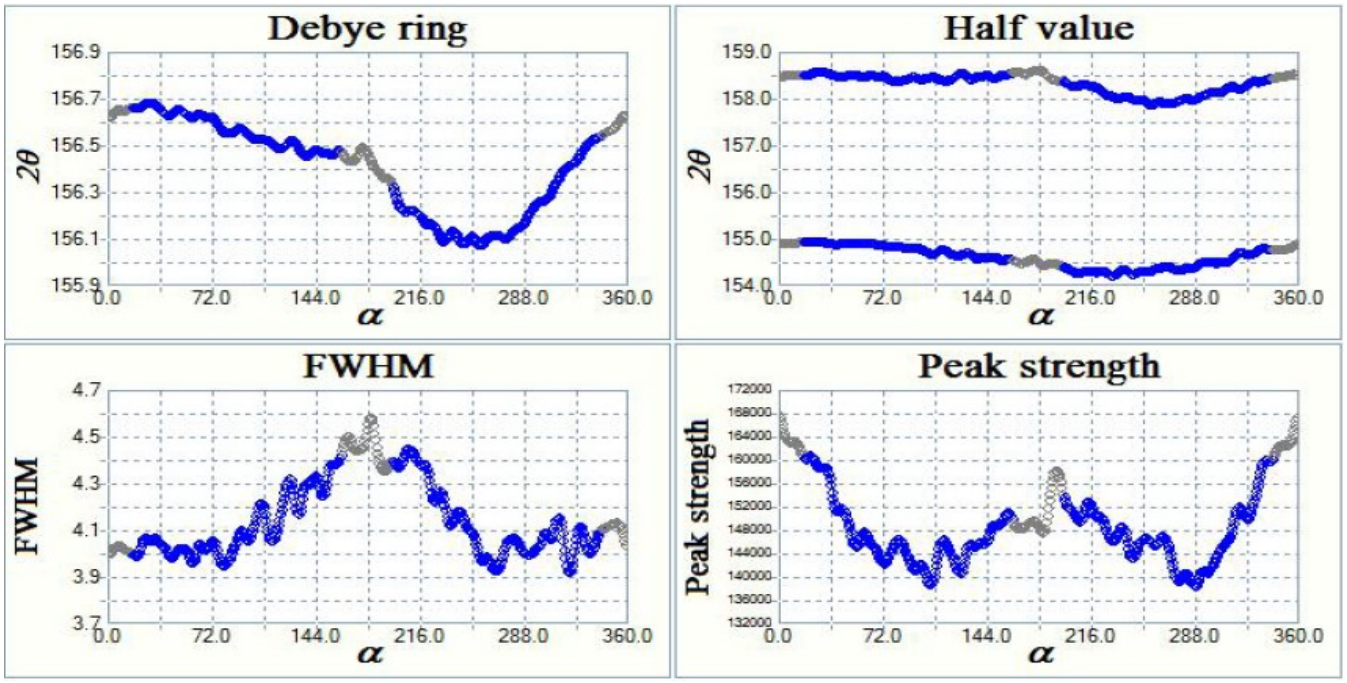

(d) FWHM graph of EN-36C tempered at 500^0C

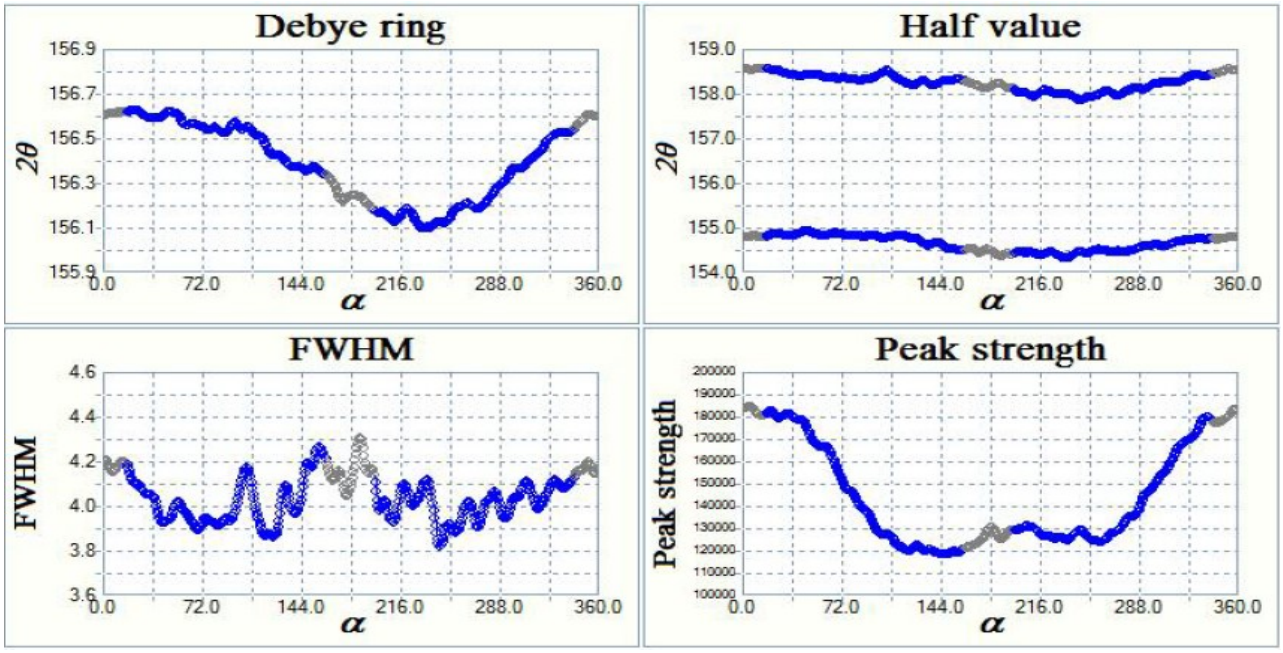

(e) FWHM graph of EN-36C tempered at 700^0C

Fig.29: FWHM graphs of EN-36C (a) Untempered (b) Tempered at 200ºC (c) Tempered at 300ºC (d) Tempered at 500°C (e) Tempered at700°C

Figure 30 (a) and (b) shows the residual stress profile of untempered and tempered EN-36C alloy steel. It can be seen clearly from Figure30 (a) that untempered sample has higher peak strength than the sample tempered at 500°C.The lower value of peak strength confirms the minimum residual stress of the tempered sample.

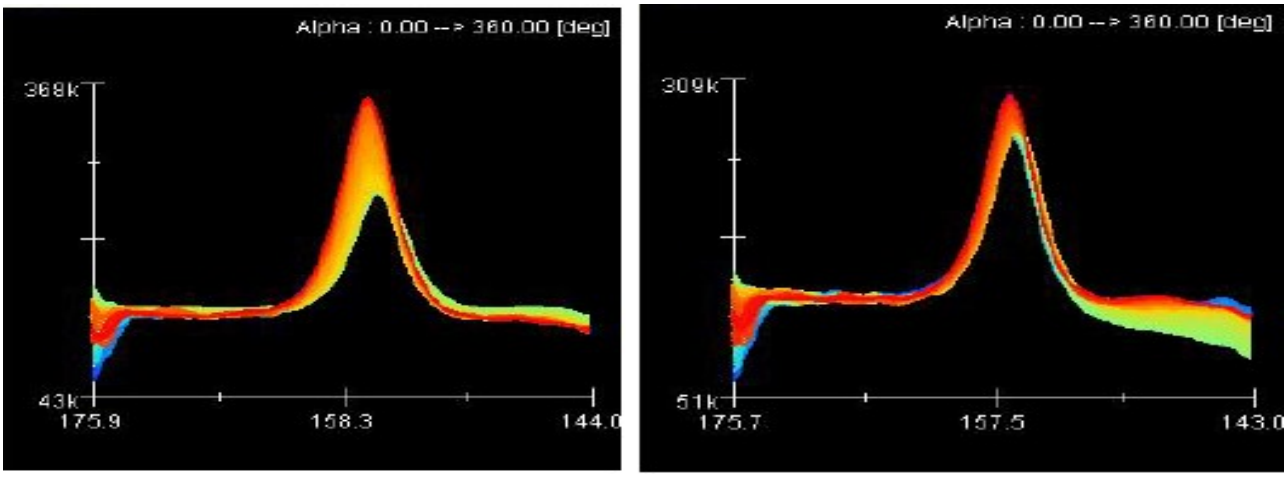

Figure 30: Residual stress profile of EN-36C (a) Untempered (b) Tempered at 500°C.

7.6 Optimization of Residual Stresses

It is very difficult to measure residual stresses in different machining processes and to model this phenomenon as well. In literature surveys, it was found that many researchers claim that the nature of residual stresses is tensile, while some claim that they are compressive. The main cause of the different natures is due to the different material properties and machining conditions [140]. Here, the residual stresses of all turned samples were measured with the help of a (μ-X360n full 2D) device based on Japan Company. Residual stresses in each sample were measured at a distance of 4 mm from the start of the turning, as shown in Figure 31. It could be seen that all the values are positive; hence it is of a tensile nature. The results obtained in experiments are analysed with the use of statistical tool design software. The normal probability and main effect plots generated by RSM can confirm the significance of the factors, as shown in Figure26 (a) and (b). In ANOVA, the condition for significance is 95% or a p-value of 0.05.Typically, turning causes the generation of Type I and Type II residual stresses: Type I: Compressive plastic deformation of the machined surface along the cutting direction results from pressure applied to the work-piece material during the turning process by the rake face. Tensile residual stress (+σ) is created in the surface layer and compressive residual stress (-σ) is created in the inner layer as a result of the interaction between the compressive plastic deformation on the machined surface and the unaffected material beneath. Type II: As the turning process progresses, the material of the work-piece is subjected to friction and extrusion from the flank face. The machined surface experiences tensile plastic deformation along the cutting direction as a result. Compressive residual stress (-σ) is produced in the surface layer as a result of the interaction between this tensile plastic deformation and the inner undeformed material, while tensile residual stress (+σ) is produced in the inner layer [141-142].

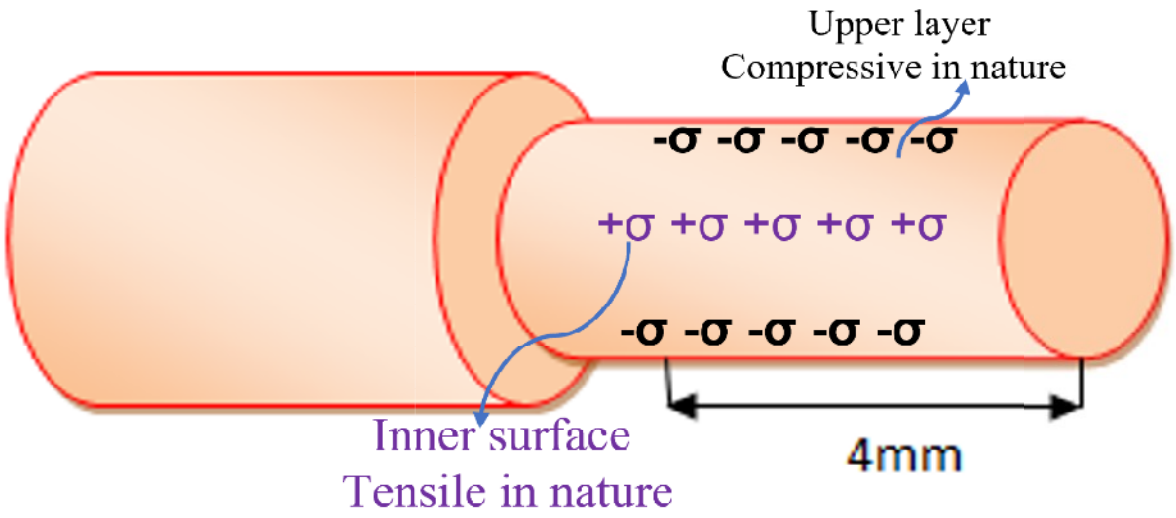

Fig.31: Measuring position of residual stresses from start of the turning

The residual stress data are analysed with the help of ANOVA table before and after eliminating insignificant terms, as presented in Tables 10 and 11, respectively. Table 11 is formed by eliminating all the insignificant terms through a backward elimination process using RSM. If $p < 0.05$, then terms are significant; otherwise, they will be insignificant. Lack of fits is insignificant since ($p > 0.05$. The final equation after the backward elimination process is given in Equation (13). The equation based on actual factors is used to predict the responses of each factor at given levels.

It could be seen from ANOVA in Table 11 that there is significant contribution of cutting speed 77.58 % and feed rate12.58% towards the residual stresses whereas the percentage contribution of depth of cut 5.08% is very less.

CHAPTER-8

Result analysis and discussion

This chapter describes the results and discussion part of the investigations in this thesis. The effect of tempering on mechanical properties and behavioral of microstructure as well as the various process parameters such as cutting speed (V), feed rate (f) and depth of cut (d) on their responses like residual stress, material removal rate(MRR), tool wear, surface roughnes is studied.

8.1 Effect of tempering on Mechanical Properties

The stress-strain graphs of test specimens were shown in Figure 17 (c). The tensile test results values are tabulated in Table 3.It was observed that the values of tensile strength of tempered specimens had significantly reduced in stress and strain curve. The results depicted that the peak value of tensile strength specimen tempered at 500ºC was observed 680.42 MPa. Further it was noticed that the tensile strength was minimum in the specimens tempered at 700ºC. However, maximum percentage elongation was found in the specimen tempered at 700ºC. It was observed that the higher tempered specimens exhibited large grain size [118, 130].

The average hardness values of specimens were represented in graph with respect to untempered and tempered temperatures shown in Figure 17 (b) and tabulated in Table 4.The curve is almost straight. It can be seen from the graph that values of hardness get increased slightly at tempering temperature of 500ºC and 700ºC [136].The main cause of this variation was due to the change in the microstructure of the alloy steel during the tempering [118,129]

The Impact tests of each specimen of EN-36C alloy steel were evaluated and tabulated in the Table 5. It has been seen that there is a less significant effect of tempering temperature on the hardness than toughness for the EN-36C alloy steel. Figure17 (a) shows that the toughness behaviour of investigated material at different tempered temperatures [129]. The effect of tempering causes the change in microstructure which results a little bit variation in hardness. The more dominating effect has been seen on specimen tempered at 500ºC.

8.2 Effect of tempering on Microstructure

The 36-composition and microstructural analysis of ENC have been done by Energy Dispersive X-ray Analysis (EDAX) using a scanning electron microscope (SEM).Figure 23 (c) shows the microstructure of the specimens tempered at 500°C (for 2hours). The martensite and retained austenite microstructure has been obtained after tempering process at 300^0C and 500°C (for 2 hours). It was observed that untempered specimens have ferrite (white) and pearlite (black) as the two major constituents in their microstructure as shown in Figure 23 (a). Further, optical micrographs show that the specimen tempered at 200°C has needle (like bainite) microstructure having good mechanical properties.

The specimens tempered at 300°C and 500°C (for 2 hours) show better mechanical properties than the specimen tempered at 200°C [129, 131].

8.3 Effect of tempering on machining

The tempering process has significant impact on machining. The tempered specimens exhibited more material removal rate (MRR) than untempered specimens at the same process parameters. The MRR vs. tempering temperature bar graph is shown in Figure 32 (a). Further, Figure 32 (a) shows that untempered specimen has less material removal rate (11028.33 mm^3/min) than tempered specimens. Figure 32 (b) shows the average tool tip temperature vs. tempering temperature bar graph for investigating material. The tool tip temperatures were measured at the time of specimen during turning operation. It was observed that the tool tip temperature was higher for untempered specimens than tempered specimens. All tempered specimens have less tool tip temperature during turning except specimen tempered at 700°C. It was due to the secondary hardening at this temperature. The effect of tempering on surface roughness of specimens was discussed in result section 8.4. It was concluded from above discussion that tempering had great effect on machinability of EN-36C alloy steel.

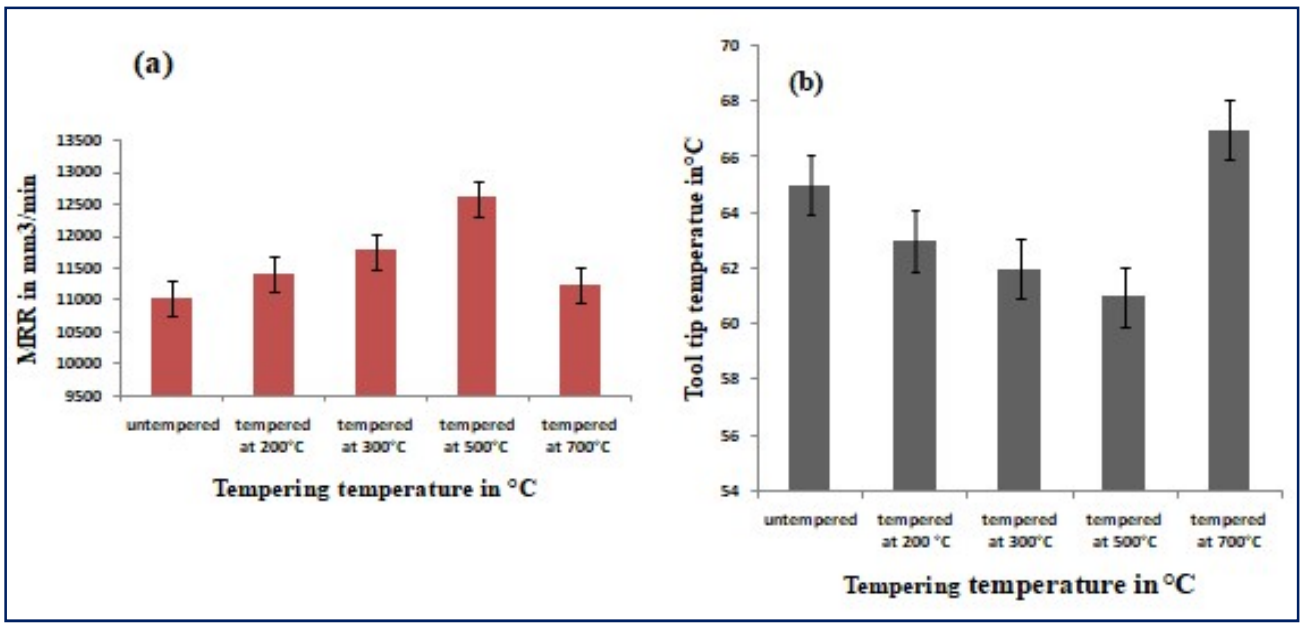

Fig.32: Bar chart of untempered and tempered specimens at 200ºC,300 ºC,500 ºC, and 700ºC for (a) Material removal rate (b) Average tool tip temperature

8.4 Effect of tempering on surface roughness

Surface roughness of test specimens was measured with the help of a portable stylus-type profilometer, talysurf. The process parameter (cutting speed, depth of cut, feed rate) in turning operation were taken same for each specimen. The cut off length 0.8 mm and Gaussian filter with a ratio of 2.5µm was used in the surface roughness experiments. All the roughness parameters (R_a, R_q, and $R_{z)}$ were measured on the specimens repeatedly five places in the transverse direction. The average value of surface roughness is presented in Table 6. The results were depicted that specimen tempered at 500ºC have lowest surface roughness among other samples. The surface roughness profiles of untempered and tempered specimens are shown in Figure 21 (a) and (b) respectively. In graphs of surface roughness X-axis represents length in mm and Y-axis represents the total height of the primary profile P_t in µm.

8.5 Effect of Process parameters on Residual Stresses

Using analysis of variance, the impact of various process parameters on percentage reduction in residual stress (%ΔRS) has been investigated.

8.5.1 Effect of cutting speed on %ΔRS

Cutting speed is most significant process parameter for increasing the percentage reduction in residual stress (%ΔRS) during the turning of samples having the contribution of 77.58 % obtained from ANOVA analysis. As cutting speed is increased, the %ΔRS get increased. It is due to increase in cutting forces and temperature during the turning at high speed. Increase in friction between cutting tool and work-piece contact also causes increase in residual stress. This can be observed in Figure 33.1 depicting the effect of cutting speed on %ΔRS.

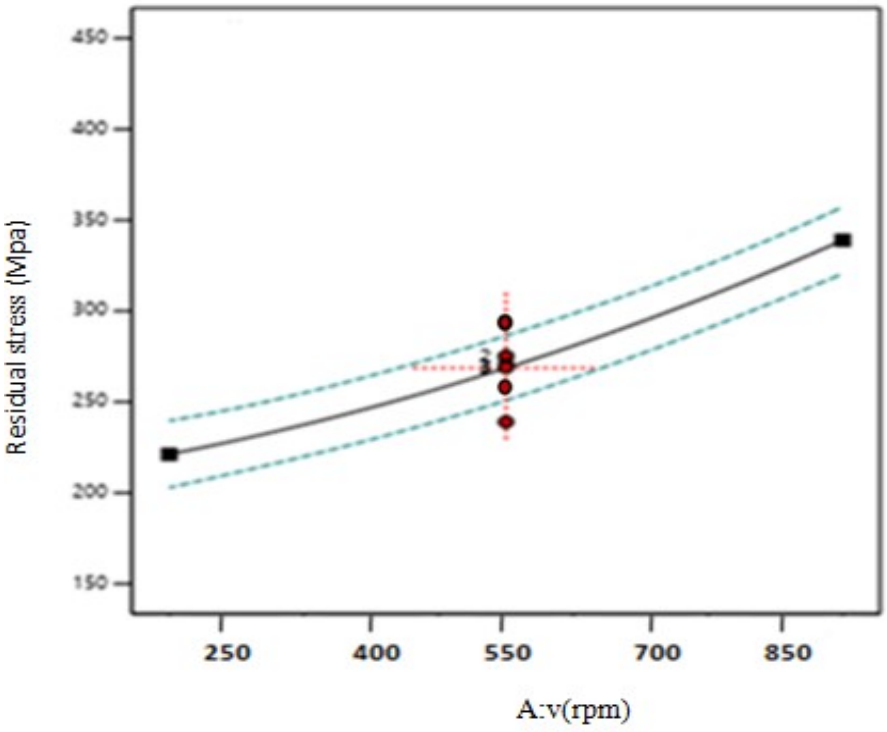

Fig. 33.1: Effect of Cutting speed on %ΔRS

8.5.2 Effect of feed rate on %ΔRS

Increase in feed rate (f) causes slightly increase in %ΔRS during turning as shown in Figure 33.2. The main reason is due to high feed rate, the subsurface compressive residual stresses get increased. The percentage contribution of feed rate in %ΔRS is 12.58%as depicted from statistical tool.

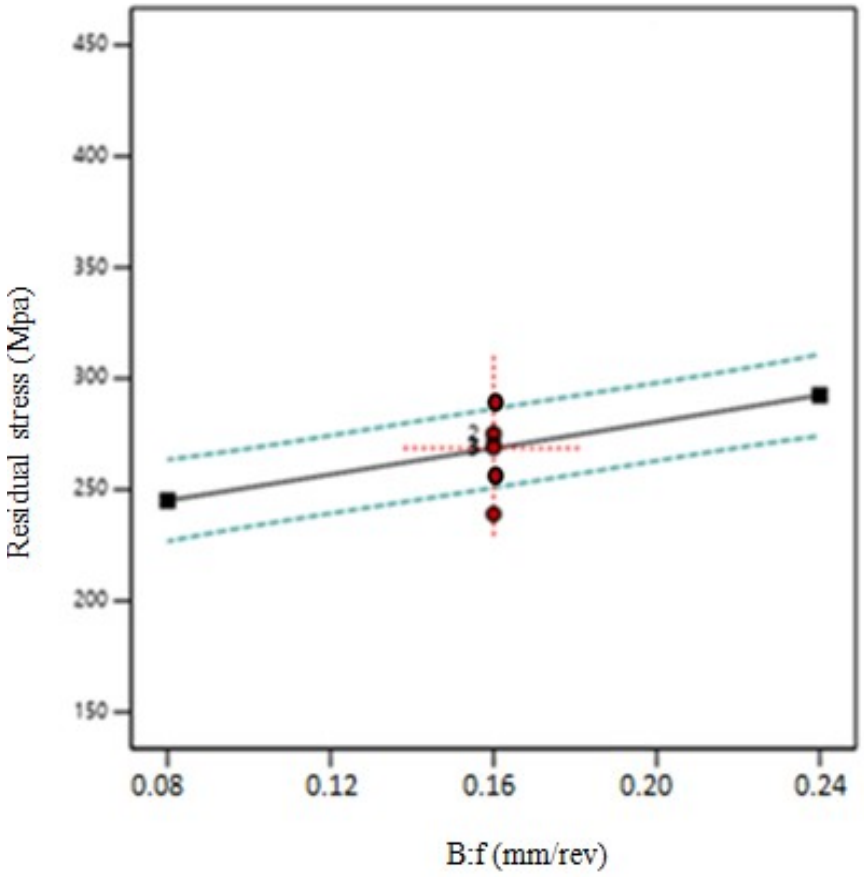

Fig. 33.2: Effect of feed rate (f) on %ΔRS

8.5.3 Effect of depth of cut on %ΔRS

Increase in depth of cut causes slightly reduce in residual stress during the turning of EN-36C alloy steel as shown in Figure 33.3. The percentage contribution of depth of cut in %ΔRS is 5.08% depicted from statistical tool analysis.

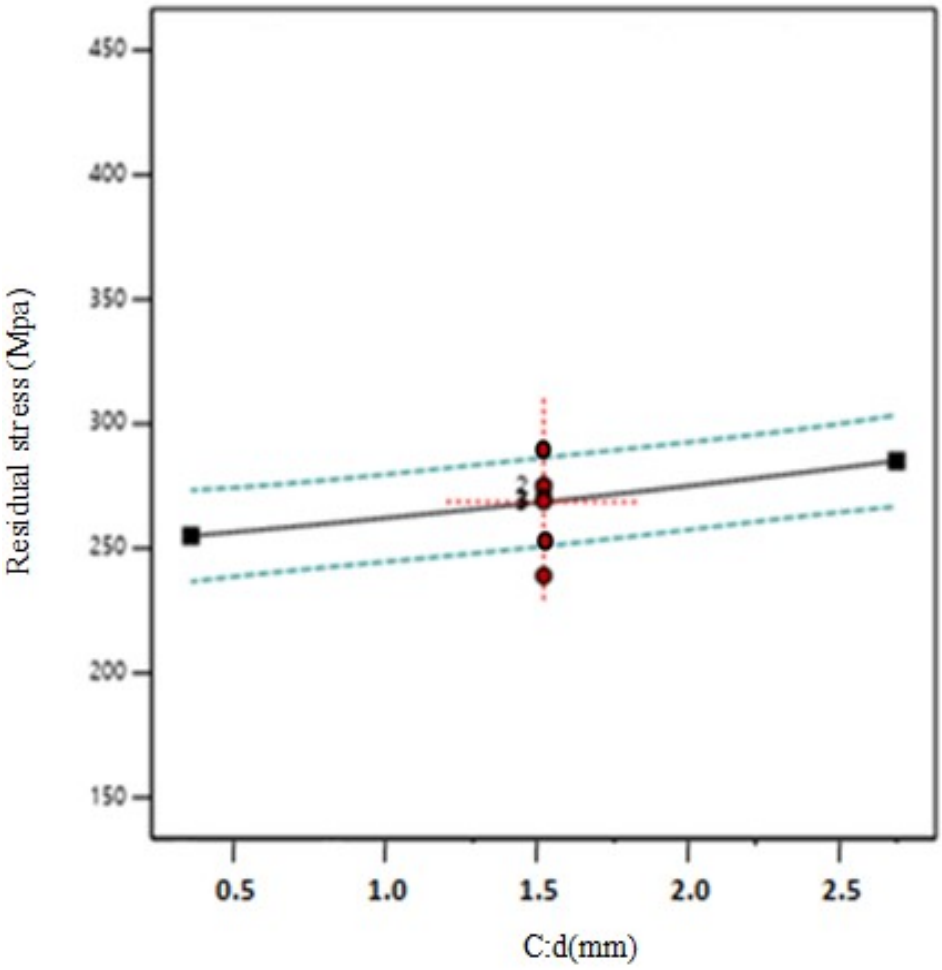

Fig. 33.3: Effect of depth of cut (d) on %ΔRS

The individual effect of process parameters (cutting speed, feed rate and depth of cut) on %ΔRS is shown in Figure 33.4 (a). From Figure 33.4 (b), it can be observed that the predicted value of %ΔRS is close to the actual value obtained after conduction of experiments. Figure 33.4 (b) justified the magnificent acceptability of the regression model. The observed values were consistent with the predicted values, as depicted in Figure 33.4 (b) indicating a fair consistency between the predicted and actual values. Figure 33.4 (b) demonstrates a fair consistency between predicted and actual values, with actual values closer to the predicted line, indicating satisfactory

experimental results. The interaction of process parameters on %ΔRS can be observed through contour surface graphs depicted in Figure 33.5

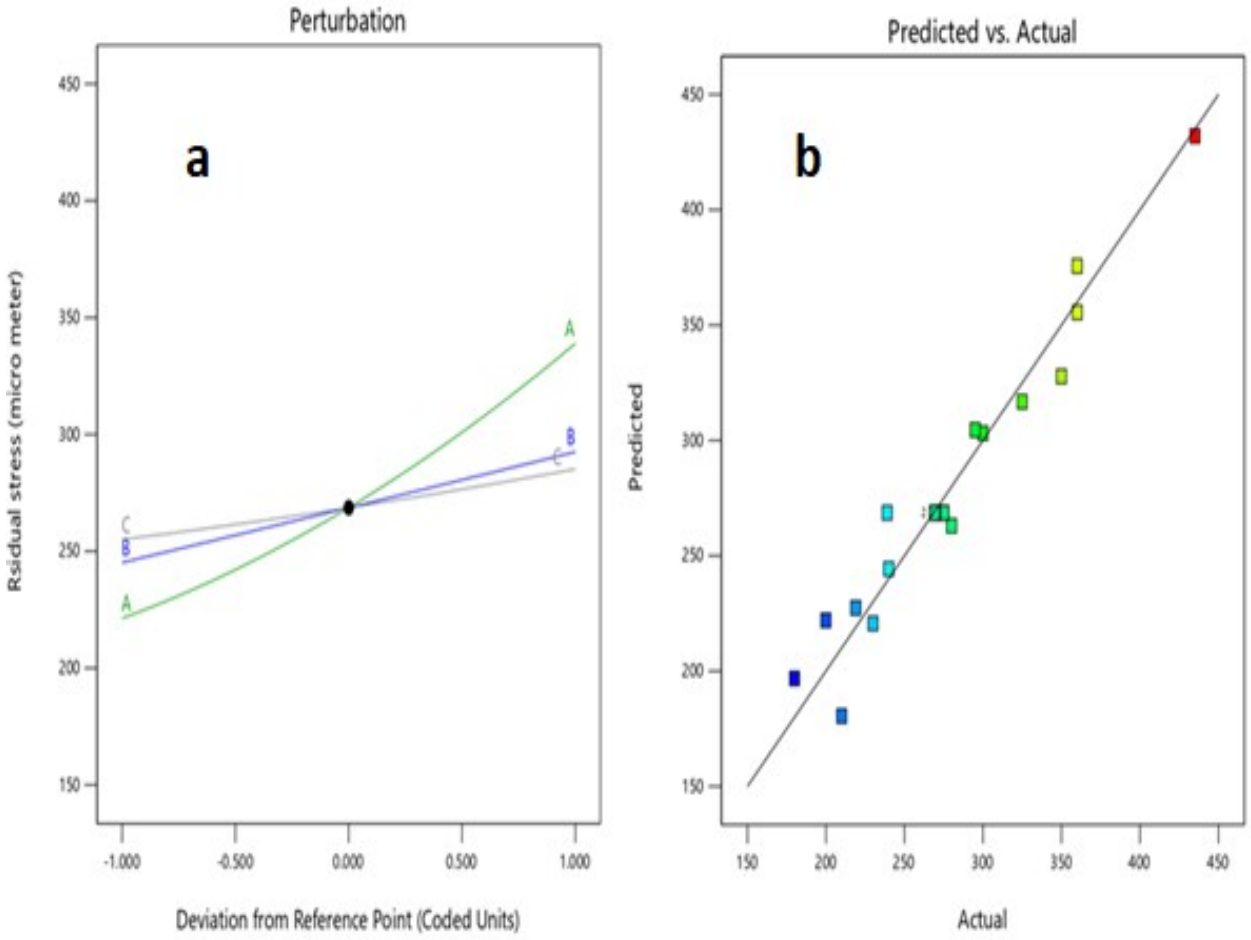

Fig.33.4:(a) Perturbation diagram for %ΔRS with (A- cutting speed, B- feed rate, C- depth of cut) (b) Actual vs predicted graph

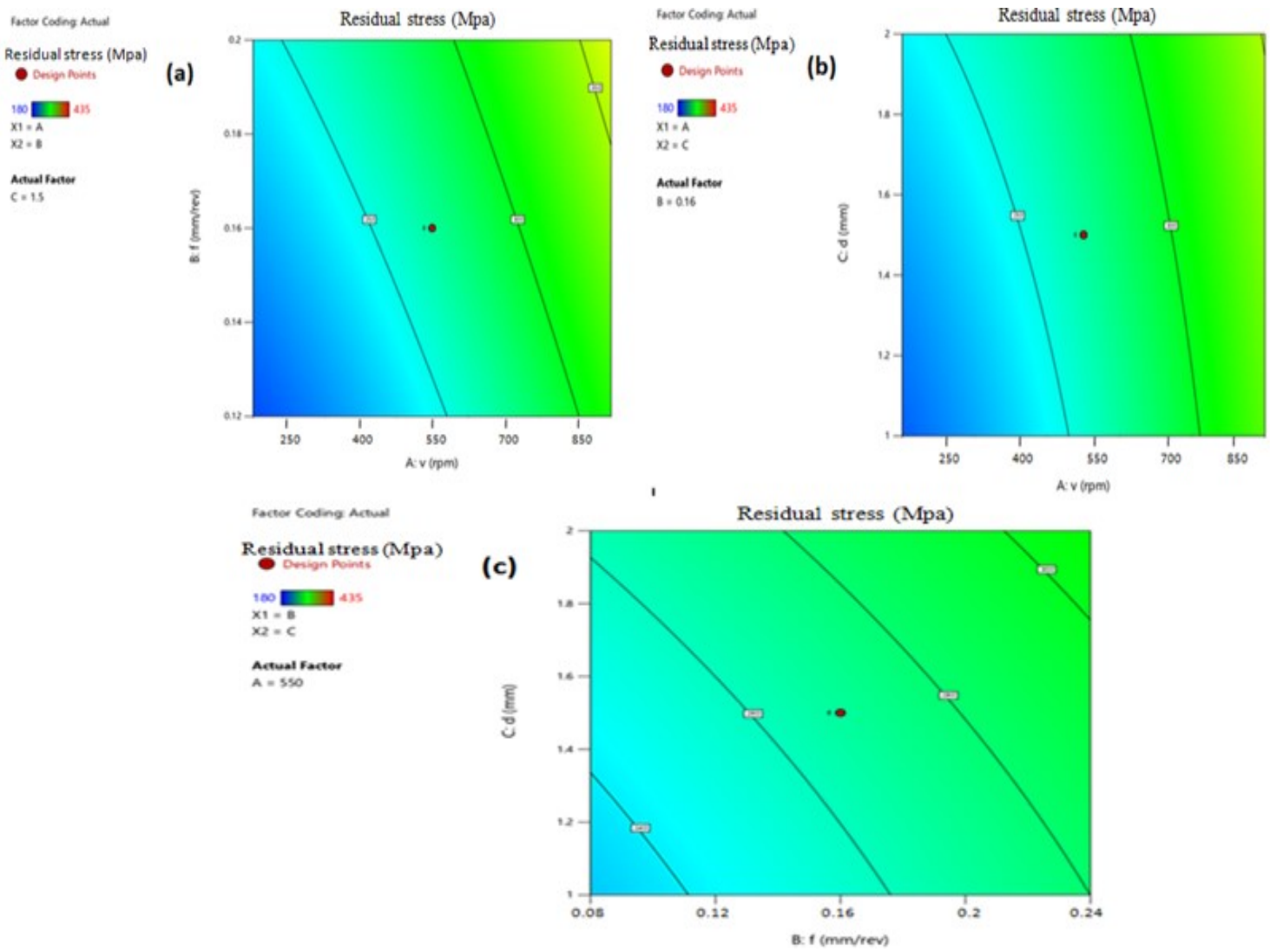

Fig.33.5: Contour surface graph between (a) Feed rate and cutting speed (b) Depth of cut and cutting speed (c) Depth of cut and feed rate.

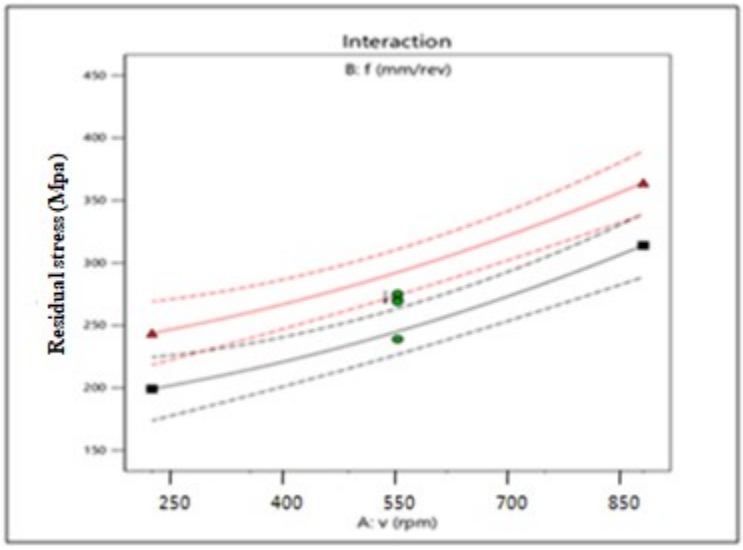

Fig. 33.6: Interaction graph between cutting speed and feed rate on %ΔRS

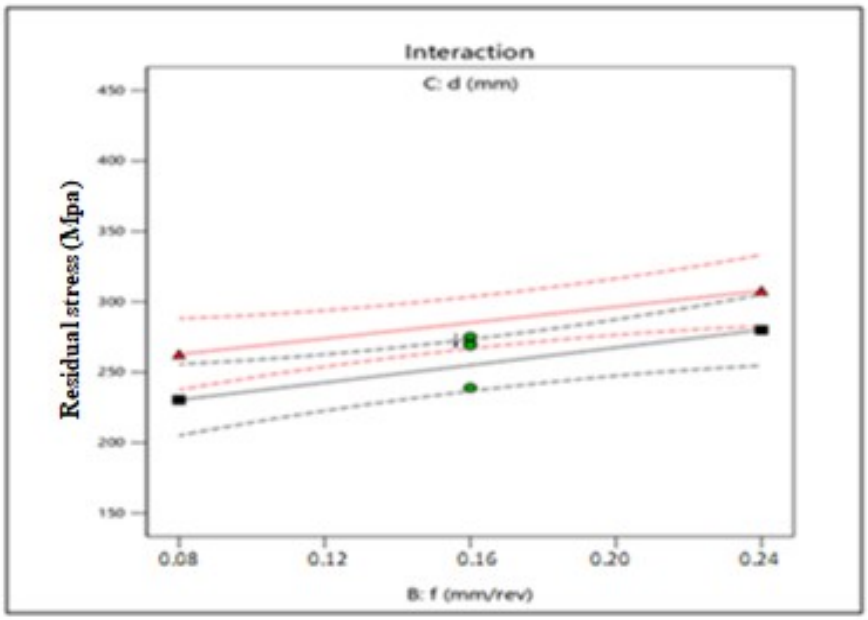

Fig. 33.7: Interaction graph between depth of cut and feed rate on %ΔRS

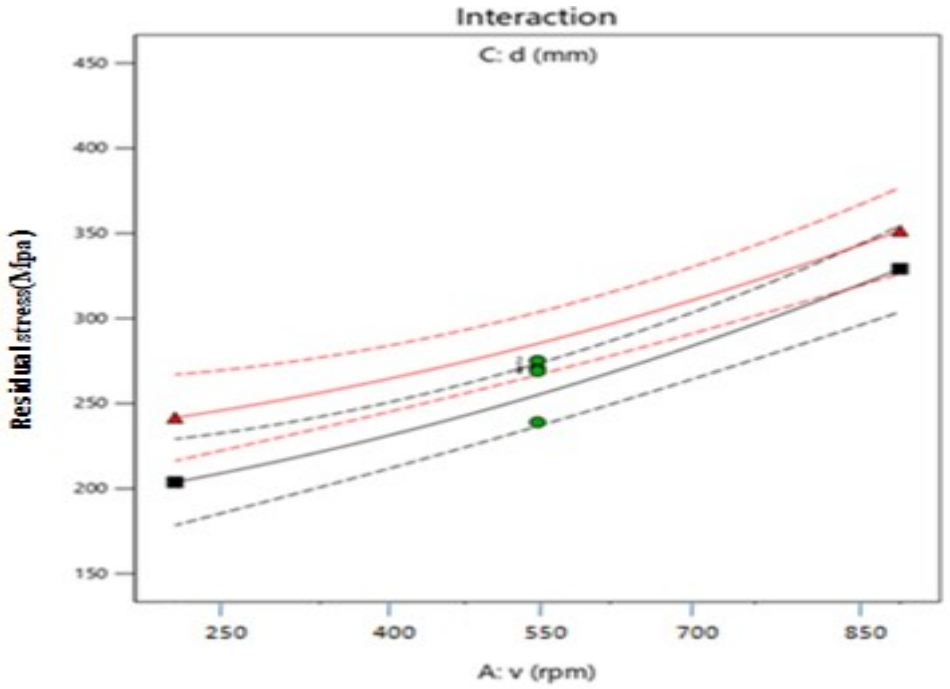

Fig. 33.8: Interaction graph between feed rate and cutting speed on %ΔRS

The interaction graph analysis reveals that the %ΔRS increases with an increase in cutting speed and decreases with an increase in feed rate as shown in Figure 33.6. The %ΔRS increases with increase in feed rate and decreases with increase in depth of cut as shown in Figure 33.7.The %ΔRS increases with increase in cutting speed and decreases with increase in depth of cut as shown in Figure.33.8.

The adjusted R^2 and R^2 values are quite near to one another (0.9296 and 0.9444 respectively), indicating strong agreement between the reaction (residual stress) and turning variables (independents). Figure 33.9 (a) shows the probability curve for residual stress. Since the mistakes in this case are distributed appropriately, they surround a straight line. The primary variables influencing the residual stresses during EN-36C turning are depicted in Figure 33.9(b). The graph shows that, in comparison to feed rate, cutting speed has a larger effect with residual stress. However, because of the slope's nature, cutting depth has relatively little impact.

8.5.4 3-D plot pattern of normal probability, main effect and surface for MRR

The 3-D surface plots of residual stresses for different combination of machining parameters are shown in Figure 34 (a), (b) and (c). It could be seen from the statistical data of response optimization that residual stress gets minimize at feed rate 0.08 mm/rev, cutting speed 250 rpm, and depth of cut 1.9 mm. The predicted value of residual stress by this model was found to be 180.528 MPa. Residual stress graph at confirmatory test are shown in Figure 35.

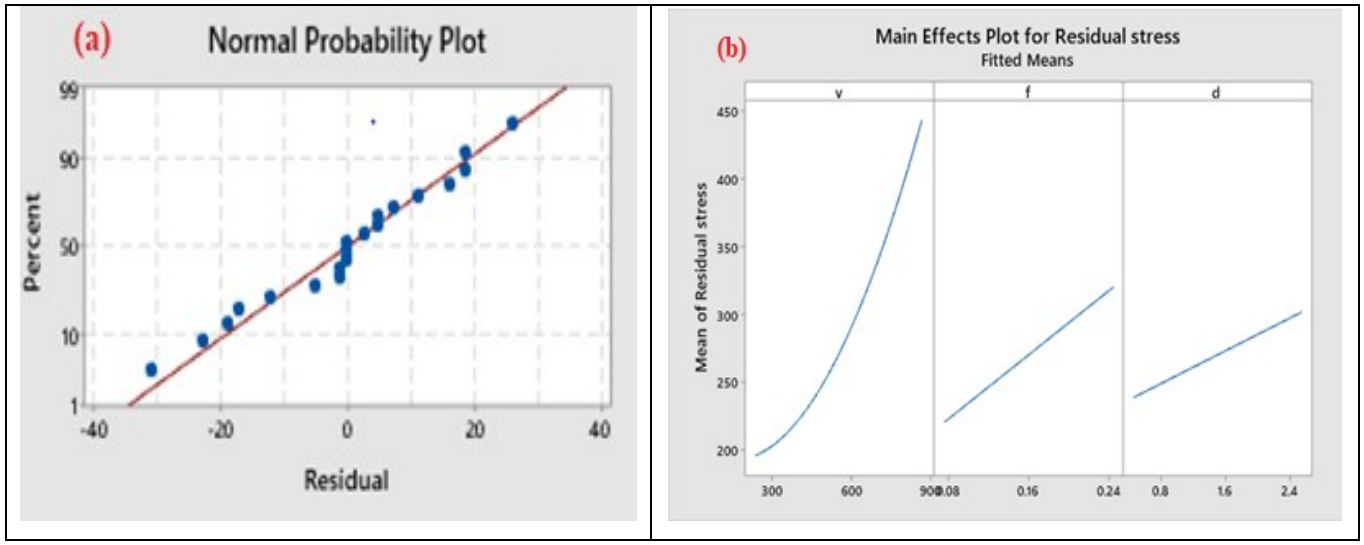

Fig.33.9: (a) Normal probability graph for residual stress (b) Main effect plot for residual stress

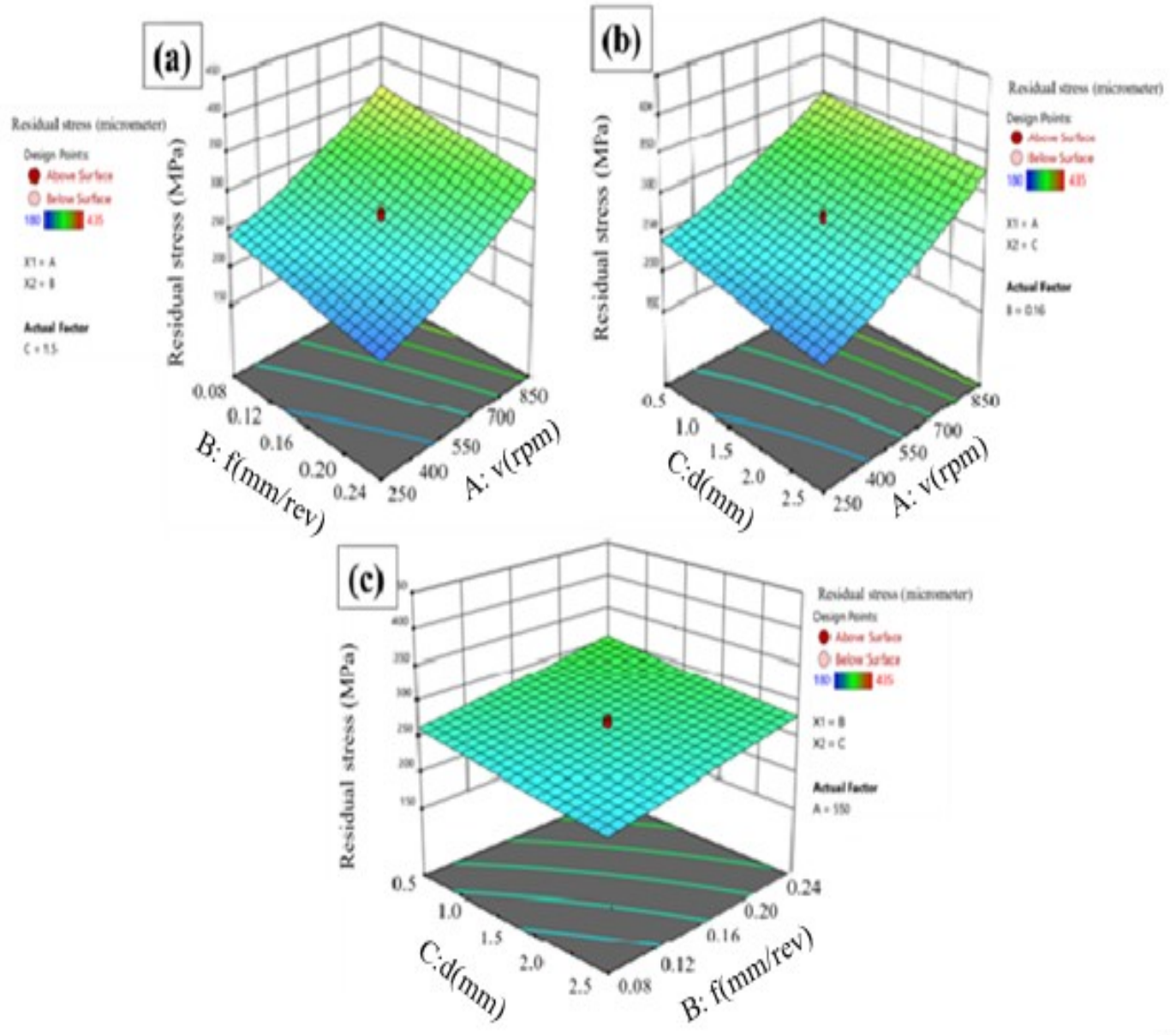

Fig.34**:** 3-D surface plot of (a) Residual stress vs speed, feed (b) Residual stress vs speed, depth of cut (c) Residual stress vs feed, depth of cut.

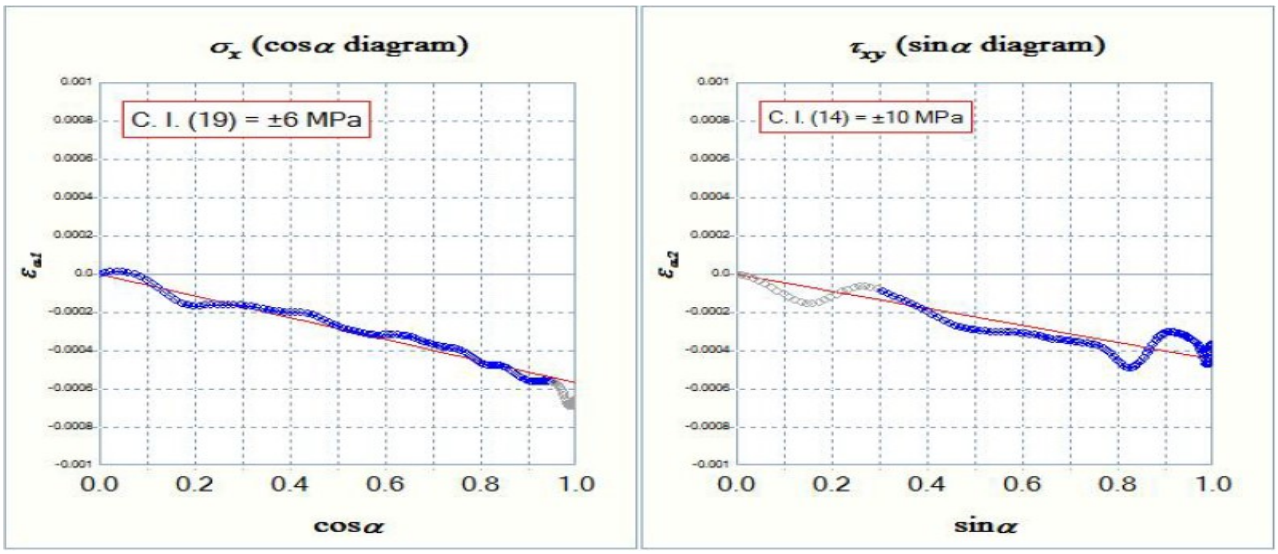

Fig.35: Residual stress graph of turned sample at cutting speed of 250 rpm, feed rate of 0.08 mm/rev and depth of cut 1.9 mm.

8.6 Effect of process parameters on tool wears

8.6.1 Effect of feed rate (f) on tool wear

It has been observed that the impact of feed rate (f) on tool wear is very less as compared to cutting velocity during turning operation as shown in Figure.36.1. The main reason is due to the less contribution in built-up edge at high and low feed rate. The percentage contribution of feed rate in tool wear is 9.04% as depicted from statistical tool.

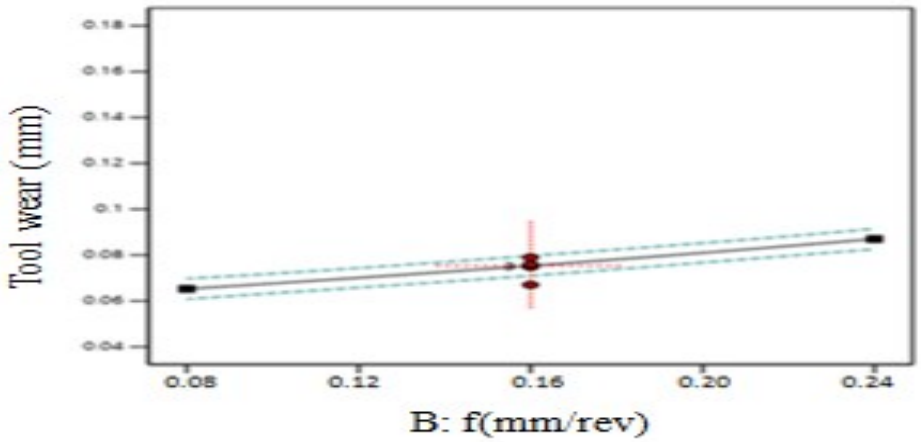

Fig.36.1: Effect of feed rate (f) on tool wear

8.6.2 Effect of Cutting speed (V) on tool wear

Cutting speed is most significant process parameter for tool wear during the turning of EN-36C alloy steel having contribution of 74.28 % obtained from ANOVA analysis. As cutting speed is increased, the tool wear gets increased. It is due to increase in built-up edge (BUE) during the turning at high speed. Increase in friction between cutting tool and work-piece contact also causes increase in tool wear. This can be observed in Figure. 36.2 depicting the effect of cutting speed on tool wear.

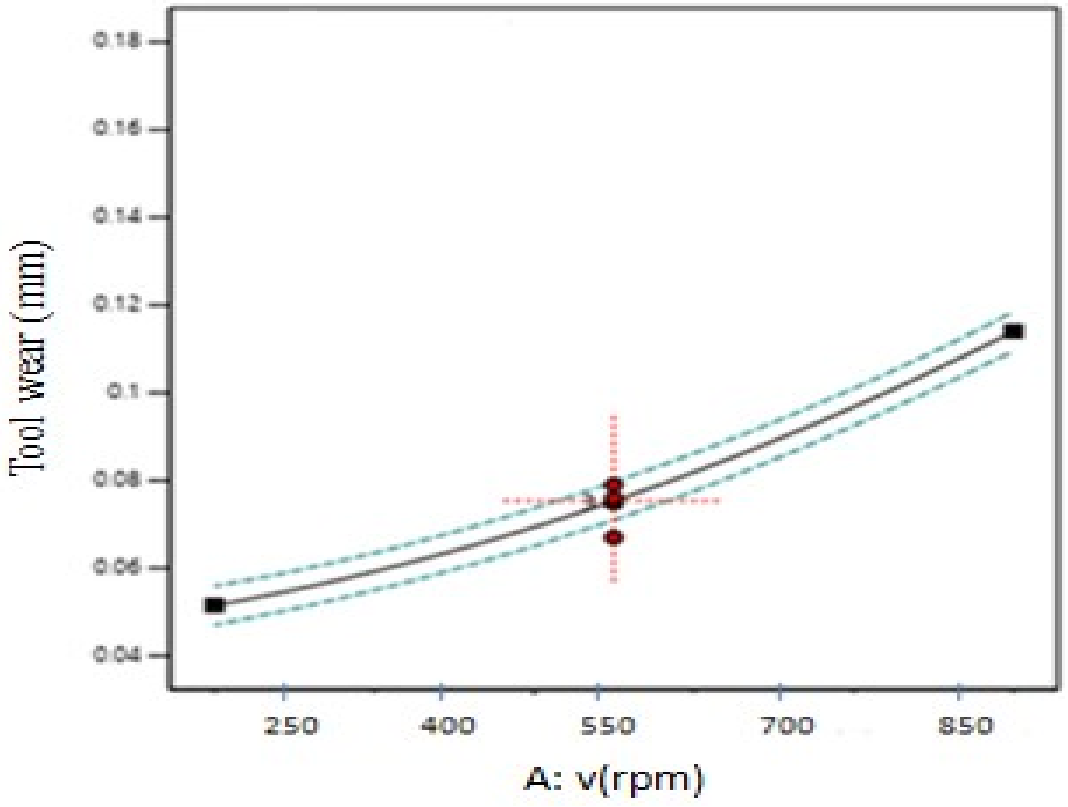

Fig.36.2: Effect of cutting speed (V) on tool wear

8.6.3 Effect of depth of cut (d) on tool wear

The contribution of depth of cut (d) in tool wear is also very less as compared to cutting velocity during the turning of EN-36C alloy steel as shown in Figure.36.3. The percentage contribution of depth of cut in tool wear is 8.57% as depicted from statistical tool analysis.

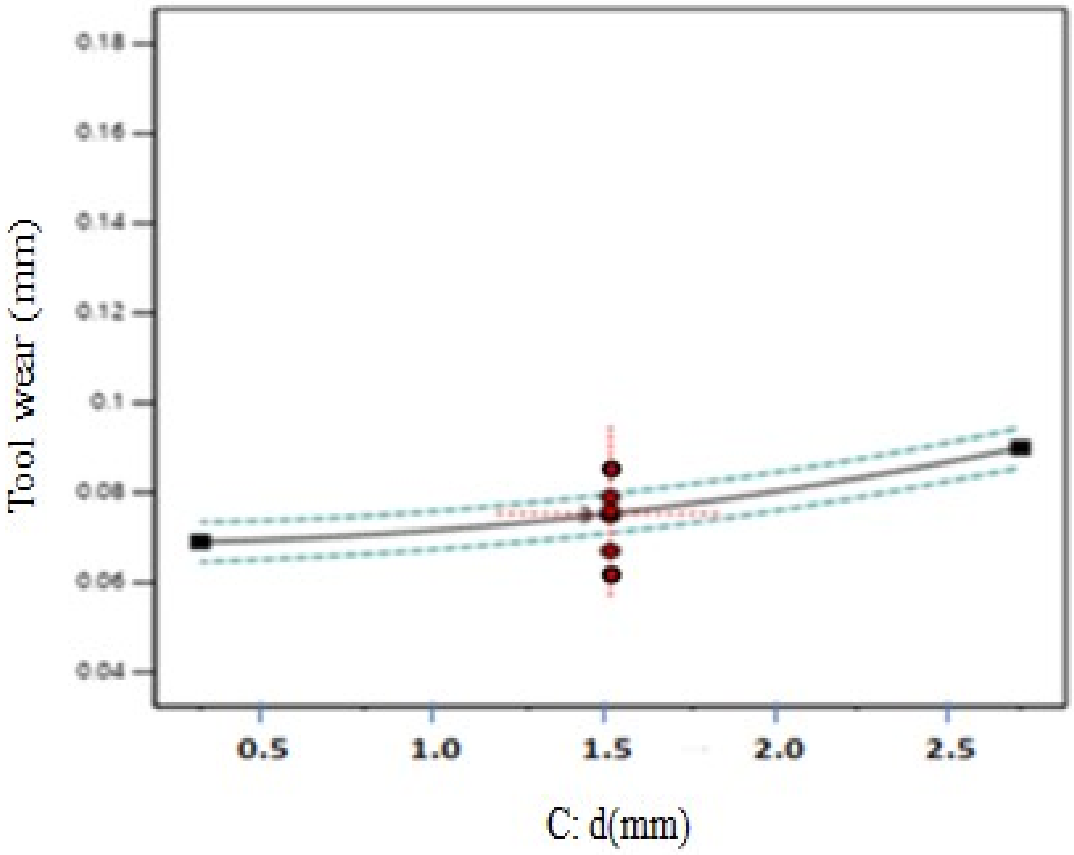

Fig.36.3: Effect of depth of cut (d) on tool wear

8.6.4 3-D plot pattern of normal probability, main effect and surface for MRR

In Figure 36.4, errors are normally distributed since they lie around a straight line. It could be seen from the main effect plot that cutting speed and depth of cut are the most influential parameters for tool wear, whereas feed rate has less effect. The normal probability chart and the main effect plot for tool wear are shown in Figure 36.4 (a) and (b), respectively. The percentage contributions of speed (74.28%), feed (9.04%), and depth of cut (8.57%) for tool wear are shown in Table 13. The optimization of tool wear shows the best conditions for the process parameters of cutting speed of 672.233 rpm, feed rate of 0.12 mm/rev, and depth of cut of 1 mm, at which the tool wear was found to be minimum as 0.089 mm

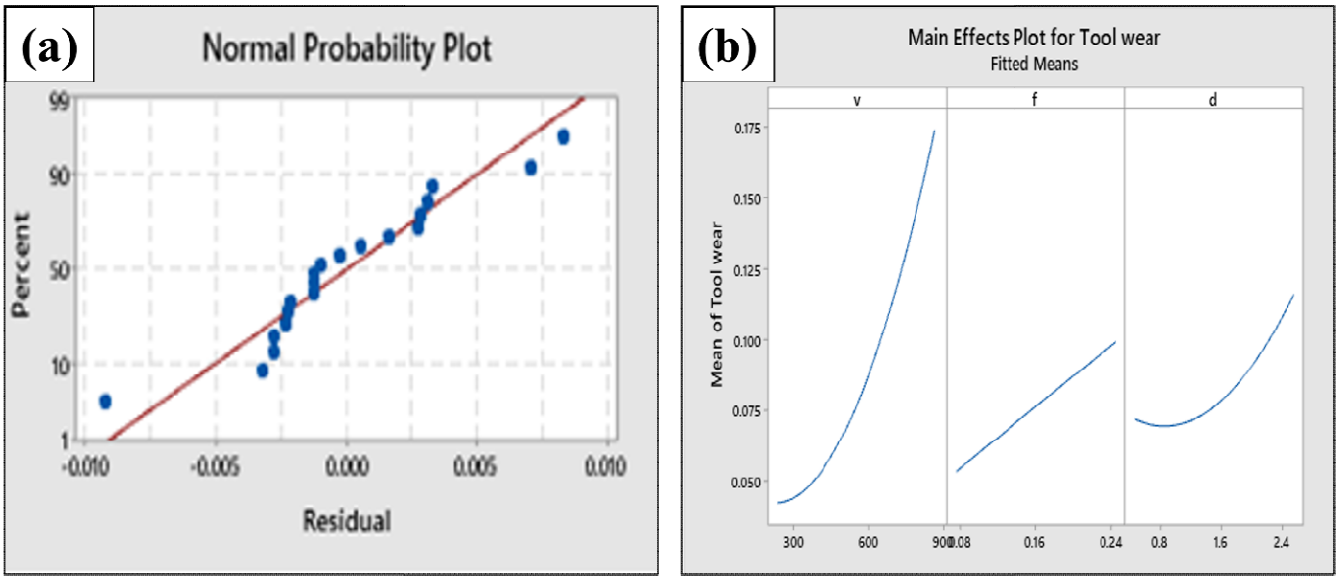

Fig.36.4:a) Normal probability plot for tool wear, (b) Main effect graph for tool wear

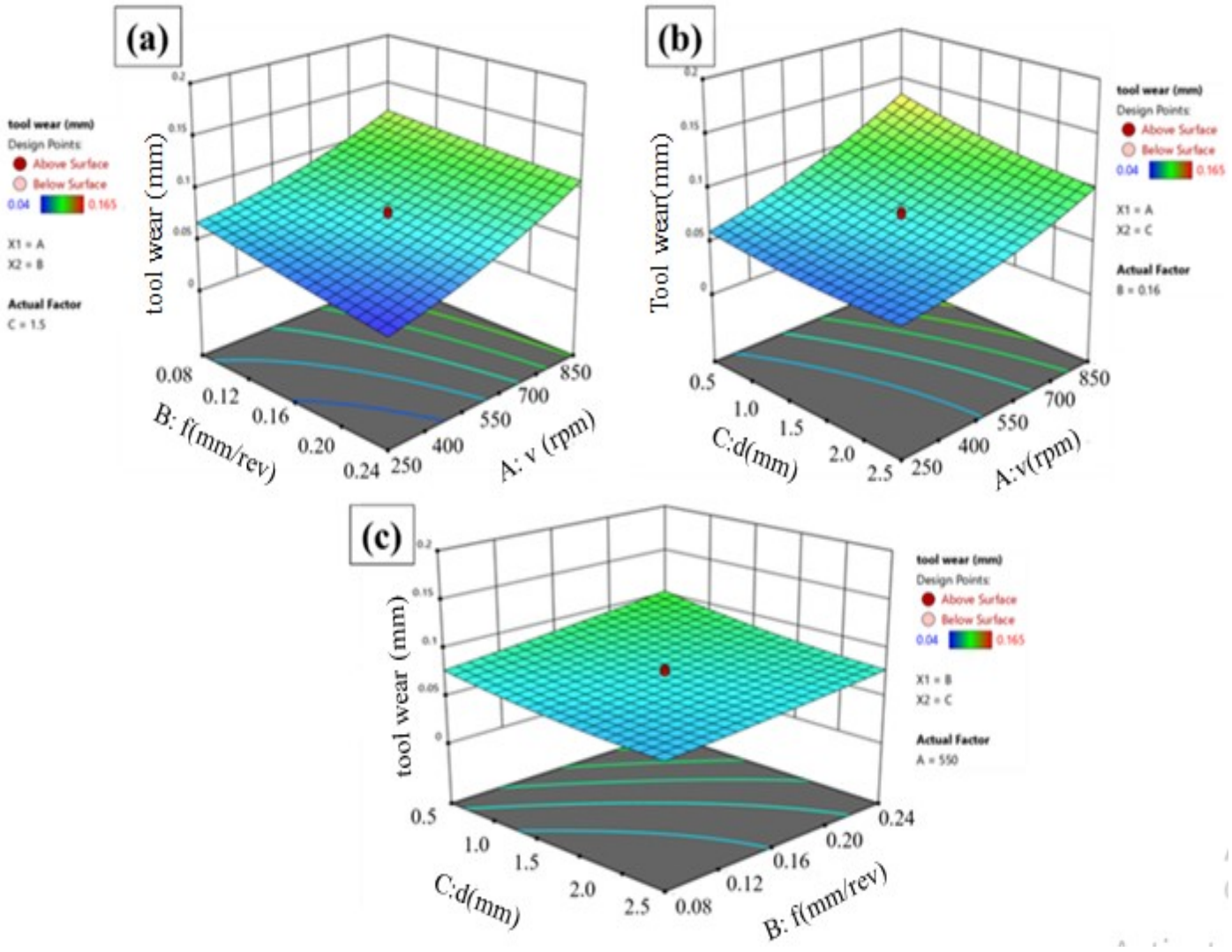

Fig.37**:** 3-D surface plots interaction effects for tool wear between (a) Cutting speed and feed rate, (b) Cutting speed and depth of cut (c) Depth of cut and feed rate

The 3-D surface plots of tool wear for different combination of machining parameters are shown in Figure 37 (a), (b) and (c).Microstructure of tool wear for confirmatory test at cutting speed 672.233rpm, feed rate 0.12mm/rev and depth of cut 1mm is shown in Figure 38 (a) and (b).

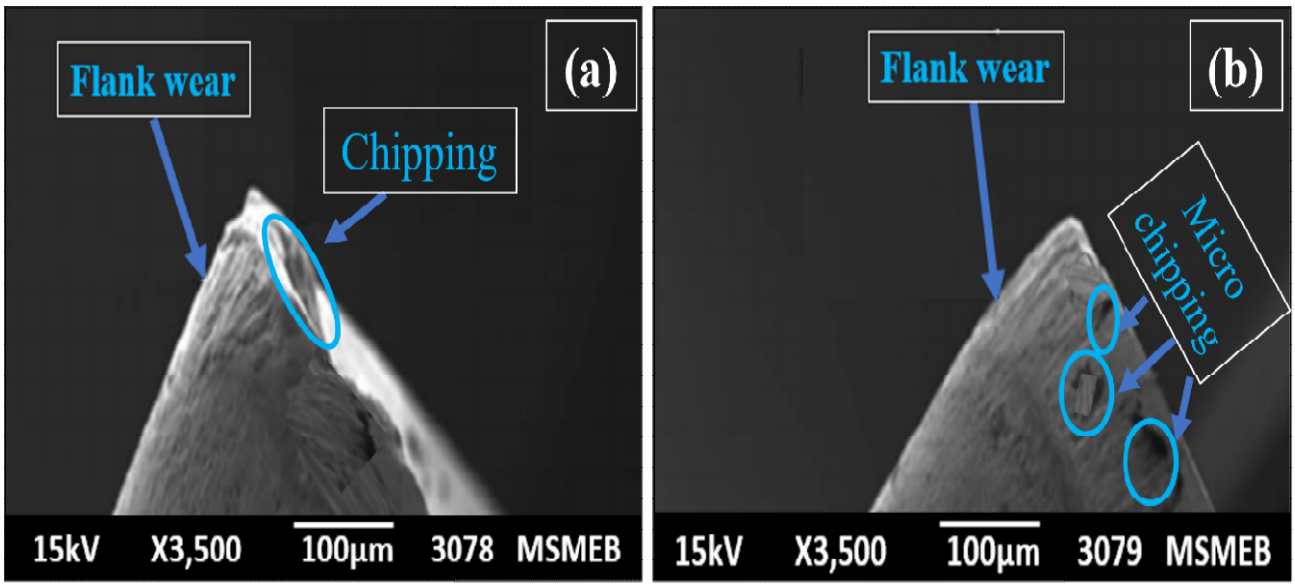

Fig.38: Microstructure of tool wear for confirmatory test at cutting speed 672.2 rpm, feed rate 0.12mm/rev and depth of cut 1mm

8.7 Effect of process parameters on material removal rate (MRR)

There is a striking degree of agreement between the experimental or real values and the anticipated values, as seen by the residual values in Figure 40 (a), which closely match a straight line. Though there may not be much of a difference between the two, the actual numbers differ somewhat from the anticipated values at 2.5 residual values. The primary effect plot for MRR may be shown in Figure 40 (b). Process parameters like cutting speed (v) and depth of cut (d) have a significant contribution in MRR since the slope of speed and depth of cut is quiet steep. Feed rate contribution toward MRR is lesser as compared to speed and depth of cut. It could be seen from ANOVA Table 15 that there is significant percentage contribution of cutting speed 40.48 % and depth of cut 35.16 % towards the MRR whereas for the feed rate it is observed as 18.16 %.

8.7.1 Effect of Cutting speed (V) on MRR

Cutting speed is most significant process parameter for MRR during the turning of samples having the contribution of 40.48 % obtained from ANOVA analysis. As cutting speed is

increased the percentage contribution of MRR gets increased. This can be observed in Figure.39.1 depicting the effect of cutting speed on material removal rate.

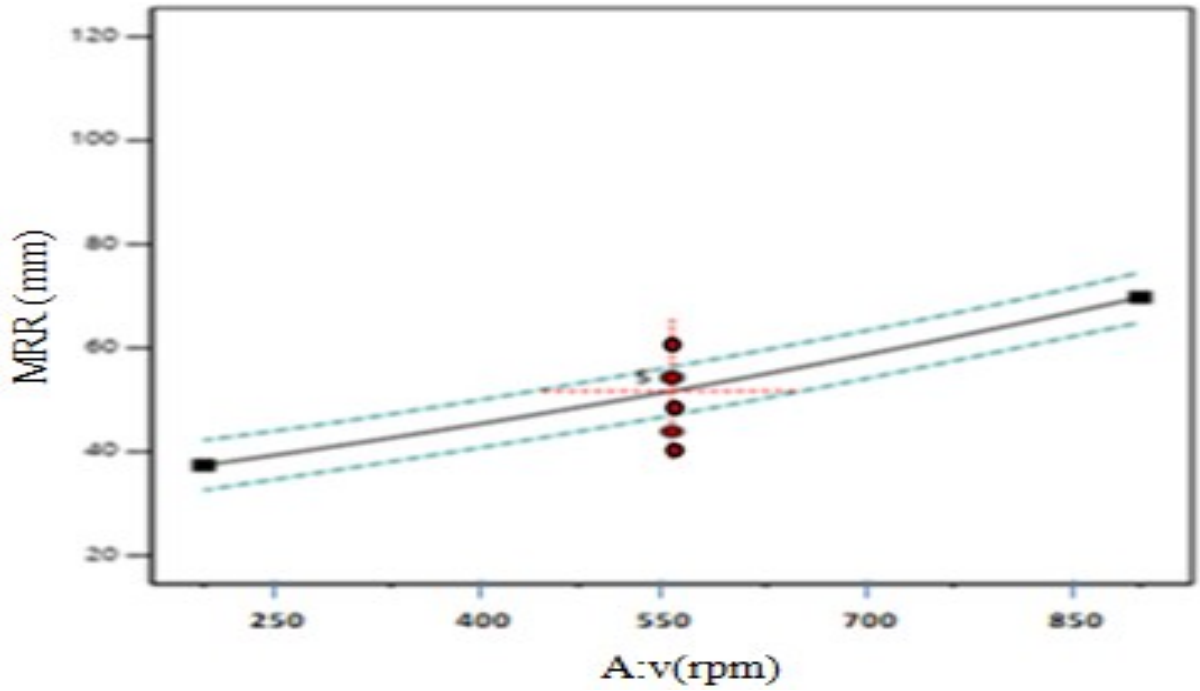

Fig.39.1: Effect of cutting speed (V) on MRR

8.7.2 Effect of depth of cut on MRR

Depth of cut (d) also has a significant contribution on MRR but slightly less than cutting velocity during the turning of EN-36C alloy steel as shown in Figure.39.2. The percentage contribution of depth of cut in MRR is 35.16% depicted from statistical tool analysis.

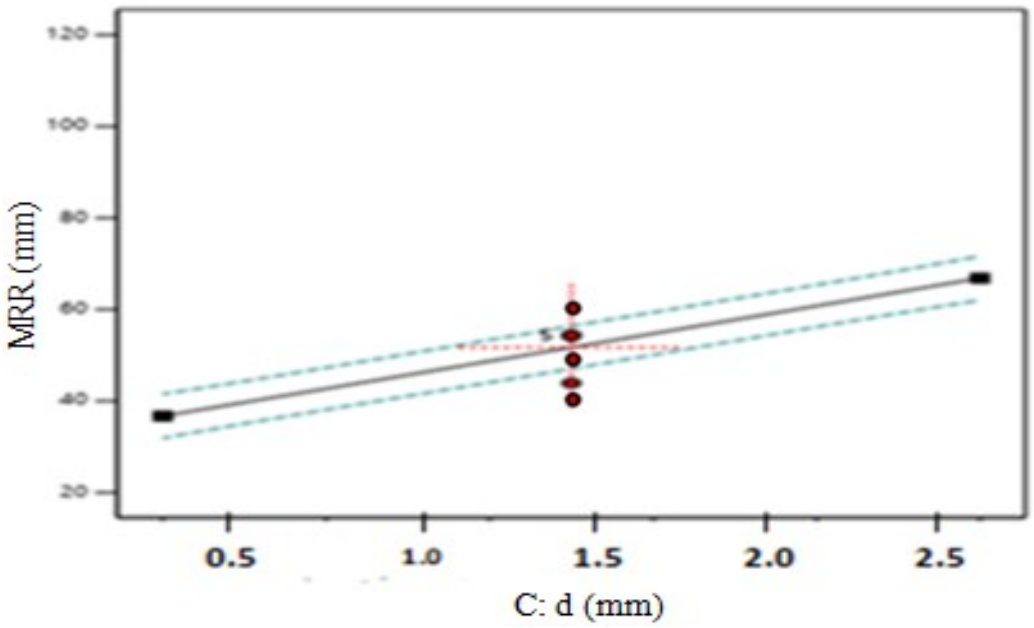

Fig.39.2: Effect of depth of cut (d) on MRR

8.7.3 Effect of feed rate on MRR

Feed rate (f) has less contribution on material removal rate as compared to Cutting velocity (V) and depth of cut (d) during turning as shown in Figure.39.3. The percentage contribution of feed rate in material removal rate is 18.16% as depicted from statistical tool.

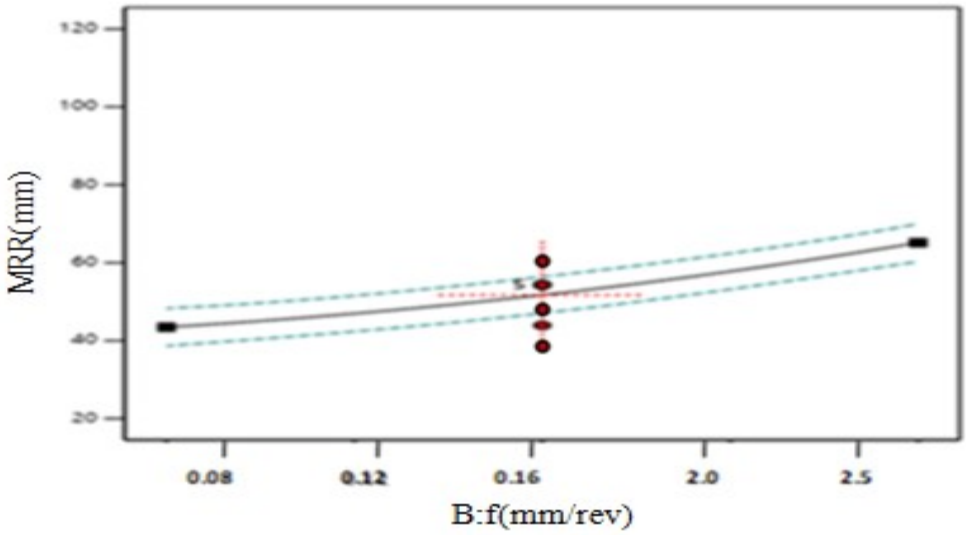

Fig.39.3: Effect of feed rate (f) on MRR

8.7.4 3-D plot pattern of normal probability, main effect and surface for MRR

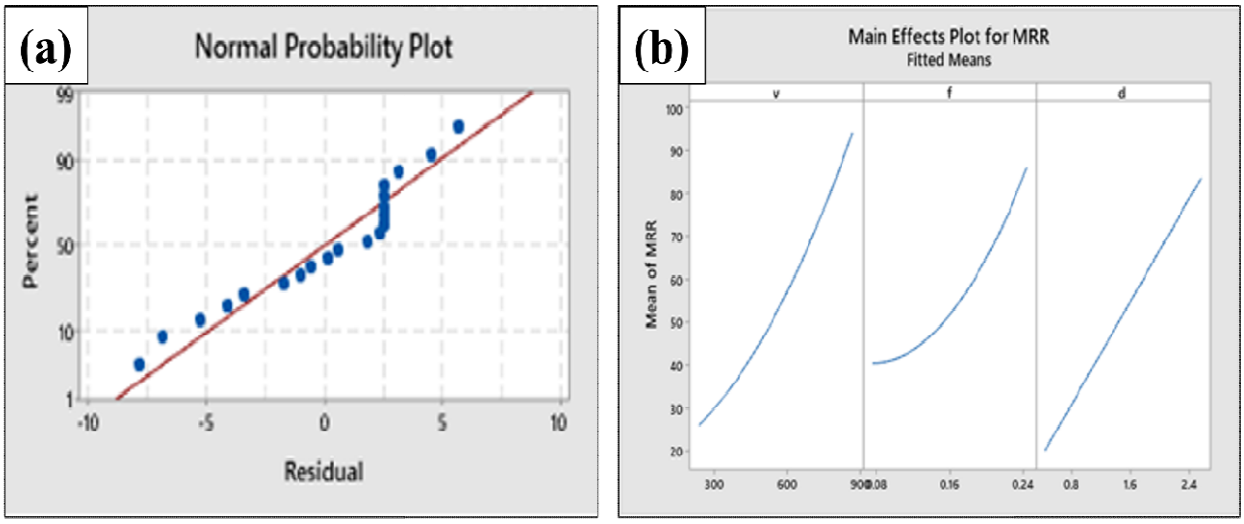

Fig.40: (a) Normal probability plot for MRR, (b) main effect plot for MRR

The 3-D surface plots of MRR for different combinations of machining parameters are shown in Figure 41 (a), (b), and (c). The optimisation result of RSM confirmed that MRR is found to be maximum at cutting speeds of 700 rpm, cutting depths of 2 mm, and feed rates of 0.2 mm/rev. The predicted value of MRR was observed at 113.298 g/min.

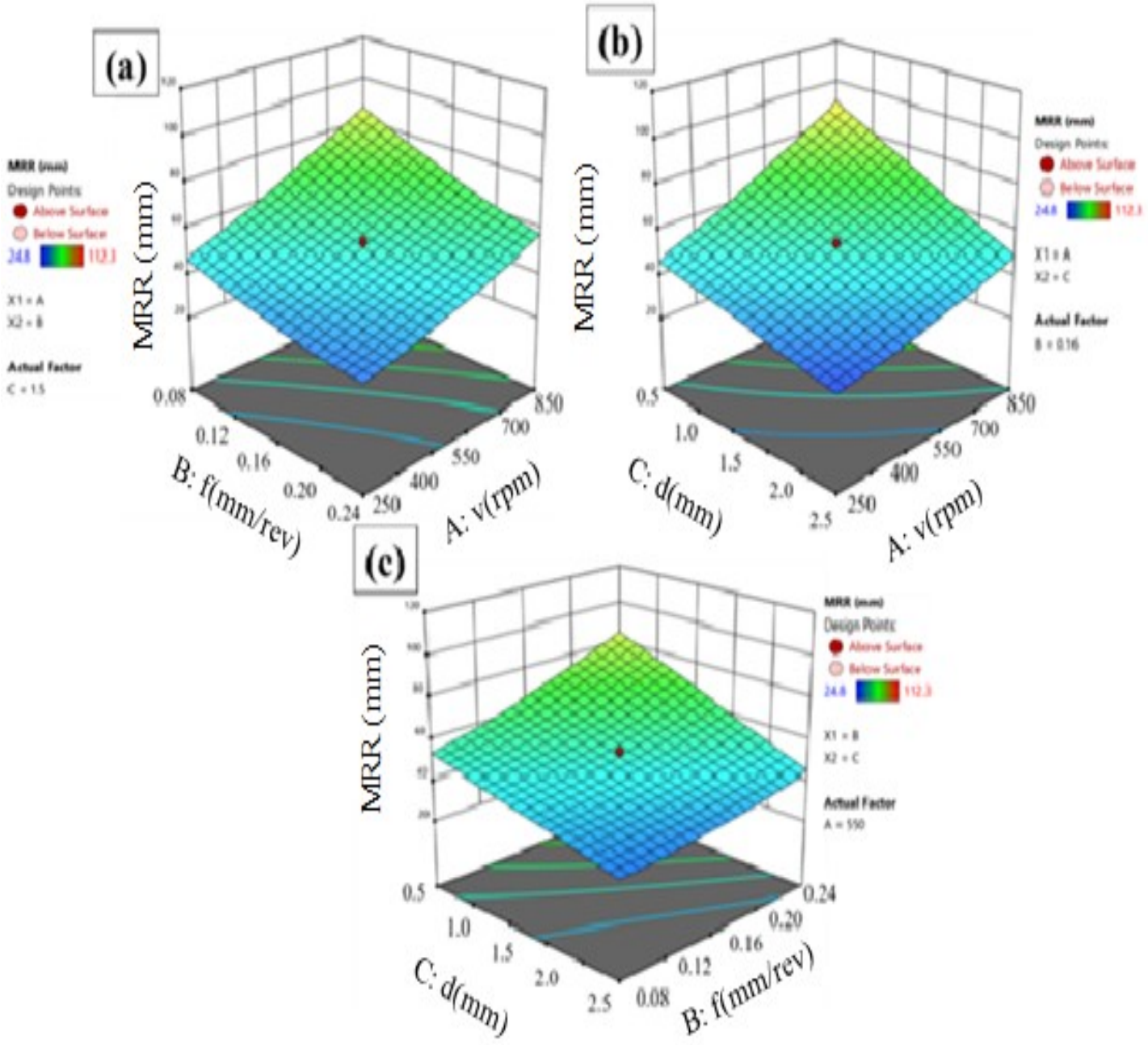

Fig.41: 3-D surface plots interaction effects on MRR (a) Cutting speed and feed rate (b) Depth of cut and cutting speed and (c) Depth of cut and feed rate.

8.8 Confirmation Experiments

Confirmatory tests were carried out at ideal process settings for reactions including residual stress, tool wear, and MRR in order to validate the outcomes of the anticipated model created using RSM, as shown in Table 16. When the actual experiment findings and the projected model were compared, they were discovered to be almost in agreement. Additionally, the data shows that for every answer in this experiment, the percentage errors between the anticipated and experimental values are quite modest.

Table 16: Results of confirmation tests for residual stress, tool wear and MRR

S. no.	Process Parameters	Speed (rpm)	Feed rate (f), mm/rev	Depth of cut(d), mm	Predicted	Actual	Errors (%)
1.	Residual stress (MPa)	250	0.08	1.9	180.528	180	-0.293
2.	Tool wear(mm)	672.2	0.12	1	0.089	0.093	3.54
3.	MRR(g/min)	700	0.2	2	113.298	111.5	-1.612

CHAPTER-9

Conclusions and Future Scope

This chapter contains the conclusions obtained from experimental investigations on EN-36C alloy steel with and without tempered during CNC turning. The process is thoroughly analyzed mechanical properties such as tensile strength, hardness, toughness and percentage elongation, microstructural properties, surface roughness and residual stress by statistical analysis using response surface methodology. The results have been explained in brief and scope of future work is discussed.

9.1 Conclusions

The following conclusions are drawn based on experimental investigations into enhancing the Machinability of EN-36C.

1. Tempering of EN-36C has been done at different temperatures. It has been observed that the residual stress was found minimum as 217 MPa in the specimen tempered at 500°C while it was observed as 732 MPa in the untempered specimen after turning at same process parameters.

2. The FWHM of tempered specimens is observed smaller than untempered specimens.

3. The hardness of the untempered specimen was found to be 93 HRB (Rockwell hardness of scale B) and that of tempered specimen at 500°C was observed as 92 HRB which indicates that hardness of tempered and untempered specimen was almost same.

4. The toughness of specimen tempered at 500°C was observed maximum 187 J than untempered specimen 35 J which shows significant improvement in toughness.

5. It has been observed that the average value of tensile strength of specimen tempered at 500°C was found minimum (680.418 MPa) as compared to untempered specimens1024.001MPa which shows reduction in tensile strength in tempered specimen.

6. Optical microscopic analysis shows the improvement over partial ferrite and residual austenite in tempered specimens and enhanced machinability as compared to untempered specimens.

7. Analysis of variance shows more contribution towards cutting speed and feed rate than depth of cut for minimum residual stress and tool wear, while more contribution towards cutting speed and depth of cut was observed than feed rate for maximum MRR.

8. Minimum residual stress was found to be 180.528 MPa at a cutting speed of 250 rpm, a feed rate of 0.08 mm/rev, and a cutting depth of 1.914 mm.

9. Minimum tool wear of 0.0899 mm was found at a cutting speed of 672.233 rpm, a feed rate of 0.12 mm/rev, and depth of cut of 1mm.

10. Maximum MRR of 298 g/min was observed at a cutting speed of 700 rpm, depth of cut of 2 mm, and feed rate of 0.2 mm/rev.

9.2 Scope of future work

1. Experimental investigations on EN-36C alloy steel can also be carried out for analyzing of mechanical properties and microstructural behaviour with and without treatment of cryogenic.

2. Mathematical modeling and simulation can also be conducted.

3. Study can also be extended for all hard metals.

4. Further research can be also extended for force measurement and power requirement during turning .

5. Study of chips formation of EN-36C can be added at different stage of tempering.

6. Study of tool and machine vibration due to the tempered and untempered work-piece can be studied

REFERENCES

[1] Abhang, L. B., & Hameedullah, M. (2012). Optimization of machining parameters in steel turning operation by Taguchi method. *Procedia Engineering*, *38*, 40-48.

[2] Bouzid, L., Boutabba, S., Yallese, M. A., Belhadi, S., & Girardin, F. (2014). Simultaneous optimization of surface roughness and material removal rate for turning of X20Cr13 stainless steel. *The International Journal of Advanced Manufacturing Technology*, *74*, 879-891.

[3] Lou, M. S., Chen, J. C., & Li, C. M. (1998). Surface roughness prediction technique for CNC end-milling. *Journal of industrial technology*, *15*(1), 1-6.

[4] Kalpak jian, S., Schmid, S. R., & Werner, E. (2011). *Werkstofftechnik*. Pearson Deutschland GmbH.

[5] Rao, C. J., Rao, D. N., & Srihari, P. (2013). Influence of cutting parameters on cutting force and surface finish in turning operation. *Procedia Engineering*, *64*, 1405-1415.

[6] Abhang, L. B., & Hameedullah, M. (2011). Multi performance optimization in machining of En-31 steel alloy using Taguchi-utility concept. *Journal of Manufacturing Technology Research*, *3*(3/4), 265.

[7] Günay, M., & Yücel, E. (2013). Application of Taguchi method for determining optimum surface roughness in turning of high-alloy white cast iron. *Measurement*, *46*(2), 913-919.

[8] Zerti, O., Yallese, M. A., Khettabi, R., Chaoui, K., & Mabrouki, T. (2017). Design optimization for minimum technological parameters when dry turning of AISI D3 steel using Taguchi method. *The International Journal of Advanced Manufacturing Technology*, *89*, 1915-1934.

[9] Zhang, B., Katinas, C., & Shin, Y. C. (2018). Robust tool wear monitoring using systematic feature selection in turning processes with consideration of uncertainties. *Journal of Manufacturing Science and Engineering*, *140*(8), 081010.

[10]Kaladhar, M., Subbaiah, K. V., & Rao, C. S. (2012). Determination of optimum process parameters during turning of AISI 304 austenitic stainless steels using Taguchi method and ANOVA. *International Journal of lean thinking*, *3*(1), 1-19.

[11] Gosai, M., & Bhavsar, S. N. (2016). Experimental study on temperature measurement in turning operation of hardened steel (EN36). *Procedia Technology*, *23*, 311-318.

[12] Reddy, P. M., Reddy, P. V. B., Reddy, Y. A. K., & Naresh, N. (2014). Optimization of machining parameter for turning of EN16 steel using grey based Taguchi method. *ARPN Journal of Engineering and Applied Sciences*, *9*(3), 215-222.

[13] Aggarwal, A., Singh, H., Kumar, P., & Singh, M. (2008). Optimizing power consumption for CNC turned parts using response surface methodology and Taguchi's technique—a comparative analysis. *Journal of materials processing technology*, *200*(1-3), 373-384.

[14] Işık, B. (2008). Experimental investigations of surface roughness in orthogonal turning of unidirectional glass-fiber reinforced plastic composites. *The International Journal of Advanced Manufacturing Technology*, *37*, 42-48.

[15] Kumar, N. S., Shetty, A., Shetty, A., Ananth, K., & Shetty, H. (2012). Effect of spindle speed and feed rate on surface roughness of carbon steels in CNC turning. *Procedia Engineering*, *38*, 691-697.

[16] Abhang, L. B., & Hameedullah, M. (2010). Chip-tool interface temperature prediction model for turning process. *International Journal of Engineering Science and Technology*, *2*(4), 382-393.

[17] Routara, B. C., Sahoo, A. K., Parida, A. K., & Padhi, P. C. (2012). Response surface methodology and genetic algorithm used to optimize the cutting condition for surface roughness parameters in CNC turning. *Procedia engineering*, *38*, 1893-1904.

[18] Aslan, E., Camuşcu, N., & Birgören, B. (2007). Design optimization of cutting parameters when turning hardened AISI 4140 steel (63 HRC) with Al2O3+ TiCN mixed ceramic tool. *Materials & design*, *28*(5), 1618-1622.

[19] Sahoo, A. K., & Sahoo, B. (2013). Performance studies of multilayer hard surface coatings (TiN/TiCN/Al2O3/TiN) of indexable carbide inserts in hard machining: Part-II (RSM, grey relational and techno economical approach). *Measurement*, *46*(8), 2868-2884.

[20] Suresh, R., & Basavarajappa, S. (2014). Effect of process parameters on tool wear and surface roughness during turning of hardened steel with coated ceramic tool. *Procedia Materials Science*, *5*, 1450-1459.

[21] Das, S. R., Dhupal, D., & Kumar, A. (2015). Study of surface roughness and flank wear in hard turning of AISI 4140 steel with coated ceramic inserts. *Journal of Mechanical Science and Technology*, *29*, 4329-4340.

[22] Aouici, H., Yallese, M. A., Fnides, B., Chaoui, K., & Mabrouki, T. (2011). Modeling and optimization of hard turning of X38CrMoV5-1 steel with CBN tool: Machining parameters effects on flank wear and surface roughness. *Journal of mechanical science and technology*, *25*, 2843-2851.

[23] Gaitonde, V. N., Karnik, S. R., Figueira, L., & Davim, J. P. (2011). Performance comparison of conventional and wiper ceramic inserts in hard turning through artificial neural network modeling. *The International Journal of Advanced Manufacturing Technology*, *52*, 101-114.

[24] Horng, J. T., Liu, N. M., & Chiang, K. T. (2008). Investigating the machinability evaluation of Hadfield steel in the hard turning with Al2O3/TiC mixed ceramic tool based on the response surface methodology. *Journal of materials processing technology*, *208*(1-3), 532-541.

[25] HAFIZ, A. (2008). Prediction of tool life in end milling of hardened steel AISI D2. *European Journal of Scientific Research*, *21*(4), 592-602.

[26] Dolinšek, S., Šuštaršič, B., & Kopač, J. (2001). Wear mechanisms of cutting tools in high-speed cutting processes. *Wear*, *250*(1-12), 349-356.

[27] Grzesik, W., Bartoszuk, M., & Nieslony, P. (2005). Finite element modelling of temperature distribution in the cutting zone in turning processes with differently coated tools. *Journal of Materials Processing Technology*, *164*, 1204-1211.

[28] YİĞİT, R., Findik, F., & Celik, E. (2010). Performance of multilayer coated carbide tools when turning cast iron. *Turkish Journal of Engineering and Environmental Sciences*, *33*(3), 147-158.

[29] Aslantas, K., Ucun, I., & Cicek, A. (2012). Tool life and wear mechanism of coated and uncoated Al2O3/TiCN mixed ceramic tools in turning hardened alloy steel. *Wear*, *274*, 442-451.

[30] Kamdar, N. M., & Patel, V. K. (2012). Experimental investigation of machining parameters of EN 36 steel using tungsten carbide cutting tool during hot machining. *International Journal of Engineering Research and Applications*, *2*, 1833-1838.

[31] Singh, K. P., Gautam, G. D., Yadav, R., Bisht, L., & Norkey, G. (2014). Selection of Optimum Machining Parameters for EN36 Alloy Steel in CNC Turning Using Taguchi Method. *International Journal of Scientific & Engineering Research*, *5*(3).

[32] Salvi, S. B., Deshmukh, R. R., & Deshmukh, S. D. (2013). Analysis of surface roughness in hard turning by using Taguchi method. *International Journal of Engineering Science and Technology*, *5*(02), 365-370.

[33] Suresh, R., & Basavarajappa, S. (2014). Effect of process parameters on tool wear and surface roughness during turning of hardened steel with coated ceramic tool. *Procedia Materials Science*, *5*, 1450-1459.

[34] Sahoo, A. (2014). Application of Taguchi and regression analysis on surface roughness in machining hardened AISI D2 steel. *International Journal of Industrial Engineering Computations*, *5*(2), 295-304.

[35] Zahia, H., Athmane, Y., Lakhdar, B., & Tarek, M. (2015). On the application of response surface methodology for predicting and optimizing surface roughness and cutting forces in hard turning by PVD coated insert. *International Journal of Industrial Engineering Computations*, *6*(2), 267-284.

[36] Lawrence, I. D., Pandiarajan, M., & Kaviprakash, G. (2015). Prediction of machining parameters in turning on EN36. *International Journal of Applied Engineering Research*, *10*(55), 4070-75.

[37] Rashid, W. B., Goel, S., Davim, J. P., & Joshi, S. N. (2016). Parametric design optimization of hard turning of AISI 4340 steel (69 HRC). *The International Journal of Advanced Manufacturing Technology*, *82*, 451-462.

[38] Aouici, H., Fnides, B., Elbah, M., Benlahmidi, S., Bensouilah, H., & Yallese, M. (2016). Surface roughness evaluation of various cutting materials in hard turning of AISI H11. *International Journal of Industrial Engineering Computations*, *7*(2), 339-352.

[39] Lister, P. M., & Barrow, G. (1986). Tool condition monitoring systems. In *Proceedings of the Twenty-Sixth International Machine Tool Design and Research Conference: held in Manchester 17th–18th September 1986* (pp. 271-288). Macmillan Education UK.

[40] Shaw, M. C., & Cookson, J. O. (2005). *Metal cutting principles* (Vol. 2, No. 3). New York: Oxford university press.

[41] Honeycombe, R. W. K. (1995). Steels microstructure and properties. *Metallurgy and materials science*, *1*.

[42] Dobrzański, L. A., Kasprzak, W., & Mazurkiewicz, J.(1995) The structure and properties W-Mo-V-Co high-speed steel of the type 11-2-2-5 after heat treatment. In *Proceedings of the 4th International Scientific Conference „Achievements in Mechanical and Materials Engineering" AMME* (Vol. 95, pp. 83-86).

[43] Taylor, K. A., Olson, G. B., Cohen, M., & Sande, J. V. (1989). Carbide precipitation during stage I tempering of Fe-Ni-C martensites. *Metallurgical Transactions A*, *20*, 2749-2765.

[44] Di Gianfrancesco, A., Cipolla, L., Venditti, D., Neri, S., & Calderini, M. (2008). Creep behaviour and microstructural analysis of FB2 trial rotor steel. In *Proc of the Fifth International Conference on Advances in Materials Technology for Fossil Power Plants, Marco Island, FL, USA, ASM International* (pp. 366-376).

[45] Wang, X., & Feng, C. X. (2002). Development of empirical models for surface roughness prediction in finish turning. *The International Journal of Advanced Manufacturing Technology*, *20*, 348-356.

[46] Suresh, P. V. S., Rao, P. V., & Deshmukh, S. G. (2002). A genetic algorithmic approach for optimization of surface roughness prediction model. *International Journal of Machine Tools and Manufacture*, *42*(6), 675-680.

[47] Neşeli, S., Yaldız, S., & Türkeş, E. (2011). Optimization of tool geometry parameters for turning operations based on the response surface methodology. *Measurement*, *44*(3), 580-587.

[48] Attanasio, A., Gelfi, M., Giardini, C., & Remino, C. A. R. L. O. (2006). Minimal quantity lubrication in turning: Effect on tool wear. *Wear*, *260*(3), 333-338.

[49] Dhar, N. R., Ahmed, M. T., & Islam, S. (2007). An experimental investigation on effect of minimum quantity lubrication in machining AISI 1040 steel. *International Journal of Machine Tools and Manufacture*, *47*(5), 748-753.

[50] Dhar, N. R., Islam, M. W., Islam, S., & Mithu, M. A. H. (2006). The influence of minimum quantity of lubrication (MQL) on cutting temperature, chip and dimensional accuracy in turning AISI-1040 steel. *Journal of materials processing technology*, *171*(1), 93-99.

[51] Autret, R., Liang, S. Y., & Woodruff, G. W. (2003, March). Minimum quantity lubrication in finish hard turning. In *Proceedings of International Conference on Humanoid, Nanotechnology, Information Technology, Communication and Control, Environment, and Management, Manila*.

[52] Khan, M. M. A., Mithu, M. A. H., & Dhar, N. R. (2009). Effects of minimum quantity lubrication on turning AISI 9310 alloy steel using vegetable oil-based cutting fluid. *Journal of materials processing Technology*, *209*(15-16), 5573-5583.

[53] Vyas, A. S. M. E., & Shaw, M. C. (1999). Mechanics of saw-tooth chip formation in metal cutting.

[54] Jena, P. K., Mishra, B., RameshBabu, M., Babu, A., Singh, A. K., SivaKumar, K., & Bhat, T. B. (2010). Effect of heat treatment on mechanical and ballistic properties of a high strength armour steel. *International journal of impact engineering*, *37*(3), 242-249.

[55] Yang, J. R., Yu, T. H., & Wang, C. H. (2006). Martensitic transformations in AISI 440C stainless steel. *Materials Science and Engineering: A*, *438*, 276-280.

[56] Bhat, T. B. (1984). Principles of armour design. *Trans Indian Inst Met*, *57*(4), 313-34.

[57] Ulutan, D., & Ozel, T. (2011). Machining induced surface integrity in titanium and nickel alloys: A review. *International Journal of Machine Tools and Manufacture*, *51*(3), 250-280.

[58] Zhuang, W. Z., & Halford, G. R. (2001). Investigation of residual stress relaxation under cyclic load. *International journal of fatigue*, *23*, 31-37.

[59] Hoffmeister, J., Schulze, V., Hessert, R., & Koenig, G. (2012). Residual stresses under quasi-static and cyclic loading in shot peened Inconel 718. *International journal of materials research*, *103*(1), 66-72.

[60] Cullity, B. D. (1956). *Elements of X-ray Diffraction*. Addison-Wesley Publishing.

[61] Noyan, I. C., & Cohen, J. B. (2013). *Residual stress: measurement by diffraction and interpretation*. Springer.

[62] Prevey, P. S. (1976). A method of determining the elastic properties of alloys in selected crystallographic directions for X-ray diffraction residual stress measurement. *Advances in X-ray Analysis*, *20*, 345-354.

[63] Noyan, I. C., & Cohen, J. B. (2013). *Residual stress: measurement by diffraction and interpretation*. Springer.

[64] Pineault, J. A., Belassel, M., & Brauss, M. E. (2002). X-ray diffraction residual stress measurement in failure analysis. *Failure Analysis and Prevention*, *11*, 484-497.

[65] Wojciechowski, S., Krajewska-Śpiewak, J., Maruda, R. W., Krolczyk, G. M., Nieslony, P., Wieczorowski, M., & Gawlik, J. (2023). Study on ploughing phenomena in tool flank face–workpiece interface including tool wear effect during ball-end milling. *Tribology International*, *181*, 108313.

[66] Zębala, W., Struzikiewicz, G., & Rumian, K. (2021). Cutting forces and tool wear investigation during turning of sintered nickel-cobalt alloy with CBN tools. *Materials*, *14*(7), 1623.

[67] Tu, L., Lin, L., Liu, C., Zheng, T., Deng, Y., Han, L., ... & Chen, M. (2023). Tool wear characteristics analysis of cBN cutting tools in high-speed turning of Inconel 718. *Ceramics International*, *49*(1), 635-658.

[68] Poulachon, G., Albert, A., Schluraff, M. A., & Jawahir, I. S. (2005). An experimental investigation of work material microstructure effects on white layer formation in PCBN hard turning. *International Journal of Machine Tools and Manufacture*, *45*(2), 211-218.

[69] Lescano, D. E., & Silvetti, S. P. (2012). Study of microestructure and tempered martensite embrittlement in AISI 15B41 steel. *Procedia Materials Science*, *1*, 134-140.

[70] Jian, Z. H. O. U., CHI, H. X., CHEN, Z. Z., & LI, X. Y. (2013). Microstructure and properties of hot working die steel H13MOD. *Journal of Iron and Steel Research, International*, *20*(9), 117-125.

[71] Stoicanescu, M., Ene, E., Zara, A., Giacomelli, I., & Crisan, A. (2016). The heat treatment influence of 1.3343 high speed steel on content of residual austenite. *Procedia Technology*, *22*, 161-166.

[72] Deng, X., & Ju, D. (2013). Modeling and simulation of quenching and tempering process in steels. *Physics Procedia*, *50*, 368-374.

[73] Sasaki, T., Takahashi, S., Iwfuchi, K., Satoh, Y., Kanematsu, Y., Chiba, M., & Takago, S. (2006, September). Residual stress in railway rails by IP/cosα method. In *Materials science forum* (Vol. 524, pp. 381-386). Trans Tech Publications Ltd.

[74] Sasaki, T., Maruyama, Y., Ohba, H., & Ejiri, S. (2014). Two-dimensional imaging of Debye-Scherrer ring for tri-axial stress analysis of industrial materials. *Journal of Instrumentation*, *9*(07), C07006.

[75] Savaria, V., Bridier, F., & Bocher, P. (2016). Predicting the effects of material properties gradient and residual stresses on the bending fatigue strength of induction hardened aeronautical gears. *International Journal of Fatigue*, *85*, 70-84.

[76] Arrazola, P. J., Kortabarria, A., Madariaga, A., Esnaola, J. A., Fernandez, E., Cappellini, C.,& Özel, T. (2014). On the machining induced residual stresses in IN718 nickel-based alloy: Experiments and predictions with finite element simulation. *Simulation Modelling Practice and Theory*, *41*, 87-103.

[77] Hua, Y., & Liu, Z. (2018). Experimental investigation of principal residual stress and fatigue performance for turned nickel-based superalloy Inconel 718. *Materials*, *11*(6), 879.

[78] Reddy, N. S. K., & Rao, P. V. (2006). Selections of an optimal parametric combination for achieving a better surface finish in dry milling using genetic algorithms. *The International Journal of Advanced Manufacturing Technology*, *28*, 463-473.

[79] Jain, A., & Pandey, A. K. (2019). Modeling and optimizing of different quality characteristics in electrical discharge drilling of titanium alloy (Grade-5) sheet. *Materials Today: Proceedings*, *18*, 182-191.

[80] Jain, A., & Pandey, A. K. (2017). Multiple quality optimizations in electrical discharge drilling of mild steel sheet. *Materials Today: Proceedings*, *4*(8), 7252-7261.

[81] Hou, T. H., Su, C. H., & Liu, W. L. (2007). Parameters optimization of a nano-particle wet milling process using the Taguchi method, response surface method and genetic algorithm. *Powder technology*, *173*(3), 153-162.

[82] Kilickap, E., Huseyinoglu, M., & Yardimeden, A. (2011). Optimization of drilling parameters on surface roughness in drilling of AISI 1045 using response surface methodology and genetic algorithm. *The International Journal of Advanced Manufacturing Technology*, *52*, 79-88.

[83] Pai, D., Rao, S. S., & D'souza, R. (2011). Multi objective optimization of surface grinding process by combination of RSM and nondominated sorting GA. *Int J Comp Appl*, *36*(3), 19-24.

[84] Wibowo, A., & Desa, M. I. (2012). Kernel based regression and genetic algorithms for estimating cutting conditions of surface roughness in end milling machining process. *Expert Systems with Applications*, *39*(14), 11634-11641.

[85] Davis, J. R. (Ed.). (1992). *ASM materials engineering dictionary*. ASM international.

[86] Snis, M., & Olsson, J. (2008). Reduce costs for storage and distribution of desalted water—Use duplex stainless steel. *Desalination*, *223*(1-3), 476-486.

[87] Agrawal, S., Chakrabarti, A. K., & Chattopadhyay, A. B. (1995). A study of the machining of cast austenitic stainless-steels with carbide tools. *Journal of materials processing technology*, *52*(2-4), 610-620.

[88] Kumar, A. S., Durai, A. R., & Sornakumar, T. (2006). The effect of tool wear on tool life of alumina-based ceramic cutting tools while machining hardened martensitic stainless steel. *Journal of Materials Processing Technology*, *173*(2), 151-156.

[89] Noordin, M. Y., Venkatesh, V. C., & Sharif, S. (2007). Dry turning of tempered martensitic stainless tool steel using coated cermet and coated carbide tools. *Journal of materials processing technology*, *185*(1-3), 83-90.

[90] Saï, W. B., Salah, N. B., & Lebrun, J. L. (2001). Influence of machining by finishing milling on surface characteristics. *International Journal of Machine Tools and Manufacture*, *41*(3), 443-450.

[91] Mandal, N., Doloi, B., Mondal, B., & Das, R. (2011). Optimization of flank wear using Zirconia Toughened Alumina (ZTA) cutting tool: Taguchi method and Regression analysis. *Measurement*, *44*(10), 2149-2155.

[92] Asiltürk, I., & Akkuş, H. (2011). Determining the effect of cutting parameters on surface roughness in hard turning using the Taguchi method. *Measurement*, *44*(9), 1697-1704.

[93] Matsumoto, Y., Barash, M. M., & Liu, C. R. (1986). Effect of hardness on the surface integrity of AISI 4340 steel.

[94] Thiele, J. D., Melkote, S. N., Peascoe, R. A., & Watkins, T. R. (2000). Effect of cutting-edge geometry and workpiece hardness on surface residual stresses in finish hard turning of AISI 52100 steel. *J. Manuf. Sci. Eng.*, *122*(4), 642-649.

[95] Thiele, J. D., & Melkote, S. N. (2000). Effect of tool edge geometry on workpiece subsurface deformation and through-thickness residual stresses for hard turning of AISI 52100 steel. *Journal of Manufacturing Processes*, *2*(4), 270-276.

[96] Matsumoto, Y., Hashimoto, F., & Lahoti, G. (1999). Surface integrity generated by precision hard turning. *CIRP Annals*, *48*(1), 59-62.

[97] Abrão, A. M., & Aspinwall, D. K. (1996). The surface integrity of turned and ground hardened bearing steel. *Wear*, *196*(1-2), 279-284.

[98]Agha, S. R., & Liu, C. R. (2000). Experimental study on the performance of superfinish hard turned surfaces in rolling contact. *Wear*, *244*(1-2), 52-59.

[99] Mittal, S., & Liu, C. R. (1998). A method of modeling residual stresses in superfinish hard turning. *Wear*, *218*(1), 21-33.

[100] Özel, T., Karpat, Y., Figueira, L., & Davim, J. P. (2007). Modelling of surface finish and tool flank wear in turning of AISI D2 steel with ceramic wiper inserts. *Journal of materials processing technology*, *189*(1-3), 192-198.

[101] Thamizhmnaii, S., Bin Omar, B., Saparudin, S., & Hasan, S. (2008). Tool flank wear analyses on martensitic stainless steel by turning. *Archives of Materials Science and Engineering*, *32*(1), 41-44.

[102] Lin, H. M., Liao, Y. S., & Wei, C. C. (2008). Wear behavior in turning high hardness alloy steel by CBN tool. *Wear*, *264*(7-8), 679-684.

[103] Thamizhmanii, S., Kamarudin, K., Rahim, E. A., Saparudin, A., & Hassan, S. (2007, July). Tool Wear and Surface Roughness in Turning AISI 8620 using Coated Ceramic Tool. In *World Congress on Engineering* (pp. 1157-1161).

[104] Mahfoudi, F., List, G., Molinari, A., Moufki, A., & Boulanouar, L. (2008). High speed turning for hard material with PCBN inserts: tool wear analysis. *International Journal of Machining and Machinability of Materials*, *3*(1-2), 62-79.

[105] Arsecularatne, J. A., Zhang, L. C., & Montross, C. (2006). Wear and tool life of tungsten carbide, PCBN and PCD cutting tools. *International Journal of Machine Tools and Manufacture*, *46*(5), 482-491.

[106] Huang, Y., & Dawson, T. G. (2005). Tool crater wear depth modeling in CBN hard turning. *Wear*, *258*(9), 1455-1461.

[107] Xie, L. J., Schmidt, J., Schmidt, C., & Biesinger, F. (2005). 2D FEM estimate of tool wear in turning operation. *Wear*, *258*(10), 1479-1490.

[108] Lorentzon, J., & Järvstråt, N. (2008). Modelling tool wear in cemented-carbide machining alloy 718. *International Journal of Machine Tools and Manufacture*, *48*(10), 1072-1080.

[109] Wang, X., Wang, W., Huang, Y., Nguyen, N., & Krishnakumar, K. (2008). Design of neural network-based estimator for tool wear modeling in hard turning. *Journal of intelligent manufacturing*, *19*, 383-396.

[110] Mamalis, A. G., Kundrák, J., Markopoulos, A., & Manolakos, D. E. (2008). On the finite element modelling of high speed hard turning. *The International Journal of Advanced Manufacturing Technology*, *38*, 441-446.

[111] Bouzid Sai, W. (2005). An investigation of tool wear in high-speed turning of AISI 4340 steel. *The International Journal of Advanced Manufacturing Technology*, *26*, 330-334.

[112] Sharma, V. S., Sharma, S. K., & Sharma, A. K. (2008). Cutting tool wear estimation for turning. *Journal of Intelligent Manufacturing*, *19*, 99-108.

[113] Astakhov, V. P. (2007). Effects of the cutting feed, depth of cut, and workpiece (bore) diameter on the tool wear rate. *The International Journal of Advanced Manufacturing Technology*, *34*, 631-640.

[114] Maranhão, C., & Davim, J. P. (2010). Finite element modelling of machining of AISI 316 steel: numerical simulation and experimental validation. *Simulation Modelling Practice and Theory*, *18*(2), 139-156.

[115] Coelho, R. T., Ng, E. G., & Elbestawi, M. A. (2007). Tool wear when turning hardened AISI 4340 with coated PCBN tools using finishing cutting conditions. *International Journal of Machine Tools and Manufacture*, *47*(2), 263-272.

[116] Bäker, M. (2006). Finite element simulation of high-speed cutting forces. *Journal of Materials Processing Technology*, *176*(1-3), 117-126.

[117] Shi, G., Deng, X., & Shet, C. (2002). A finite element study of the effect of friction in orthogonal metal cutting. *Finite Elements in Analysis and Design*, *38*(9), 863-883.

[118] Umbrello, D., Filice, L., Rizzuti, S., Micari, F., & Settineri, L. (2007). On the effectiveness of finite element simulation of orthogonal cutting with particular reference to temperature prediction. *Journal of materials processing technology*, *189*(1-3), 284-291.

[119] Arunachalam, R. M., Mannan, M. A., & Spowage, A. C. (2004). Residual stress and surface roughness when facing age hardened Inconel 718 with CBN and ceramic cutting tools. *International Journal of Machine Tools and Manufacture*, *44*(9), 879-887.

[120] Gunnberg, F., Escursell, M., & Jacobson, M. (2006). The influence of cutting parameters on residual stresses and surface topography during hard turning of 18MnCr5 case carburised steel. *Journal of Materials Processing Technology*, *174*(1-3), 82-90.

[121] Attanasio, A., Ceretti, E., Fiorentino, A., Cappellini, C. R. I. S. T. I. A. N., & Giardini, C. (2010). Investigation and FEM-based simulation of tool wear in turning operations with uncoated carbide tools. *Wear*, *269*(5-6), 344-350.

[122] Caruso, S., Outeiro, J. C., Umbrello, D., & M'Saoubi, R. (2010). Modeling and experimental validation of the surface residual stresses induced by hard machining of AISI H13 tool steel. *International journal of material forming*, *3*, 515-518.

[123] Ulutan, D., Alaca, B. E., & Lazoglu, I. (2007). Analytical modelling of residual stresses in machining. *Journal of Materials Processing Technology*, *183*(1), 77-87.

[124] Outeiro, J. C., Pina, J. C., M'saoubi, R., Pusavec, F., & Jawahir, I. S. (2008). Analysis of residual stresses induced by dry turning of difficult-to-machine materials. *CIRP annals*, *57*(1), 77-80.

[125] Rizzuti, S., Umbrello, D., Filice, L., & Settineri, L. (2010). Finite element analysis of residual stresses in machining. *International Journal of Material Forming*, *3*, 431-434.

[126] Jena, P. K., & Senthil P, P. (2016). Effect of tempering time on the ballistic performance of a high strength armour steel. *Journal of applied research and technology*, *14*(1), 47-53.

[127] Jha, S. K. (2017). Investigation of micro-structure and mechanical properties of three steel alloys. *International Journal of Automotive and Mechanical Engineering*, *14*(2), 4315-4331.

[128] Gaitonde, V. N., Karnik, S. R., Figueira, L., & Davim, J. P. (2009). Analysis of machinability during hard turning of cold work tool steel (type: AISI D2). *Materials and Manufacturing Processes*, *24*(12), 1373-1382.

[129] Taira, S., Tanaka, K., & Yamasaki, T. (1978). A method of X-ray microbeam measurement of local stress and its application to fatigue crack growth problems. *Japan Society of Materials Science, Journal*, *27*, 251-256.

[130] Jena, P. K., Mishra, B., RameshBabu, M., Babu, A., Singh, A. K., SivaKumar, K., & Bhat, T. B. (2010). Effect of heat treatment on mechanical and ballistic properties of a high strength armour steel. *International journal of impact engineering*, *37*(3), 242-249.

[131] Qu, S. G., Zhang, Y. L., Lai, F. Q., & Li, X. Q. (2018). Effect of tempering temperatures on tensile properties and rotary bending fatigue behaviors of 17Cr2Ni2MoVNb steel. *Metals*, *8*(7), 507.

[132] Krawczyk, J., Bała, P., & Pawłowski, B. (2010). Kinetics of phase transformations of undercooled austenite in 18CrNiMo7-6 steel applied for toothed wheels. *Archives of Foundry Engineering*, *10*(3), 29-34.

[133] Kam, M., & Şeremet, M. (2021). Experimental investigation of the effect of machinability on surface quality and vibration in hard turning of hardened AISI 4140 steels using ceramic cutting tools. *Proceedings of the Institution of Mechanical Engineers, Part E: Journal of Process Mechanical Engineering*, *235*(5), 1565-1574.

[134] Ranjole, C., Singh, V. P., Kuriachen, B., & Vineesh, K. P. (2022). Numerical prediction and experimental investigation of temperature, residual stress and mechanical properties of dissimilar friction-stir welded AA5083 and AZ31 alloys. *Arabian Journal for Science and Engineering*, *47*(12), 16103-16115.

[135] Kumar, R., Dwivedi, R. K., Singh, V. P., Kuriachen, B., & Krishnan, N. A. (2023). Influence of toughness and retained austenite on wear behaviour of carbide-free bainite in high silicon steel. *Transactions of the Indian Institute of Metals*, *76*(9), 2425-2434.

[136] Arrazola, P. J., Kortabarria, A., Madariaga, A., Esnaola, J. A., Fernandez, E., Cappellini, C.& Özel, T. (2014). On the machining induced residual stresses in IN718 nickel-based alloy: Experiments and predictions with finite element simulation. *Simulation Modelling Practice and Theory*, *41*, 87-103.

[137]Tanaka, K. (2018). X-ray measurement of triaxial residual stress on machined surfaces by the cosα method using a two-dimensional detector. *Journal of Applied Crystallography*, *51*(5), 1329-1338.

[138] Jiang, G. U. O., Haiyang, F. U., Bo, P. A. N., & Renke, K. A. N. G. (2021). Recent progress of residual stress measurement methods: A review. *Chinese Journal of Aeronautics*, *34*(2), 54-78.

[139]Tanaka, K. (2019). The cosα method for X-ray residual stress measurement using two-dimensional detector. *Mechanical Engineering Reviews*, *6*(1), 18-00378

[140] Sharma, V., & Pandey, P. M. (2016). Recent advances in turning with textured cutting tools: a review. *Journal of Cleaner Production*, *137*, 701-715..

[141] Panchal, D. (2020). Optimization of surface roughness of EN-36 alloy steel on CNC turning machine using Box Behnken method under RSM. *Int. J. Res. Appl. Sci. Eng. Technol*, *8*, 608-625.

[142] Singh, G., & Pandey, K. N. (2022). Effect of cryogenic treatment on properties of materials: A review. *Proceedings of the Institution of Mechanical Engineers, Part E: Journal of Process Mechanical Engineering*, *236*(4), 1758-1773.